

Alma Mater Studiorum – Università di Bologna

DOTTORATO DI RICERCA IN
Automotive Engineering for Intelligent Mobility

Ciclo 36

Settore Concorsuale: 09/A3

Settore Scientifico Disciplinare: ING-IND/15

IDeS Methodology Applied to Automotive Component Re-Engineering
Focused on Lightweight and High-Strength by Additive Manufacturing

Presentata da: Christian Edmundo Leon Cardenas

Coordinatore Dottorato

Supervisore

Nicolo Cavina

Alfredo Liverani

Esame finale anno 2023

Table of Contents

Index of Figures	4
Index of Tables	4
1. Engineering Background	11
2. Industrialization in the new century> Challenges for product design	12
2.1 Additive Manufacturing (AM)	14
2.2 3D Scanning.....	16
3. IDeS method.....	17
4. IDES method applied to technical product design.....	22
4.1 Analysis Methods from IDES used in this project:	23
4.1.1 QFD Methodology.....	23
4.1.2 TRIZ Methodology.....	25
5. Additive Manufacturing Introspective	25
6. Project Objectives and Engineering targets	31
6.1 Objectives	31
6.2 Methodology Achievement Phases	32
7. Methods for fast product prototyping and optimal solution assessment	32
8. Case Study> Reverse Engineering applied to product design with technical approach	33
Case study: front suspension control arm	33
8.1 Starting up input element data: geometry, materials, and mechanical requirements.....	34
A) QFD – To find out technical characteristics.....	35
A1) Six Questions and Overall Requirements.....	36
A2) Independence Matrix	37
A3) Importance Matrix.....	38
A4) What–How Matrix	39
B) Benchmarking – to find out market solutions to the issue.....	40
C) TRIZ method application	43
8.2 Vehicle Dynamics forces analysis	45
8.1.1 Static Case	47
8.1.2 Dynamic Cases	48
8.1.3 Braking on The Flat.....	48
8.1.4 Accelerated on The Flat	49
8.1.5 Curb.....	50
8.1.6 Downward Braking.....	52
8.3 Vehicle Dynamics Simulation analysis in FEM software – ANSYS	56
8.4 Results from Dynamic Analysis and Topological Analysis Set Up.....	61

8.5 Product Design for Additive Manufacturing (DfAM) > Topological Optimization	62
Topological Optimization: Reticular and Lattice Structural Deployment.	62
8.5.1 Lattice Structures	62
8.5.2 Response to the Same Loads of Different Latex Structures	65
8.5.3 Lattice Structures with Additive Manufacturing	70
9. Material choice and Engineering approach	71
9.1 3-point bending test (ASTM D790)	75
9.1.3.1 Test probes	75
9.2 Carbon Fiber Lamination Strategy over PETG-CF reinforced polymer	82
9.2.1 Carbon fiber characteristics	82
9.2.2 Epoxy Resin characteristics	83
10. IDES Method Tools and Software Accuracy Exercise	84
11. Product design> Topological Optimization	87
11.1 Lower Suspension – Steering Arm	87
11.2 Upper Suspension – Control Arm.....	94
11.2.1 Optimization of internal structure:	96
11.2.1 SLM AM solution – AlSiMg10 material.....	96
11.2.2 PETG-CF Reinforced Core with Carbon Fiber laminate	101
12. Design Reengineering> methods for fast prototyping and optimal solution assessment	105
12.1 Upper Arm Prototyping.....	106
12.1.1 Part G-Coding for 3D printing: Slicing	107
12.1.2 FDM printing	109
12.1.3 3D scanning	111
12.1.3.1 Repeatability Assessment:	112
12.2 Lower Arm Prototyping.....	114
12.2.1 Lower Arm 3D Scanning	115
13. Achievements.....	117
14. Conclusions	118
15. Future works	118
16. Bibliography	119

Index of Figures

Figure 1. Manufacturing Complexity Assessment.....	12
Figure 2. Manufacturing 4.0 technologies in product development	13
Figure 3. FDM printing layout	14
Figure 4. SLM process	15
Figure 5. Comparison assessment of machining, AM, and hybrid combinations	15
Figure 6. Comparison assessment of machining, AM, and hybrid combinations	16
Figure 7. Faro 3D Laser Scanning Arm.....	17
Figure 8. IDeS methodology for product and process design.	18
Figure 9. IDeS Method Deployment: Tool Overview.....	18
Figure 10. DFSS and IDeS tool comparison and overlap	19
Figure 11. Integration of DFSS into IDeS	20
Figure 12. Importance of Design to reach the goals of an organization.	21
Figure 13. Ideal tradeoff for initial product decisions.....	21
Figure 14. Project Development using IDeS sequence.	22
Figure 15. Tooling used in IDeS that including Styling an Engineering design areas	23
Figure 16. Outline of IdeS Method.....	23
Figure 17. Defect appearance on a PLA specimen: (a) material voids between adjacent lines.....	26
Figure 18. Optimization Process Loop Cycle	27
Figure 19. Flow Chart of the Optimization Process.....	28
Figure 20. Printing quality on the microscope (20x): (a) No optimized (b) Increasing Performance and (c) Fully Optimized	28
Figure 21. AM medical applications - orthopedics: surgery planning (left); customized surgery tooling (right)	29
Figure 22. Part orientation on the buildplate, part helpers in blue.	30
Figure 23. Steps followed during the design of the mold cad model.	30
Figure 24. Comparison between the scan of mold 1 pre and post smoothing (A) and comparison of mold 2 pre and post smoothing (B).	31
Figure 25. Comparison between the two molds after smoothing.....	31
Figure 26. Targets inside each phase of DMADV.....	33
Figure 27. Process line sequence for the project.....	33
Figure 28. 3D Scan result from a Tesla model S front suspension	34
Figure 29. Tesla Model S Front Suspension 3D parametric model.....	35
Figure 30. Design for Additive Manufacturing Guidelines	45
Figure 31. Source Vehicle Main dimensions	46
Figure 32. Forces Acting on the Vehicle in a Static Case.....	47
Figure 33. dynamic diagram of the car when braking.....	48
Figure 34. Schematization of the Car Acceleration Case.....	50
Figure 35. schematization of the forces acting on the vehicle during a curve.....	51
Figure 36. model of the forces acting on the vehicle in the event of braking downhill also considering the aerodynamic resistance.....	53
Figure 37. model of the left suspension (in brown the aluminum components and in gray the steel components).....	56
Figure 38. Vehicle suspension for analysis: A: Upper Arm; B: Lower Arm 1; C: Steering, Lower Arm 257	
Figure 39. Simulation Project Schematic for Vehicle Dynamics	58
Figure 40. Engineering Data Input and Material details for Aluminum Alloy (left) and Structural Steel (right).	59

Figure 41. Results on Dynamic 4 cases analysis on: Upper arm and stub axle	59
Figure 42. Results on Dynamic 4 cases analysis on: reactions between the lower arm and stub axle.	60
Figure 43. Results on Dynamic 4 cases analysis on: Lower Arm 2 - steering arm and the spindle.	60
Figure 44. Maximum deformation results on the entire suspension for 4 different Dynamic cases.	61
Figure 45. <i>Reference Systems of The Upper and Lower Arm</i>	62
Figure 46. a) Unique beam-based building blocks generated by diverse-connected boundary nodes; b) $n \times n$ non-uniform unit cells with $n = 3$ by different combinations of building blocks, design a and its 90°-rotated version b (identified by a darker green).....	64
Figure 47. Reticular Structures Used in the study.....	65
Figure 48. Von-Misses Stress vs Lattice Thickness and Fillet Radius for best scored Structure geometries.	70
Figure 49. AM-sourced lattice structures.....	70
Figure 50. SISMA® MySint 100 SLM Printer	71
Figure 51. Artillery® Sidewinder X1 FDM Printer	73
Figure 52. UTS vs number of cycles assessment for PETG material.....	74
Figure 53. Probe printing with different internal structures: Honeycomb Transversal (Top) and Square Honeycomb (Down)	75
Figure 54. Reinforced walls Honeycomb Structure	76
Figure 55. Test Probes – Material: PETG + CF and 3 point bending test (ASTM D790).....	76
Figure 56. Test Probes 1, 2, 3 – with transversal Honeycomb structure, showed the best overall mechanical performance. Note that probe 3 has 3 layers of CF.	79
Figure 57. Test Probes 4, 5 – with Outer layer-reinforced, Square Honeycomb structure, scored second at overall mechanical performance. Note that probe 5 has 3 layers of CF.....	80
Figure 58. Average performance results of regular, square infill by Cura® in test Probes 6 to 10 with Probe 8 that has 3 layers of CF. This structure scored last overall in the test performed	81
Figure 59. Test Probe 11 performance: this Probe was made with PLA-reinforced filament, and with 3 CF layers. Showed a rather elastic response behavior than the PETG counterparts.	81
Figure 60. Twill Carbon fabric of 600 g/m ²	82
Figure 61. MasterBond® EP42HT-2LO Polymer System	83
Figure 62. Faro Quantum® 3D Scanner	84
Figure 63. Raw lower arm component for Topological Optimization Exercise in Ansys	88
Figure 64. Top) Total Deformation Distribution; and Down) Equivalent Stress Distribution pre- Optimization.....	88
Figure 65. Optimization Solution Information, shows convergence after 28 iterations	88
Figure 66. Obtained Part distribution density after optimization. Grey zones are to keep, and the brown zones are parts in which the material is cut up to 60%.....	89
Figure 67. Early Proposal for Topological Optimized Lower Arm	89
Figure 68. Total Deformation for Early Proposal – Lower Arm.....	90
Figure 69. Equivalent Von Misses Stress – Lower Arm.....	90
Figure 70. Fatigue assessment according to Soderberg’s theory.	90
Figure 71. Geometry Optimization performed in the joint area, the best solution (right) delivered a reduction of 57% of the max Equivalent Stress.	91
Figure 72. Optimized Lower Arm Solution.	92
Figure 73. Geometry Optimization performed in the joint area, the best solution (right) delivered a reduction of 74% of the max total Deformation.....	92
Figure 74. The best solution delivered a reduction of 42% of the max Equivalent Stress.....	93
Figure 75. The best solution delivered an important increase of 3 orders of magnitude of the lowest Life Cycle expectation.	93

Figure 76. Raw component for Topological Optimization Exercise in Ansys.....	94
Figure 77. Left)Total Deformation Distribution; and Right)Equivalent Stress Distribution pre Optimization.....	95
Figure 78. Optimization Solution Information, shows convergence after 22 iterations	95
Figure 79. Upper arm distribution density after optimization. Grey zones are to keep, and the brown zones are parts in which the material is cut up to 60%	95
Figure 80. Project Schematic layout of the Upper Arm focused on SLM process.....	97
Figure 81. First Iteration with geometry V1; Max Stress= 58.302 Mpa; 1.38 mm Max deflection	97
Figure 82. Iteration #7 geometry no TO- V7 Equivalent Stress distribution – part without Lattice.....	98
Figure 83. Results on Initial lattices Iteration: Square mesh. Note the lower Stress Distribution	99
Figure 84. Iteration with optimized ball joint geometry and Honeycomb TO. Max Stress = 28.453MPa; Deformation is still high at 1.96 mm.....	99
Figure 85. Final Iteration with lighter structure and Honeycomb TO and modified Ball Joint geometry; Max Stress=35.537 MPa; Def Max= 0.15mm	100
Figure 86. Life results for the optimized AL version, Life: 1e8 cycles min; SFC 3.65 min.	101
Figure 87. Optimized Upper Arm Solution - SLM.	101
Figure 88. ANSYS Project Schematic layout of the Upper Arm focused on FDM matrix + Carbon Fiber Laminate.....	102
Figure 89. Materials used in the analysis.	102
Figure 90. Matrix Geometry: Topologically Optimized Structure	103
Figure 91. Total Deformation for total part; Max Value = 0.36528 mm.....	103
Figure 92. Equivalent Stress for PETG-CF AM Matrix; Max value of 18.562 MPa.	103
Figure 93. Equivalent Stress for Carbon Fiber layers; Max value of 102.05 MPa.....	103
Figure 94. Safety Factor (Top) 4.95 min; and Fatigue Life Cycle (Down) 9,6e4 cycles for the Solution	104
Figure 95. Optimized PETG Matrix	104
Figure 96. Carbon Fiber laminated Upper Arm Solution	105
Figure 97. Ultimaker® Cura 5.1 Interface, shows 13h 35min building time with selected parameters	108
Figure 98. G-code preview line at 50% of the total printing time.....	108
Figure 99. FDM printing of the Upper Arm at 50%	109
Figure 100. FDM printing of the Upper Arm at layer 93, the creation of the Top layer.....	109
Figure 101. Completed print (with supports)	110
Figure 102. Final printed part.....	110
Figure 103. Laminated version of the final printed element	110
Figure 104. Analysis Tab from Geomagic control X 2020.....	111
Figure 105. <i>a. Part positioning and Scan procedure with Faro® Quantum 3D Scanner.</i>	111
Figure 106. Comparison results of scanned part vs. CAD Values.	112
Figure 107. 3D Comparison results of scanned part vs. CAD Values.	112
Figure 108. Tolerance variation results by 3D Scanning in Control X 2020.....	112
Figure 109. Tolerance variation results of second part	113
Figure 110. Tolerance variation results of the second part.....	114
Figure 111. Sisma® MySint 100 SLM Printer	114
Figure 112. Part after SLM printing – First Iteration.....	115
Figure 113. Optimized Iteration of Lower Arm, with supports after SLM printing.	115
Figure 114. Optimized Lower Arm after heat treatment.	115
Figure 115. Lower Arm V1 tolerance correlation by means of 3D scanning.....	116
Figure 116. Optimized Lower Arm tolerance correlation by means of 3D scanning.	116

Figure 117. Tolerance variation results of the second part..... 117

Index of Tables

Table 1. Six Questions and Overall Requirements.....	36
Table 2. Independence Matrix	37
Table 3. Importance Matrix.....	38
Table 4. What-How Matrix	39
Table 5. Benchmarking Analysis for a) Lower Arm; b) Upper Arm.....	41
Table 6. Inventive Ideas from Contradictions assessment via Altshuler Matrix.....	44
Table 7: Parameter Values for Calculations.....	46
Table 8. Forces at Play for Each Case Analysed	55
Table 9: data relating to the components present in figure X of the left suspension model.....	57
<i>Table 10. Load Values To Set The Topological Optimization According To The Respective Reference Systems</i>	<i>62</i>
Table 11. Mechanical Characterization for each Type of Reticular Structures.....	66
Table 12. mechanical resistance analysis results for top 3 rated internal structures from NTOP.	69
Table 13. Powder AlSi10Mg chemical composition (EOS Metal Solutions, 2022).....	72
Table 14. Typical properties (as manufactured state)	72
Table 15. Typical properties (heat Treated, EOS T6)	72
Table 16. FormFutura Carbonfil™ PETG – CF Technical Data Sheet	73
Table 17. Mechanical Properties of Polymaker® Polylite PLA-CF	74
Table 18. Test probe details for 3 bending test procedure	77
Table 19. Studied Probes Cost Deployment	78
Table 20. Results Evaluation of Analyzed Structures.....	81
Table 21. Mechanical Properties HT-Carbon Fiber:.....	82
Table 22. EP42HT-2LO Technical Data Sheet	83
Table 23. Preliminary FEM Software Computational Accuracy Analysis Differentiation.....	85
Table 24. Original Part Data – Lower Suspension Arm.....	87
Table 25. Optimized Lower Arm Summary; *: not considering tooling costs.	93
Table 26. Original Part Data – Upper Suspension Arm.....	94
Table 27. Optimized Lower Arm Summary; *: not considering tooling costs	105
Table 28. Optimized Printing Parameters for PETG-CF Filament Material	106
Table 29. Main Printing Parameters for SLM.....	114

Acknowledgements

I am utterly thankful for all the help and support of Prof. Alfredo Liverani and the entire Staff at the Department of Industrial Engineering of the University of Bologna. Professors, Researchers, and students do their best to innovate.

Dedicado a mis padres Edmundo Leon y Concepción Cardenas, su apoyo y paciencia han hecho que pueda realizar esta meta.

A Naomi

Abstract

The project aims to gather an understanding of additive manufacturing and other manufacturing 4.0 techniques with an eyesight for industrialization. First the internal material anisotropy of elements created with the most economically feasible FEM technique was established. An understanding of the main drivers for variability for AM was portrayed, with the focus on achieving material internal isotropy. Subsequently, a technique for deposition parameter optimization was presented, further procedure testing was performed following other polymeric materials and composites. A replicability assessment by means of the use of technology 4.0 was proposed, and subsequent industry findings gathered the ultimate need of developing a process that demonstrate how to re-engineer designs in order to show the best results with AM processing. The latest study aims to apply the Industrial Design and Structure Method (IDES) and applying all the knowledge previously stacked into fully reengineer a product with focus of applying tools from 4.0 era, from product feasibility studies, until CAE – FEM analysis and CAM – DfAM. These results would help in making AM and FDM processes a viable option to be combined with composites technologies to achieve a reliable, cost-effective manufacturing method that could also be used for mass market, industry applications.

1. Engineering Background

Product development in the modern era has been characterized by significant advancements in technology, increased connectivity, and a greater emphasis on sustainability and user-centric design. Here are some key trends and features that have shaped product development in this era, starting from Rapid Technological Advancements with an exponential growth in technology functionality and dependability, particularly in the fields of computing, artificial intelligence (AI), Internet of Things (IoT), and data analytics. These technological advancements have enabled the creation of smarter, more interconnected products that can collect and analyze data to offer enhanced user experiences and improved functionality. Afterwards, the Internet and Connectivity: The widespread availability of the internet and the proliferation of connected devices have given rise to the concept of the Internet of Things (IoT) (Gupta & Quamara, 2020). Products are now designed to be interconnected, allowing users to control and monitor them remotely through smartphones and other devices. This has opened up new opportunities for creating products and services with seamless integration and real-time communication (Raj et al., 2020).

Product design has been refocused in this new era as well, by means of a User-Centric Design: placing a strong emphasis on understanding and meeting the needs of users. User research, usability testing, and iterative design have become integral parts of the product development process. Companies invest significant efforts in gathering user feedback and analyzing user behavior to create products that are intuitive, enjoyable, and tailored to their customers' preferences. This evolution gave room to increase product Personalization and Customization: Advancements in technology have enabled companies to offer personalized and customized products and services to their customers. From personalized recommendations in e-commerce to tailor-made products using 3D printing, the ability to cater to individual preferences has become a competitive advantage.

Likewise, companies have evolved their practices towards the Industry 4.0 era, adopting Agile Development, in contrast to traditional waterfall product development. Agile development allows for incremental and flexible product iterations, enabling faster responses to changing market demands and reducing time to market (Peterson & Summers, 2021). This approach fosters collaboration among cross-functional teams and prioritizes frequent customer feedback. In addition to a Data-Driven Decision Making: With the abundance of data available, product development teams rely on data-driven decision making. By analyzing user data and product usage patterns, companies gain insights into user behavior, preferences, and pain points, allowing for more informed and effective product improvements.

In addition to this, Industries can exploit Innovations driven by technology in benefit of more stakeholders, with companies from different sectors collaborating and integrating technologies to develop innovative products. For example, the convergence of healthcare and technology (Han & Lee, 2021) has led to the rise of wearable health devices, telemedicine solutions, as well as important improvements in Orthopedics (Frizziero, Santi, Leon-Cardenas, Donnici, Liverani, Papaleo, et al., 2021), (Frizziero, Santi, Leon-Cardenas, Donnici, Liverani, Napolitano, et al., 2021), (Frizziero, Pagliari, et al., 2021), and transplants, by using the same technology inspired from the aerospace area. This unified platform and ecosystem product approach will help companies to create products designed to integrate seamlessly with other complementary products and services. This approach creates more value for users, enhances customer loyalty, and opens up new revenue streams.

Nevertheless, usually the practices for new product development carry a high level of risk. Which might be the high cost of development, scheduling limits for proper reengineering, as well as challenging poor manufacturability, poor product quality, and low profitability. Additionally, manufacturing

engineering and production are often brought in toward the end of the development cycle or completely left out of the development process altogether. This often results in products coming to market lacking well-defined manufacturing processes, with poor process efficiency and poor process quality. (Tambare et al., 2021).

A number of product development tools have been released that offer to mitigate these risks, and many of them fall under Lean Product Development (LPD). Conversely, some of these tools taken by mainstream product development, whereas others have not been fully implemented or tried at the industry level. The premise of a product development tool and method that improves the efficacy of the development process has long been hyped. However, it was described that many of these tools have failed to be inserted into companies (Miles & Roberts, 2019). This involves the need to enable each area of the organization to accurately understand customer-related data. Consequently, an organization could attract and retain the most valuable portion of the market by creating value to the customer; this would directly impact on the entire chain created to generate value, as later approaches on social responsibility (Ali et al., 2020). Statement confirmed also by (Narver & Slater, 1990), (Powell & Bartolome, 2020), (Seno et al., 2019) who also underlines the importance of taking into account each stakeholder across the entire value chain creation for better results in a cross-functional organization.

2. Industrialization in the new century> Challenges for product design

Moreover, as market behavior shown to head towards choosing individualized products, companies are moving for adopting a strategic opportunity of switching to customer-driven processes by creating new procedures that adopt the will of every customer (Jørgensen, 2009), (Medini et al., 2019). Other analysis by (Alt et al., 2019), (Neneh, 2018), (Oyner & Latyshova, 2009) established that nowadays the volatility of the customer behavior turned the individual customer orientation concept in a more objective way for market analysis, and differentiate or customize a product or service is useful to even get extra information about the customer maximum necessities. Therefore, increased data analysis capacity in tools from industry 4.0 have enabled companies to develop complex evaluations to gather as much detailed information (Perez et al., 2018) that can give out the optimal solutions to the challenges solved with the integration of tools for manufacturing 4.0 (Figure 1).

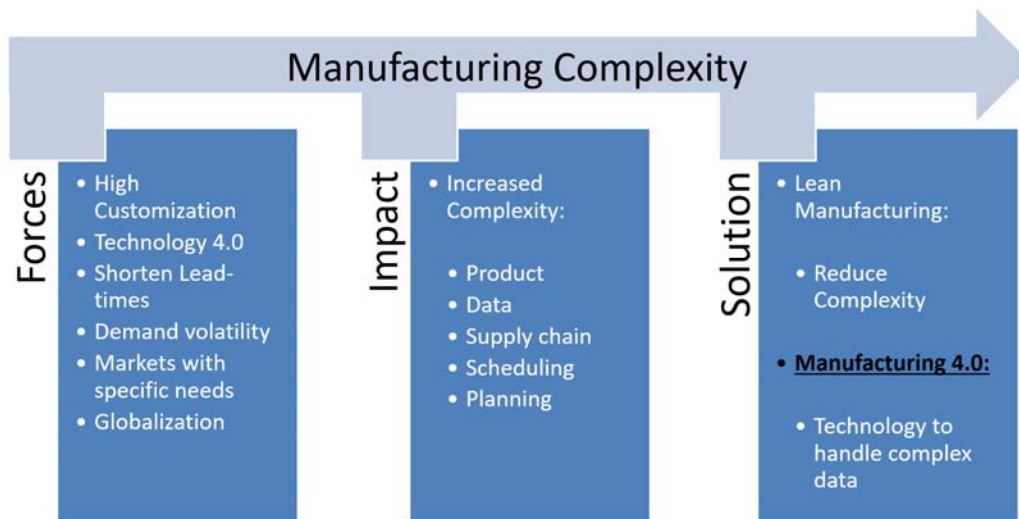


Figure 1. Manufacturing Complexity Assessment.

However, dedicated manufacturing 4.0 technologies (Lin et al., 2018), aided with artificial intelligence (Balamurugan et al., 2019) gave the opportunity to exploit high data bandwidths in order to optimize information sharing across all the organization, giving stage to new era manufacturing sequence, in which Digital technologies are present seamlessly across the entire development process, namely circular manufacturing (Delpla et al., 2022), from the early conception of customer-oriented targets (Ahmed et al., 2021), initial 3D drawing and Digital Prototyping, (Lazorík, 2021) until the ultimate automation and manufacturing with Additive Manufacturing technologies using Internet of Things (Ashima et al., 2021), (Parmar et al., 2022) (Figure 2) and quality control (Dutta et al., 2021), (Silva et al., 2021). Solutions of which offer midterm cost-effectiveness (Shivajee et al., 2019); and organizations should realize the need to change training programs to new workforce (Wulansari, et al. 2018).

Nowadays, data information management across the automotive industry is suffering of the most basic conditions of development expected from an area that employs people and whose industry is valued at \$2.6tr in 2023 (IBISWorld, 2023), which is an interesting 10 percent over year decrease from 2.86 trillion U.S. dollars, as of 2022 (Lenort et al., 2023) An accelerating industry changing scenario leaves companies without much resources to modernize internal data management platforms (Assur & Rowshankish, 2022). This old-fashionable data interchanging and integral project auditing is starting to deliver its first reactions (Lipu et al., 2021). Longer times of product development and delivery at a premium price are because of highly structured system complexities of their own. These technical and management miss has then been translated into longer deliverable processing times therefore arriving to cause many management issues that could be decreased with the adoption of an unified platform. Platform integration across global companies has been demonstrating a undoubtedly need to adopt a unified central data interchange policy (Nazarova et al., 2022).

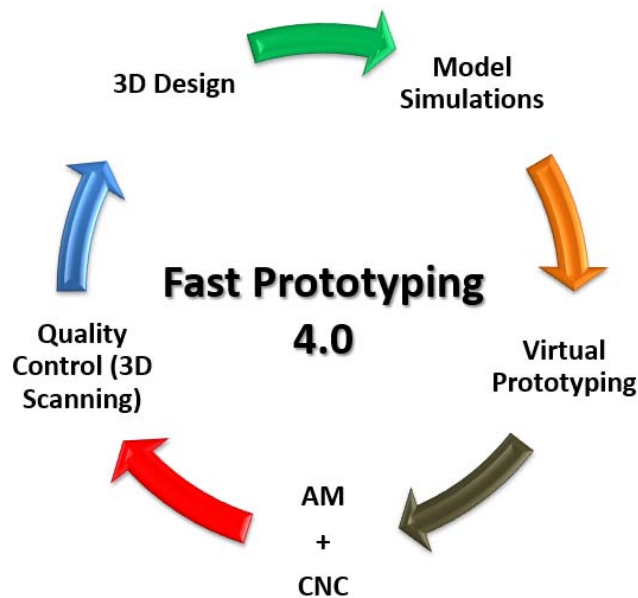


Figure 2. Manufacturing 4.0 technologies in product development

2.1 Additive Manufacturing (AM)

Additive Manufacturing (AM), also known as 3D printing, is a transformative manufacturing technology that has revolutionized various industries by enabling the creation of complex and customized objects layer by layer. Modern techniques in additive manufacturing have evolved significantly in recent years, offering improved precision, materials, and scalability. In this introduction, we will explore some of these modern techniques and their applications. AM technology has been under research and development for the past 40 years. This technology has demonstrated the capability for creating parts up to the highest quality standards.

Nowadays, there is a wide range of AM equipment proposals that offer respectable levels of productivity and repeatability, but in any case, companies have to balance the overall initial machine and materials cost with the return of investment. Part quality and overall mechanical strength are strictly related to cost. This is why AM technology has become an interesting option for companies to portray its prototypes to test in a faster way. AM's higher initial costs are balanced with the 0 initial tooling cost. This study will use two of the most known AM techniques, related to the type of material they produce, Fused Deposition Modeling (FDM) for polymeric-sourced filaments and Selective Laser Melting (SLM) for metallic components.

FDM (Figure 3) is perhaps the most common 3D printing technique. It works by extruding a thermoplastic filament through a heated nozzle, layer by layer, to create objects. FDM is widely used in industries ranging from aerospace to consumer goods due to its affordability and versatility. into a solid 3D structure. This technique is valued for its ability to work with a wide range of materials and produce parts with excellent mechanical properties.

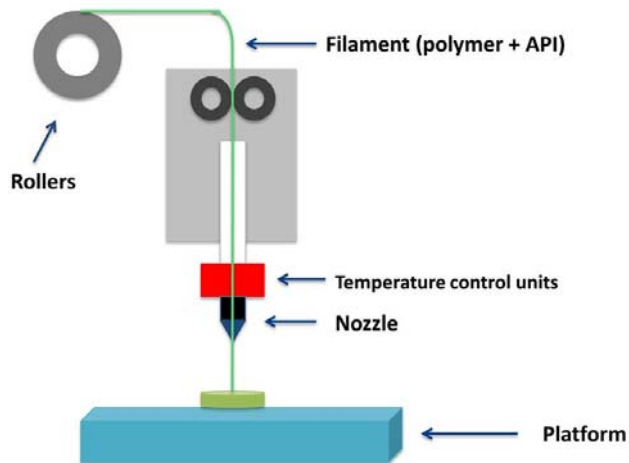


Figure 3. FDM printing layout

Afterwards, the most accepted technique of AM in the industry is metallic AM by means of the SLM technique (Figure 4), designed to use high power-density laser to melt and fuse metallic powders. A component is built by selectively melting and fusing powders within and between layers. The SLM technique is also commonly known as direct selective laser sintering, LaserCusing, and direct metal laser sintering, and this technique has been proven to produce near net-shape parts up to

99.9% relative density (Yap et al., 2015). This enables the process to build near full density functional parts and has viable economic benefits. Recent developments of fibre optics and high-power laser

have also enabled SLM to process different metallic materials, such as copper, aluminum, and tungsten. Selective Laser Melting is a crucial technique in the world of additive manufacturing, particularly in industries where high-performance metal parts are required, and it continues to advance with ongoing research and development efforts.

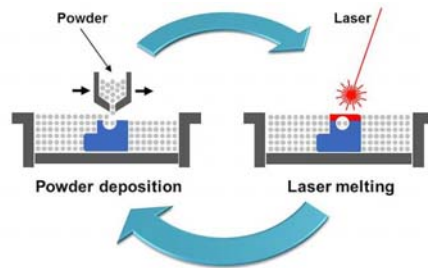


Figure 4. SLM process

In the last years, although the standard AM classification incorporates seven distinct categories (ISO 17296-2:2015 Additive Manufacturing — General Principles — Part 2: Overview of Process Categories and Feedstock, 2020), the discussion emphasizes the hybridization of the main AM technologies of material extrusion (ME), directed energy deposition (DED), and powder bed fusion (PBF) with subsequent subprocesses (Figure 5) that aids to take AM processes into mass production (Dilberoglu et al., 2021) (Figure 6).

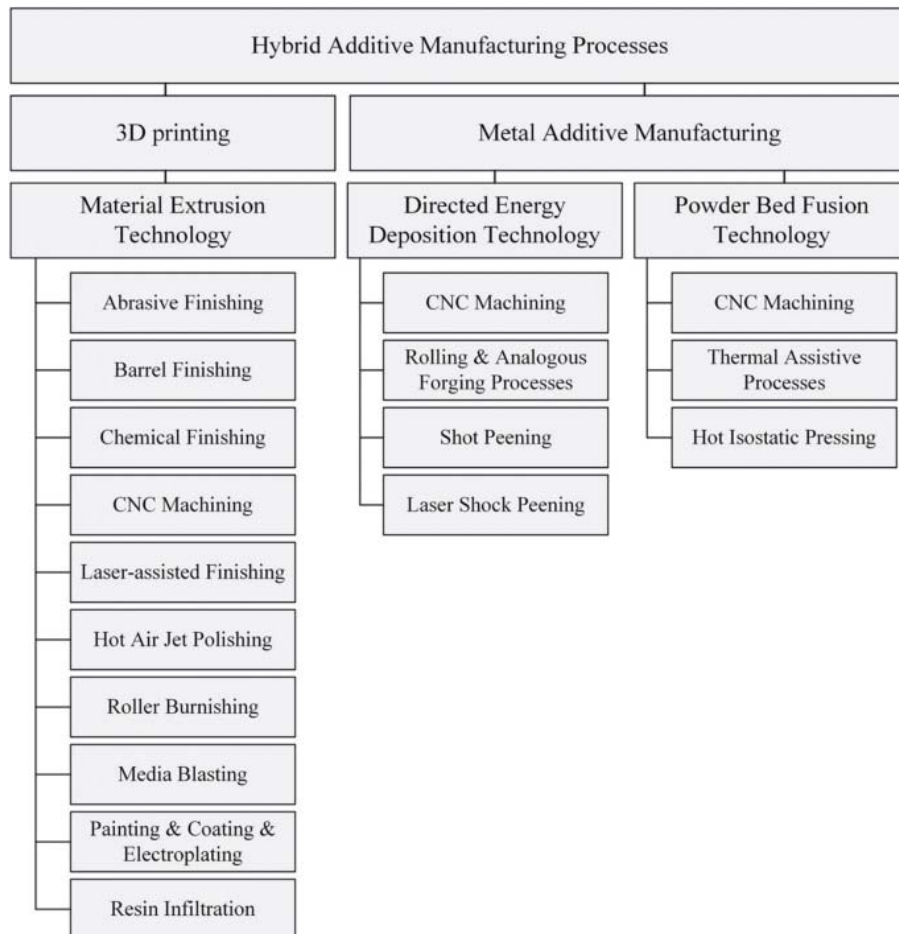


Figure 5. Comparison assessment of machining, AM, and hybrid combinations

	Properties	Machining	Additive Manufacturing	Hybrid Manufacturing
Product Quality	Shape Complexity	L H	L H	L H
	Strength	L H	L H	L H
	Surface Finish/Quality	L H	L H	L H
	Dimensional Accuracy	L H	L H	L H
	Repeatability	L H	L H	L H
Materials	Material Waste	L H	L H	L H
	Sustainability	L H	L H	L H
	Material Availability	Limited <input type="checkbox"/> <input checked="" type="checkbox"/> Several	Limited <input checked="" type="checkbox"/> <input type="checkbox"/> Flexible	Limited <input checked="" type="checkbox"/> <input type="checkbox"/> Flexible
	Multi-material Usage	Rare <input checked="" type="checkbox"/> <input type="checkbox"/> Frequent	Rare <input type="checkbox"/> <input checked="" type="checkbox"/> Frequent	Rare <input type="checkbox"/> <input checked="" type="checkbox"/> Frequent
Design	Build Volume	L H	L H	L H
	Geometric Complexity	L H	L H	L H
	Design Versatility	Limited <input checked="" type="checkbox"/> <input type="checkbox"/> Flexible	Limited <input type="checkbox"/> <input checked="" type="checkbox"/> Flexible	Limited <input type="checkbox"/> <input checked="" type="checkbox"/> Flexible
	Reshaping Products	Rare <input checked="" type="checkbox"/> <input type="checkbox"/> Frequent	Rare <input checked="" type="checkbox"/> <input type="checkbox"/> Frequent	Rare <input type="checkbox"/> <input checked="" type="checkbox"/> Frequent
Cost	Investment Cost	L H	L H	L H
	Tooling Cost	L H	L H	L H
	Labor Cost	L H	L H	L H
	Skill Requirement	L H	L H	L H
	Mass Production	Rare <input type="checkbox"/> <input checked="" type="checkbox"/> Frequent	Rare <input checked="" type="checkbox"/> <input type="checkbox"/> Frequent	Rare <input checked="" type="checkbox"/> <input type="checkbox"/> Frequent
	Batch Size	Small <input type="checkbox"/> <input checked="" type="checkbox"/> Large	Small <input checked="" type="checkbox"/> <input type="checkbox"/> Large	Small <input checked="" type="checkbox"/> <input type="checkbox"/> Large
Manufacturing	Production Speed	L H	L H	L H
	Post-processing Time	L H	L H	L H
	Customization	Yes <input type="checkbox"/> <input checked="" type="checkbox"/> No	Yes <input checked="" type="checkbox"/> <input type="checkbox"/> No	Yes <input checked="" type="checkbox"/> <input type="checkbox"/> No
	Decentralization	Yes <input type="checkbox"/> <input checked="" type="checkbox"/> No	Yes <input checked="" type="checkbox"/> <input type="checkbox"/> No	Yes <input checked="" type="checkbox"/> <input type="checkbox"/> No
	Single-step Hybrid Objects	Yes <input type="checkbox"/> <input checked="" type="checkbox"/> No	Yes <input checked="" type="checkbox"/> <input type="checkbox"/> No	Yes <input checked="" type="checkbox"/> <input type="checkbox"/> No

Figure 6. Comparison assessment of machining, AM, and hybrid combinations

Finally, the current AM applications in the Automotive Industry are concentrated in metal AM-sourced parts for Exhausts and emission-control systems, pumps, valves, as well as suspension springs, and small body panels and doors, with some exercises in engine components as well (Salifu et al., 2022); polymer-based AM instead is used to create sensor boards and control panels, as well as hubcaps, bumpers, wind breakers, but mostly related to interior dashboard panels, and seat frames. Nevertheless, the widest-known AM applications are related to customized tooling for production lines, which have proven to be economically effective and easily replaceable (Sarvankar & Yewale, 2019).

2.2 3D Scanning

3D scanning is a technology that allows the capture of three-dimensional information about objects, environments, or surfaces in the physical world and converts it into digital 3D models or point clouds. This technology has numerous applications, including manufacturing and production line usage, where it plays a crucial role in quality control, design, and process optimization. 3D scanning involves the use of various technologies and devices to capture the shape, size, and surface details of physical objects and convert this data into digital 3D representations. The most common types of 3D scanning technologies include:

Laser-based Scanning: Laser scanners project a laser beam onto an object's surface and measure the time it takes for the laser to bounce back. This data is used to create a 3D point cloud or mesh;
Structured Light Scanning: Structured light scanners project patterns of light onto an object and use the deformation of these patterns to calculate the object's 3D shape.

Moreover, 3D Scanning usage (Figure 7) has been increasing widely across production line processes, in order to aid to assess Quality Control, as it allows for the rapid and accurate inspection of parts and

components to ensure they meet design specifications; Reverse Engineering, as 3D scanning can capture the geometry of the original object; in Tool and Mold Design by allowing precise measurements of complex part geometries, ensuring that molds and tools are designed accurately; until continuously scanning and monitoring production processes, manufacturers can identify bottlenecks, defects, or inefficiencies. This information can be used to optimize production lines and improve overall productivity.

Overall, 3D scanning is a versatile technology that enhances the efficiency, accuracy, and flexibility of production lines across a wide range of industries, contributing to improved product quality and reduced production costs.



Figure 7. Faro 3D Laser Scanning Arm

3. IDeS method

The Industry Design Structure Method (IDeS) establishes the creation of continuous feedback links between the design structure with the other departments related to product development across the organization. Likewise, the main three macro phases of this concept are exposed in Figure 8 summarizing the entire industrial product design processes (Set up, Development, Production). Consequently, the main IDeS output is a customer-centered, technically and demand - wise secured product design company organization. This is obtained by structuring the organization transversally with quick adaptation in today's industrial challenges. Being able to train new professionals into the skills required for obtaining good results with manufacturing 4.0 in the company, obtained by joining all organization departments from product developers to manufacturing and quality control areas. In the end, this information would switch an organization effectiveness in maximizing consumer profitability (Burton & Obel, 2018) from the traditional, known methodologies centered in product effectiveness, as previously introduced by (Maas, 2000); this evolution has to be carried over the entire value chain (Volkov et al., 2018) until redefining the sales structure (Thaichon et al., 2018). Therefore, establishing a modern organization structure that would interactively update the knowledge of

customers behavior, and the evolving to understand the demand of specific requirements that would deliver exclusive value to its users.

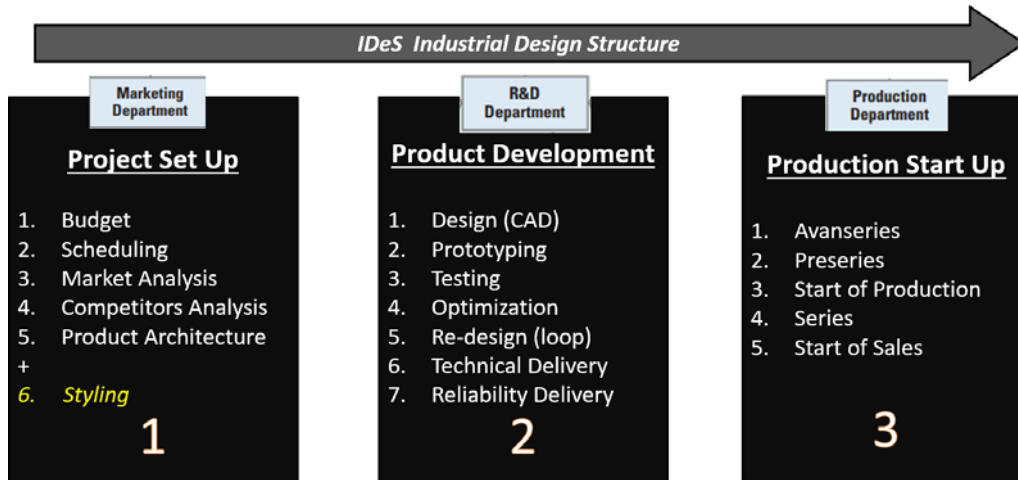


Figure 8. IDEs methodology for product and process design.

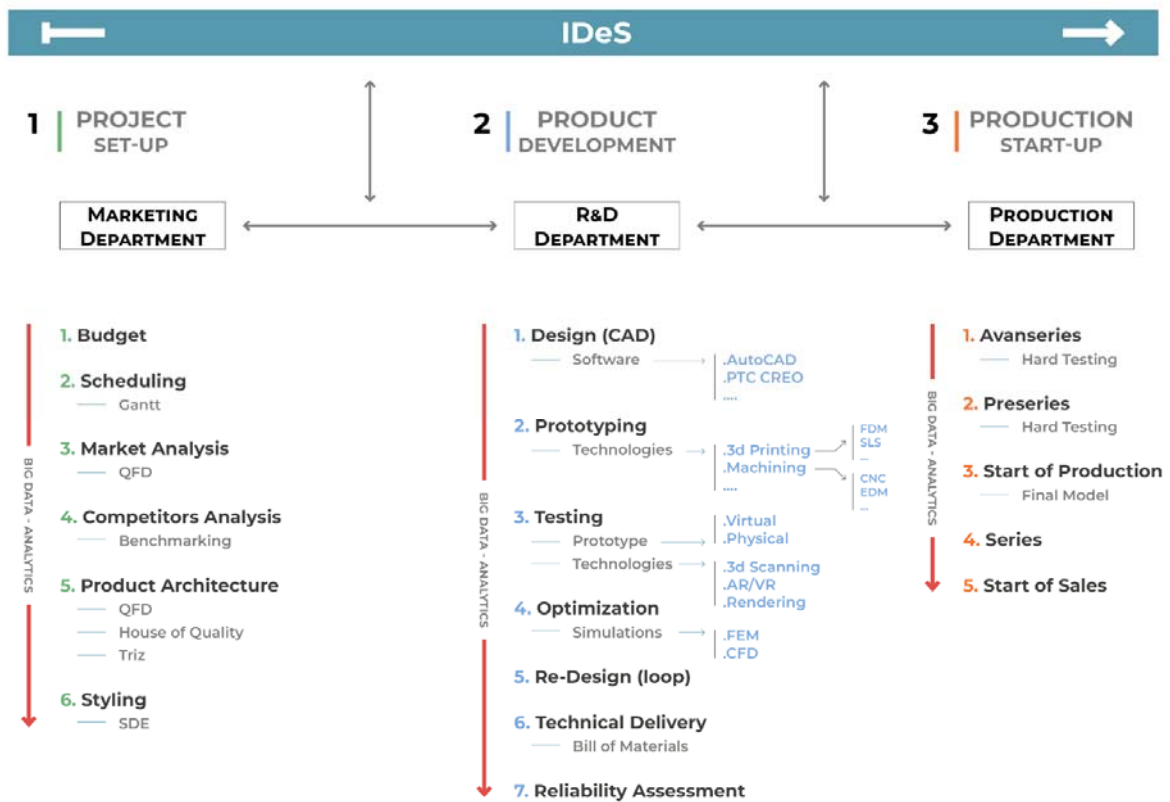


Figure 9. IDEs Method Deployment: Tool Overview

Moreover, IDEs method has proven to conduct one of the types of Design for Six Sigma, referred to by the acronym DMADV. This approach is given to achieve six sigma quality standards in the creation of a product. Therefore, a correlation was found within the tools applied across DMADV processes (F-K.

Wang et al., 2016), (Mouaky et al., 2018) and the tools applied across IDeS structure. Besides, Figure 9 shows in detail, the list of the tools used by DMADV on IDeS. The similarity on the inputs, output characteristics and target process outputs resulting of the tools of DFSS. Therefore, DFSS DMADV steps could be channeled, complemented with guidelines from lean productivity (Ikumapayi et al., 2020), and correlated in Figure 10, to be integrated into the proposed IDeS methodology across its main three phases as seen in Figure 11, in which a complete coherence of using the DFSS methods into a wide organizational methodology could be also noticed.

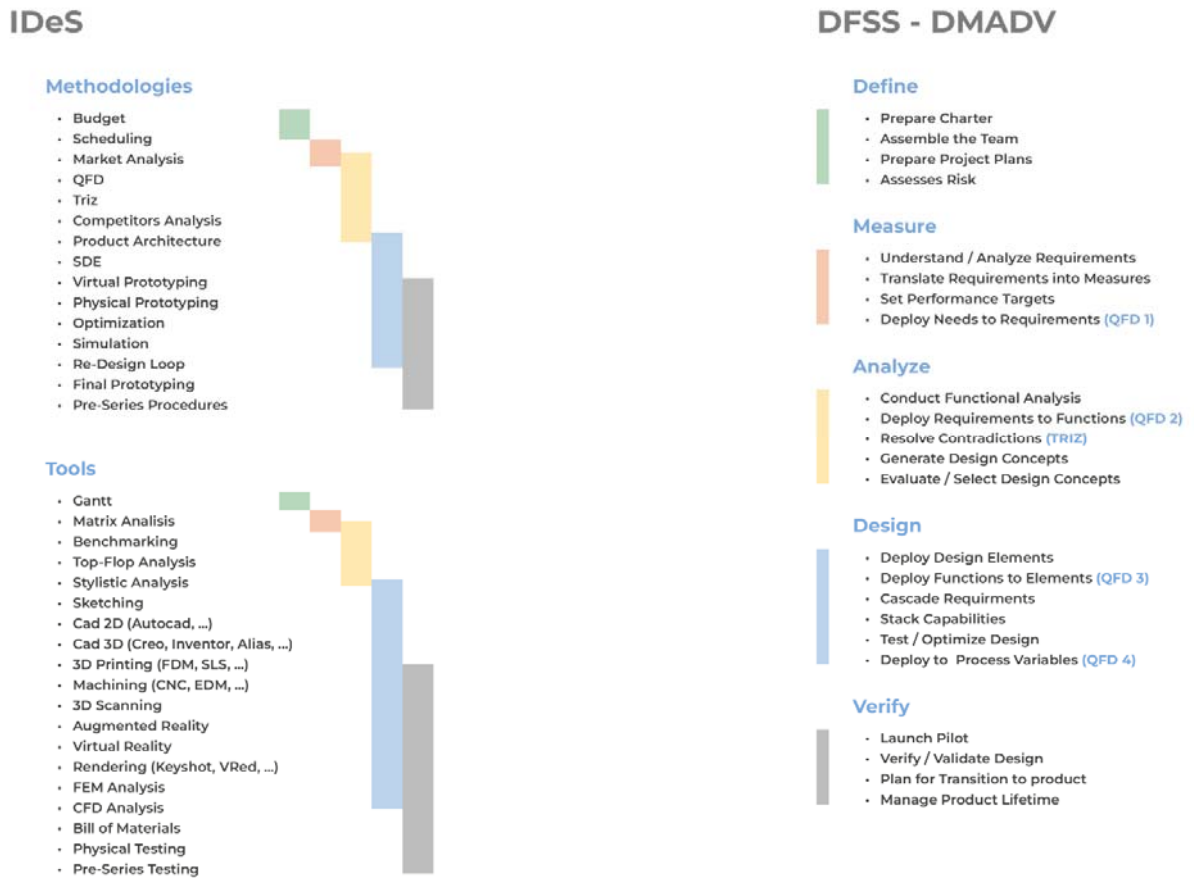


Figure 10. DFSS and IDeS tool comparison and overlap

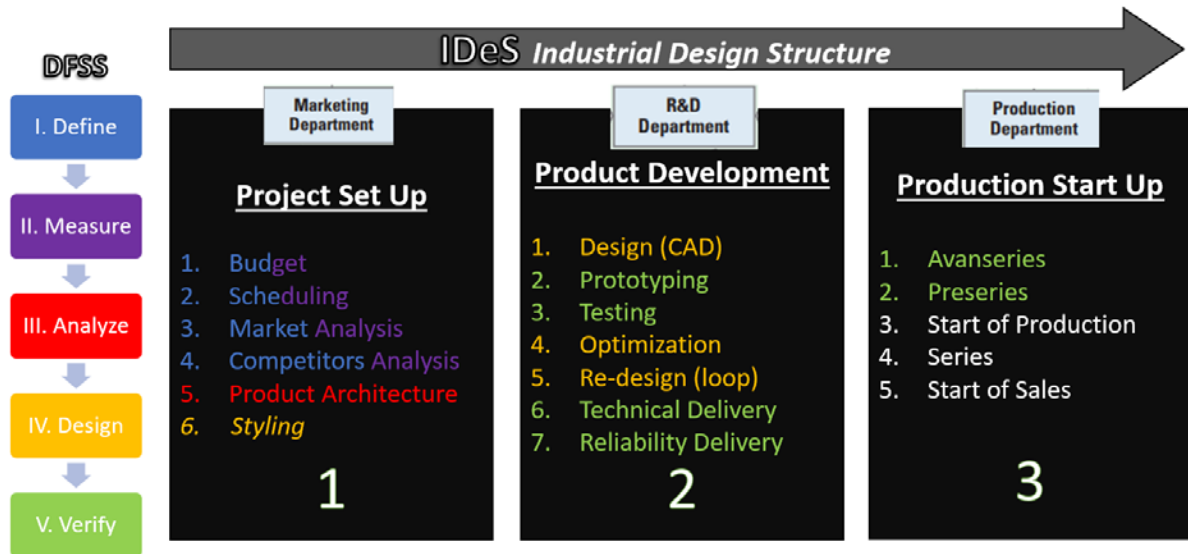


Figure 11. Integration of DFSS into IDeS

C) IDeS as a methodology for organization structuring with quick adaptation in today's industrial challenges

Historically, companies lacked to understand the compromise of including manufacturing engineering and production from the start in product development practices, that often results in a product arrival to market that lacks a defined manufacturing process, delivering poor process efficiency and poor process quality that leads to low profitability (Miles & Roberts, 2019). Even though wide research has been made about improving the existing product development methodology of DFSS, authors agree that implementing DFSS to the reality of each sector made hard to present a general process model as achieved by the Six Sigma approach (M. Patel & Desai, 2018). The results of (Miles & Roberts, 2019) shown that 42% of surveyed consultants found difficulties at implementing DFSS and 38% found QFD and Lean processes difficult to implement as well. Therefore a number of models based on DFSS have been proposed by (Shokri & Li, 2020), (Ericsson et al., 2015), (S. Patel, 2017), (Berryman, 2002), (Soderborg, 2004) among many others, findings that demonstrate how important is to have a tailored model true to every single reality. Nevertheless, a comprehensive, reliable method that considers the actual benefits of unified, cross functional interactions across the whole organization to speed up development times could be useful to conduit organizations to implement DFSS in their organizations more efficiently.

Moreover, the approach proposed with Industrial Design Structure would aid companies to systematically interact with all organization levels, therefore reaching all stakeholders involvement into each project, which is needed to reach industrial efficiency leaded by customization. Findings by Daft, Murphy and Willmott (Daft et al., 2010) correlated the concept of design into five of the author's seven main pursuals established by organizations (Figure 12), concluding that specific inputs and decisions from the top management and project leaders are key to be communicated and implemented into the design and styling department, whose outputs would spread systematically throughout the rest of the organization, affecting importantly the timing for decision making in other departments. This would determine a different strategy for adapting the cultural behavior and environment across the entire organization.

Organization exist to do the following

1. Bring together resources to achieve desired goals and outcomes
2. Produce goods and services efficiently
3. Facilitate innovation
4. Use modern manufacturing and information technologies
5. Adapt to and influence a changing environment
6. Create value for owners, customers and employees
7. Accommodate ongoing challenges of diversity, ethics, and the motivation and coordination of employees



Figure 12. Importance of Design to reach the goals of an organization.

Moreover, a different schematization would be required to arrange leadership within the organization based on the stages led by the product design phases, that is to fully interact participants from all involved departments from early product feasibility and conceptualization analysis until production start-up. This change could suggest that a different scheme is required in a modern matrix-schemed organization in which the head of product design (style and engineering) would help the Top Management to better perceive upcoming challenges and efficiently take decisions as well as finding opportunities and threats, as seen in Figure 13. This approach establishes the value to appropriately design and engineer each individual component, adding up to an overall product success. The technical and style design departments could oversight digital information sharing based on latest technologies of Industry 4.0 as Augmented Reality (AR) (Xiong et al., 2021), Cyber Physical Systems (CPS), as well as other technological tooling and methods that also aid the pro-ecological design and assessment of sustainable product development practices (Paprocki, 2019) to convey product development information across all project stakeholders, helping to ease implementation costs by saving important resources, time, and proving value savings over time (Miles & Roberts, 2019).

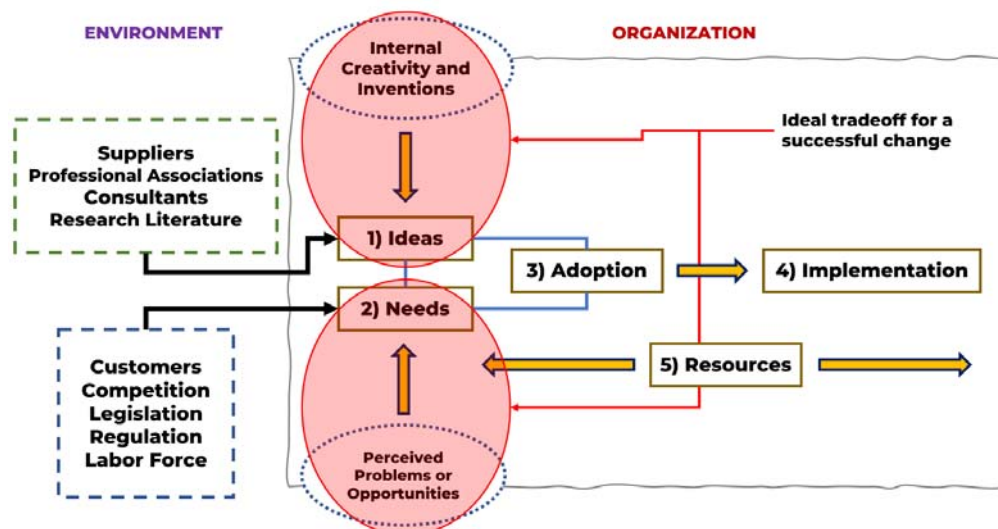


Figure 13. Ideal tradeoff for initial product decisions

4. IDES method applied to technical product design.

The implementation of the IDES method has been discussed and demonstrated in early product design research findings carried out by the affiliated institution of the authors, that proposed this methodology as an innovative organization method for product development by providing product prototypes for different industry sectors ranging from the Mobility solutions (Frizziero et al., 2022), Marine (Frizziero, Liverani, et al., 2021), until Medical (Frizziero et al., 2019); examples of which are seen in Figure 14.

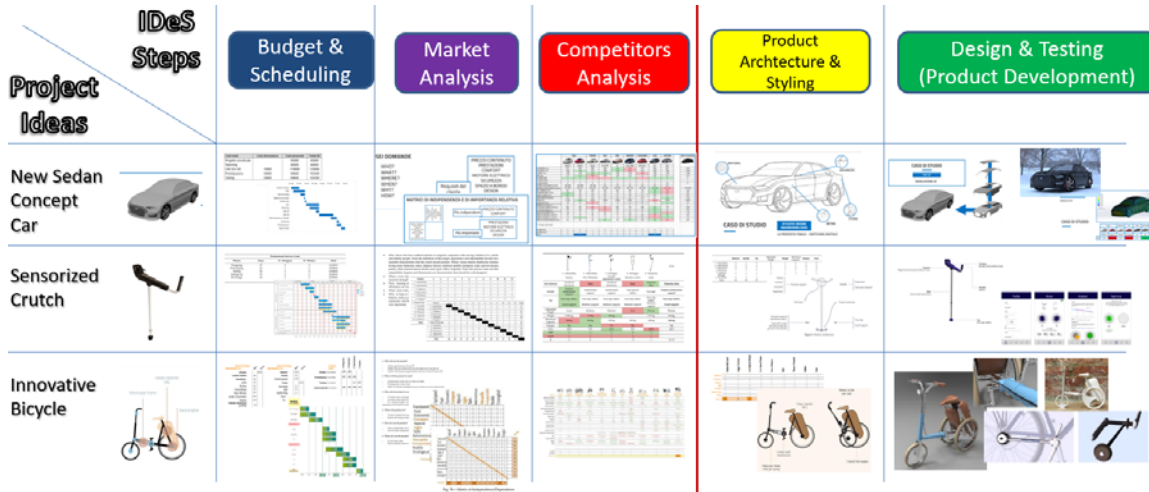


Figure 14. Project Development using IDES sequence.

Additionally, the scheme shown in Figure 9 summarizes all stages of IDES, the main technologies related to them, and the tools applied. The work divided among the three main categories (Project Set-up, Product Development and Production Start-up) is simultaneously deployed and continuously updated. The application of the Methods and Tools that IDES can use in order to bring New Product Project Development (NPPD) to be driven by DFSS engineering-based, business process management method, related to Six Sigma. The accurate combination of 15 Methods, with the 20 and increasing combination of high data processing engineering project execution, thanks to Industry 4.0. These tools would straightforwardly propose solutions across all the project development phases with the Manufacturing 4.0 technologies. Such tools will help to ease project production release by achieving outstanding quality targets. Problems that might arise throughout the product release, as well as design, validation, execution and quality are studied at the outset to speed up the timelines as much as possible, and partial overlap between the various stages is sought as far as possible to increase efficiency by decreasing time and enabling dialogue for sharing errors, problems, and solutions.

Afterwhile, IDES would englobe all individual-skilled engineers from all departments into a single area called Product Engineering (PE), in which its knowledge would be spread systematically through the development stages. This method englobes all different processes inside automotive product development and exploits the use of the internal part and technical project management tools embedded in the latest versions of CAD / CAE / CAM packages from major software suppliers like Siemens®, PTC®, and Autodesk®. These systems allow companies to fully manage and control parts and systems of new products. Allowing to seamlessly integrate part design with process, production and logistics.

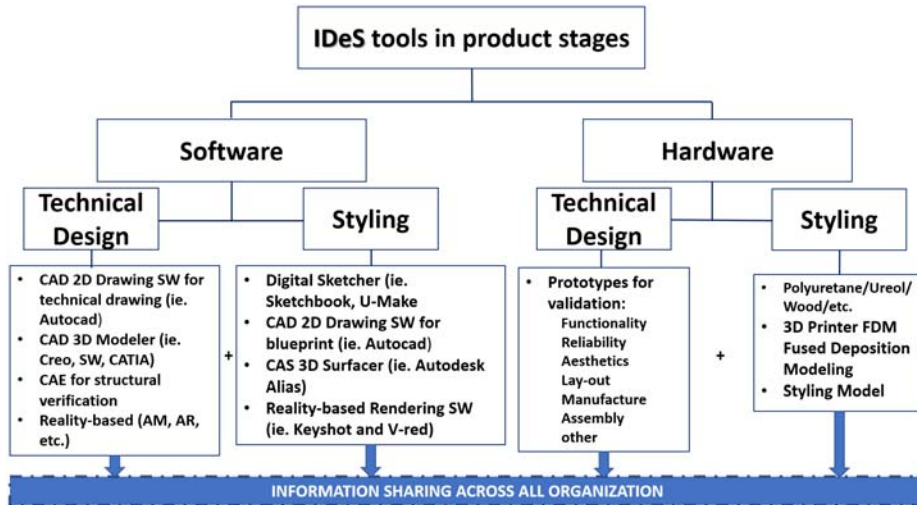


Figure 15. Tooling used in IDeS that including Styling an Engineering design areas

Moreover, the concept of IDeS has the potential to drive companies to rearrange their managerial organization to be compliant to the market reality at the present day. By unifying the platforms used to identify client requirements to share product information across the enterprise would increase the efficiency of management instruments to reach productivity and save important time and resources (Kjaer et al., 2019).



Figure 16. Outline of IDeS Method

Numerous applications of IDeS have already been presented in the literature. Remarkably, the industry application range varies from the context of automotive car design and mobility solutions to biomedical and health care. This shows that an application of the described methodology outlined in Figure 16 is not constrained to a particular context but is suitable to most industrial areas whose product has to be sold to the final customer. Different product prototypes and case studies were presented from different industry sectors like Automotive (Frizziero et al., 2022), Marine (Frizziero, Liverani, et al., 2021), until Medical (Frizziero et al., 2019).

4.1 Analysis Methods from IDeS used in this project:

4.1.1 QFD Methodology

Quality Function Deployment (QFD) is a structured approach used in product development and process improvement to translate customer needs and requirements into specific engineering or

operational characteristics. QFD helps ensure that customer expectations are met or exceeded throughout the product or process lifecycle. The QFD method allows to portray:

- A. **Identification of Customer Requirements (CRs):** The first step in QFD is to identify and prioritize customer requirements. These are the needs and expectations of the customer, both explicit and implicit. CRs can be gathered through surveys, interviews, feedback, and market research.
- B. **Identification of Technical Requirements (TRs):** Once CRs are established, the next step is to identify technical requirements, which are the specific features or characteristics of the product or process that are needed to meet the CRs. TRs are typically related to design, engineering, and production.
- C. **Creation of a House of Quality (HOQ):** The House of Quality is a matrix that serves as the central tool in QFD. It relates CRs to TRs, highlighting the interdependencies and correlations between them. The HOQ helps in prioritizing TRs based on their impact on meeting CRs.
- D. **Weighting and Prioritizing:** Weighting is assigning relative importance or priority to CRs. This is often done using a scale or ranking system. The more critical a CR is, the higher its weight. Prioritizing ensures that resources are allocated to the most critical TRs.
- E. **Development of Technical Solutions:** Cross-functional teams brainstorm and develop technical solutions to address the TRs. These solutions can involve design changes, process improvements, materials selection, or any other relevant actions.
- F. **Relationship Matrix:** This matrix helps assess the relationships between TRs and their impact on each other. It ensures that changes made to one TR don't negatively affect others.
- G. **Planning and Implementation:** Once technical solutions are identified, a plan is developed to implement these solutions. This may involve assigning responsibilities, setting timelines, and monitoring progress.
- H. **Verification and Validation:** The implemented changes are verified and validated to ensure they meet the desired quality and customer requirements.
- I. **Continuous Improvement:** QFD is not a one-time process but an ongoing one. It should be part of a company's continuous improvement efforts, with feedback loops and regular reassessment of customer needs and product/process performance.
- J. Additionally, QFD method excels in achieving the following objectives:
- K. **Cross-functional Teams:** QFD is most effective when it involves members from different departments, including marketing, design, engineering, production, and quality control. This ensures a holistic view of the project.
- L. **Customer-Centric Approach:** Keep the focus on the customer throughout the process. Understand their needs and expectations thoroughly.
- M. **Clear Documentation:** Maintain clear and well-organized documentation of CRs, TRs, the House of Quality, and all related information. This helps in communication and reference.
- N. **Use of Tools:** QFD often employs various tools such as affinity diagrams, brainstorming, and statistical analysis. Utilize these tools as needed to facilitate the process.
- O. **Regular Review:** Periodically review and update the QFD as new information becomes available or as project conditions change.
- P. **Training:** Ensure that team members are trained in QFD methodology and its tools to make the process more effective.
- Q. **Top Management Support:** QFD is most successful when it has the support and commitment of top management. They can allocate resources and ensure that QFD findings are integrated into decision-making processes.
- R. **Flexibility:** Be open to adapting the QFD process to suit the specific needs and complexities of your project or organization.

Therefore, the Quality Function Deployment is a powerful tool for aligning a company's efforts with customer needs and driving product or process improvements. When applied effectively, it can lead to increased customer satisfaction and competitive advantage.

4.1.2 TRIZ Methodology

TRIZ methodology, better known as the Theory of Inventive Problem Solving (TRIZ) is a problem-solving methodology that originated in the Soviet Union and was developed by Genrich Altshuller in the 1940s. It is based on the study of thousands of patents to identify common patterns and principles that lead to inventive solutions. TRIZ provides a systematic approach to solve complex problems and stimulate creative thinking.

Integrating TRIZ into systematic creativity methods, as suggested by Mann and Dewulf, aims to enhance the creative problem-solving process. By incorporating TRIZ principles and patterns, individuals and teams can systematically explore a broader range of potential solutions and identify innovative approaches to problem-solving.

Overall, TRIZ has been adopted in various industries and fields as a powerful tool to foster innovation and find inventive solutions to complex challenges. It encourages thinking "outside the box" and provides a structured framework for problem-solving that complements traditional creative thinking methods.

It is indeed true that many problem-solving tools, techniques, and philosophies have been integrated or compared with TRIZ to enhance their effectiveness and creative potential. Let's briefly explore some of the mentioned methods and their connections with TRIZ, as QFD, in which TRIZ principles can be employed during the QFD process to generate innovative solutions that satisfy customer needs more efficiently; Six Sigma (6σ): TRIZ can complement Six Sigma by offering inventive principles to address process issues and achieve breakthrough improvements; Robust Design, TRIZ tools can help identify potential weak points in a design and offer inventive solutions for robustness; as well as Axiomatic Design (AD), Theory of Constraints (TOC); Brainstorming; De Bono's Theories; Mind Mapping™; Neuro-Linguistic Programming (NLP), among others.

The integration of TRIZ with these various tools, techniques, and philosophies is an ongoing area of research and application, aiming to foster innovative problem-solving in different domains and industries. Researchers and practitioners continuously explore the synergies between TRIZ and other approaches to enhance their problem-solving capabilities and creativity.

The Aim of the study is to portray an exercise of product reverse engineering with main focus on exploiting the use of modern product design and production technologies, allowing agility in product research, and continuous improvement, hence capable of achieving upscale quality level. Technologies like CAD, CAM, CAE, AM, and 3D Scanning will be applied to demonstrate that a product could be promptly design with the scope of being ready to produce.

5. Additive Manufacturing Introspective

Moreover, FDM promises to solve cost problems of other non-conventional FDM methodologies like SLS (Selective Laser Sintering), Poliget (Stratasys, Object), SLA (Stereolithography), DLP (Digital Light Processing) MSLA (Masked Stereolithography). Defects plays a key role in 3D printing since they are responsible for the reduction in mechanical properties with respect to injection molded parts. As suggested in (Gordeev et al., 2018). The presence of pores/voids in the 3D printed structure leads to a

decrease in the final density of the specimen and depends on printing parameter. Also, in the FDM printing process it is necessary to optimize and reduce the presence of voids in the structure because even if the defects undergo a sintering process, they decrease in size, but still remain present in the structure.

The typology of the main FDM defect occurrence types have been identified, and the effects of the slicing parameter variation on each type of defects has been addressed. The proposed approach made possible to make a valuable comparison between the volume of defects that are present inside the specimen and the effect of the optimization procedure in the reduction of such voids, ending up to an internally symmetric element that would mechanically sustain stresses in a similar way to the material got from a regular-sourced process. Moreover, the volume of defects would also imply that mechanical characteristics of the material would also be compromised because of bad choice of parameters for a given 3D printer as internal material evenness is not guaranteed.

Previous research findings made by the author (Ferretti et al., 2021) highlighted the importance of adopting a understanding of the behavior of molten polymer materials in order to achieve the best results in terms of part surface quality and mechanical behavior by reducing material anisotropy (Figure 17).

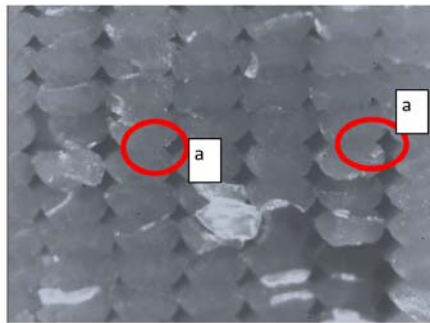


Figure 17. Defect appearance on a PLA specimen: (a) material voids between adjacent lines

Therefore, there were identified that can be summarized 2 types of defects (Ferretti et al., 2021). By defects it is said the presence of gaps in the structure that are not generated randomly but depends on how the material is deposited. This type of defect is then repeated and if the conditions during printing do not change (constant extrusion temperature, constant ambient temperature, no speed changes during printing etc), this type of defect is repeated on each layer. The proposed optimization lets to reduce the overall voids % (Eq1) with values of K_B and K_C ; where K_B and K_C consider the same type of defect, one in shell lines, the other in infill lines. Lowering the occurrence of K_B and K_C helps to diminish the total number of voids/defects existing on the specimen. The procedure is reported in Figure 18 and allows to find the best performing printing parameters given a specific 3D printer device and filament typology; the correct choice of printing parameters would guarantee optimal mechanical properties of the printed elements with zero internal voids.

$$V\% = K_A V_A + K_B V_B + K_C V_C + K_D V_D$$

$V\%$ is the total volume in percentage of the occurrence of defects, the parameters K_A, K_B, K_C, K_D allow to adjust the theoretical model to the real result.

These values can be obtained experimentally, by observing the layer in section, through a common microscope and then performing an image analysis.

$K_A V_A$: the first element of the equation is related to defects that are present on the surface of the workpiece, this term can also be related to several aspects including surface roughness which is directly related to layer height and staircase effect. It's difficult to obtain a reduction of this term by changing only the slicing parameter, but is possible to obtain a K_A value lower than 1 for some materials (eg. Polymaker PVB) related to a chemical smoothing.

K_B and K_C take into account the same type of defect, one in shell lines, the other in infill lines.

However, K_B and K_C are not identical and often have different values.

Shell lines are always stacked on top of each other with a 0° raster angle. This leads to high difficulty in reducing the defects between these lines.

Experimental evidence showed a maximum reduction of around 80% and the value of parameter K_B in the range K_B : 1-0.8

For K_C instead, related to the possibility to have a raster angle for the infill lines between different layers and related to a proper selection of printing parameters, it is possible to have a greater reduction of the gaps between lines. Value of K_C parameter is in the range between 0 and 0.9.

$K_D V_D$ is related to the presence of voids in the infill, is possible to reduce these defects by selecting the option "fill small gaps" in the slicer.

Moreover, the optimization process starts by using the recommended printing settings given by the filament producer. At a first stage the width must be set equal to the nozzle dimension. Afterwards the minimization of the layer height is performed according to the nozzle diameter and the minimum resolution value of the printer. The first optimization loop cycle, seen in Figures 18 and 19, is needed to remove the macro defects on the printed surface of the part. An additional process is focused on removing defects B and C from the part in Figure 20, in which it is possible to see the result of the proposed optimization loop on a 3D printed PLA specimen.

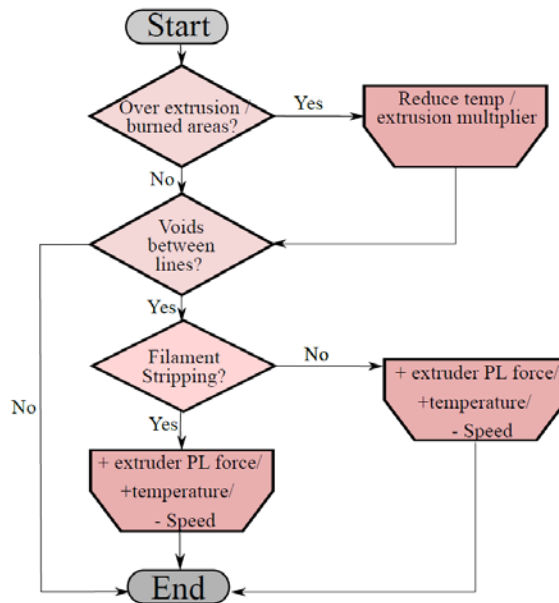


Figure 18. Optimization Process Loop Cycle

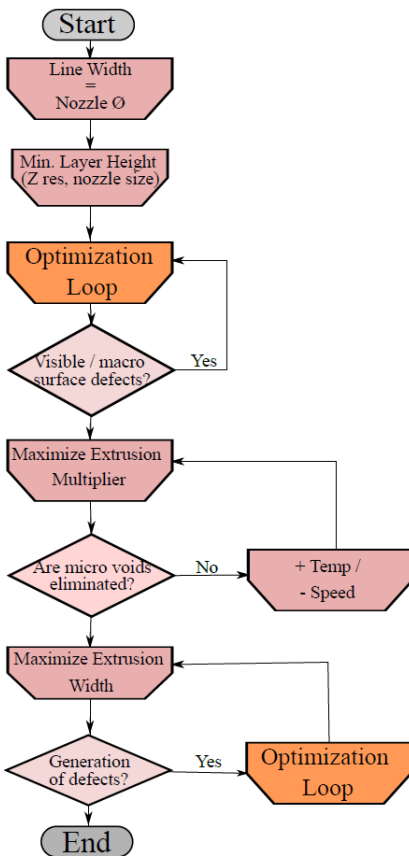


Figure 19. Flow Chart of the Optimization Process

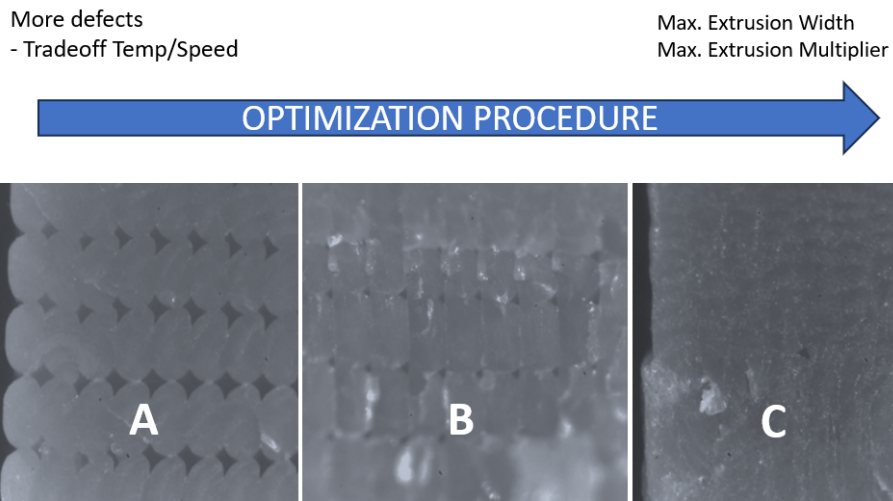


Figure 20. Printing quality on the microscope (20x): (a) No optimized (b) Increasing Performance and (c) Fully Optimized

5.1 4.0 Technologies applied in other Industry areas.

Industry 4.0 technologies have encountered valued applications across diverse areas, starting in mechanical – related issues going all the way into automotive, and aerospace submissions by gaining

flexibility in the CAE, FEM analysis that made this technology be widely spread towards other areas, including medical tenders, in which CAD, 3D modeling and construction technologies demonstrated to be a valid option to aid complex surgical planning (Frizziero, Santi, Leon-Cardenas, Donnici, Liverani, Napolitano, et al., 2021), with important achievements in orthopedics area (Frizziero, Pagliari, et al., 2021). AM technologies were found to be an important proposition to accurately and cost effectively manufacture customized surgery tooling (Figure 21) (Frizziero, Santi, Leon-Cardenas, Donnici, Liverani, Papaleo, et al., 2021), and aid to increasing reality in surgical planning and training (Leon, C., Sali, M., Frizziero, L.,Donnici, G., Liverani, 2021), (Ferretti, P., Leon, C., Sali, M., Frizziero, L.,Donnici, G., Liverani, 2021), (Leon-Cardenas et al., n.d.).



Figure 21. AM medical applications - orthopedics: surgery planning (left); customized surgery tooling (right)

5.2 Research on Improvements that make AM a viable industry alternative - applications of 3D printing to support automotive production techniques.

Subsequently, some researchers applied this technology as a support technique to create other components, especially in the case of very limited batches or prototypes; one of this application exploits the FDM 3D printed moulds to manufacture polyurethane foam parts for the automotive industry (Romero et al., 2021). Further research established that computer-aided engineering could aid to portray efficient, cost effective mould manufacturing (Francia et al., 2018), polymer moulds could be constructed by FDM printing, using polymers like ABS creating a 3D-model accordingly to eliminate material shrinkage (Krupennikov et al., 2022). Moreover, the challenges of achieving a technical feasible product often need to take back knowledge from previous trials (Piancastelli et al., 2014), the research of Chen et al. (Chen et al., 2021) proved that applying the method of polish the surface of 3D-printed moulds by solvent vapor is highly effective in reducing the surface roughness of the moulds.

We need to obtain cost-effective, high-quality moulds to reduce the costs of prototypes or small batch production. The possibility of making moulds with FDM technology is a smart solution (P. H. Wang et al., 2019), (Sudbury et al., 2017). The main challenge is related to the high surface roughness that would be transferred directly to the final component. A filler could be used on the mold, followed by manual sandblasting to improve the surface finish. This technique can be applied to components with

a relatively simple geometry with low tolerance values, but either way it would still require an important manual intervention.

This study was held to optimize and use the FDM technology as a support technique for laminated composites, opening the possibility of outstanding quality in the rapid manufacturing of parts designed for AM, ensuring a low cost especially in the realization of prototypes. Moreover, the repeatability and the possibility to use a combination of thermoplastic materials are analyzed with a 3D laser scanning method, which is used to verify the validity of the proposed manufacturing procedure. . The printing strategy adopted for this component could also be generalized to other parts with similar characteristics, with optimum printing parameters used to create the component. The first key point is the orientation of the part with respect to the build platform, as shown in Figure 22. The overall process is summarized in Figure 23. The software used for slicing was Cura v4.9.1.

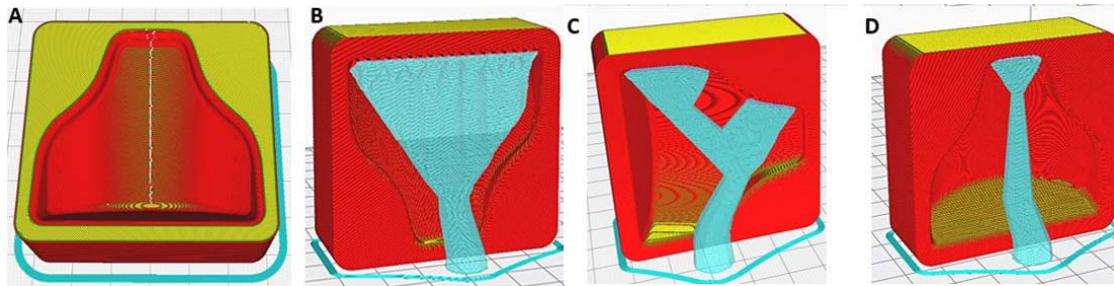


Figure 22. Part orientation on the buildplate, part helpers in blue.

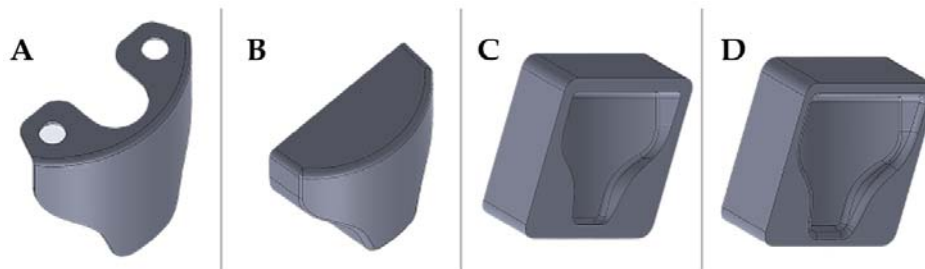


Figure 23. Steps followed during the design of the mold cad model.

A Faro 3D scanner was used to check the fidelity of the printed model compared to the designed CAD file. In order to evaluate the reproducibility of this process, two molds with the same gcode were printed. Therefore, a comparison with the theoretical, CAD file, in which the matching was good altogether, as an absolute range of 0.05 mm was obtained in most of the mold. Afterwards, thanks to the Geomagic visualization tool, a comparison was performed, and it was possible to see a greater homogenization of the surfaces, which can be seen from the zebra stripes. This was due to the smoothing process that turned the surfaces smoother and glossier. Additionally, it was possible to appreciate the effect of smoothing on the dimensional variation of the component in Figures 24 and 25. The molds before and after treatment were compared.

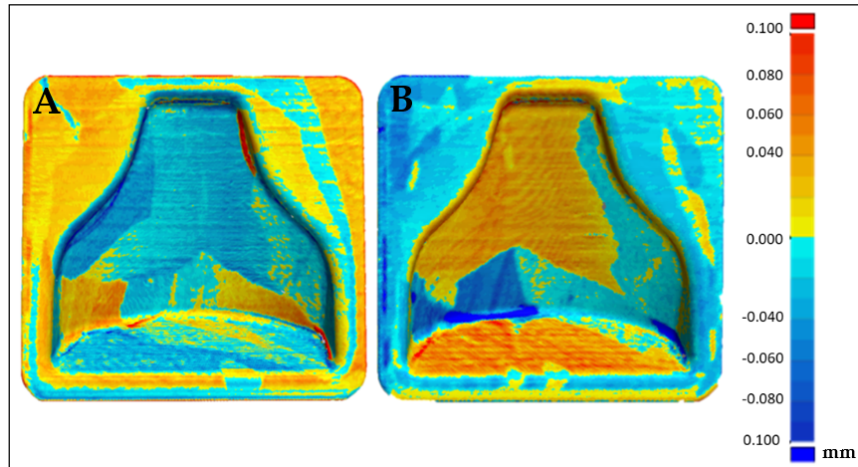


Figure 24. Comparison between the scan of mold 1 pre and post smoothing (A) and comparison of mold 2 pre and post smoothing (B).

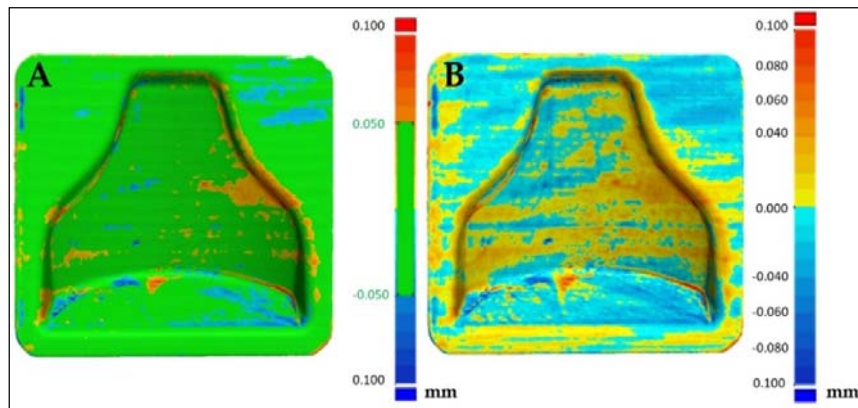


Figure 25. Comparison between the two molds after smoothing.

6 Project Objectives and Engineering targets

6.1 Objectives

- Application of the IDES methodology to portray a technical solution that complies with specific improvement targets.
- Use of the I4.0 methodologies to reengineer the source elements and optimize them to achieve the best performance focusing on manufacturing and quality control using 3D Scanning.
- Product reengineering should be done by taking into account design techniques (Design for AM), such as topological optimization, carbon fiber laminate, etc.

6.2 Methodology Achievement Phases

The IDES approach with technical focus will exemplify the use of the same tools and techniques given in early released studies of this methodology in order to assess the feasibility of conveying a technical solution, given a set of constraints and targets to achieve.

The three main targets to achieve are:

- Less energy consumption of the vehicle
- Contribute to reduce emissions target for Europe 2035
- Exploits manufacturing technologies given by the Industry 4.0

The first part of the study will examine the layout of the front suspension of a current-production vehicle with the objective of evolve the current-production parts with reengineered ones that allows the overall system to save weight, hence contribute to vehicle emissions reduction, and overall energy consumption of the vehicle.

The second part of this study would portray the complete methodology to seamlessly produce industrially acceptable elements sourced with composites and AM, whilst these elements were originally engineered to be built with traditional materials and methods for processing them. The following steps were outlined in order to pursue the main objective.

- 1) Starting up input source element data: geometry, materials, and mechanical requirements.
- 2) Definition of supply materials, processes for best efficiency
 - a) Optimize the part geometry for best results with new technologies to implement (AM, Carbon fiber)
 - b) Proper Materials Specification definition> with technical data sheets and performance tests
 - c) Printing equipment details for best quality
- 3) Optimization of the operating parameters for all processes of step 1, simulations of the optimized part to freeze the model
- 4) Development of the physical part
- 5) Part quality control assessment

7 . Methods for fast product prototyping and optimal solution assessment

IDES method drives the application of DMADV process to achieve best results, the following describes the tools applied inside each method process, which will drive the project to achieve each objective on Figure 26.

Define: Product Budget and Scheduling.

Measure: Benchmarking, Matrix Analysis

Analyze: QFD, Triz, Benchmarking

Design: QFD, CAD, CAE, CAM, AM, 3D Scanning

DFSS - DMADV



Figure 26. Targets inside each phase of DMADV.

8 Case study: Reverse Engineering Applied to Product Design with a Technical Approach

Case: front suspension control arm

The case study on which we will focus is the front suspension of the market-leading electric vehicle, the Tesla Model S. Using the IDES methodology, the components of the suspension will be analyzed and then, the components deemed suitable will be optimized and produced as summarized in (Figure 27).



Figure 27. Process line sequence for the project

This methodology will be employed to identify and analyze areas for potential improvement, design and implement improvement solutions, and finally study the effectiveness of such interventions.

The application of the methodology was given by the re-engineerization of an automotive part in order to assess its viability to be produced with composite materials by means of Additive Manufacturing and carbon fiber lamination, as well as using state of the art quality control processes. The aim is to use an existing automotive component already in production with traditional materials, in order to redesign, test, manufacture and assess the viability of use of new manufacturing technologies for manufacturing such parts.

8.1 Starting up input element data: geometry, materials, and mechanical requirements.

The starting point procedure began with obtaining the original geometry from the part to redesign. To do this, a cloud of points was obtained after scanning, via 3D laser scanner that was used to obtain a .stl file from which the main geometrical properties, dimensions and shape characteristics of the front powertrain unit of a Tesla model S vehicle were obtained.

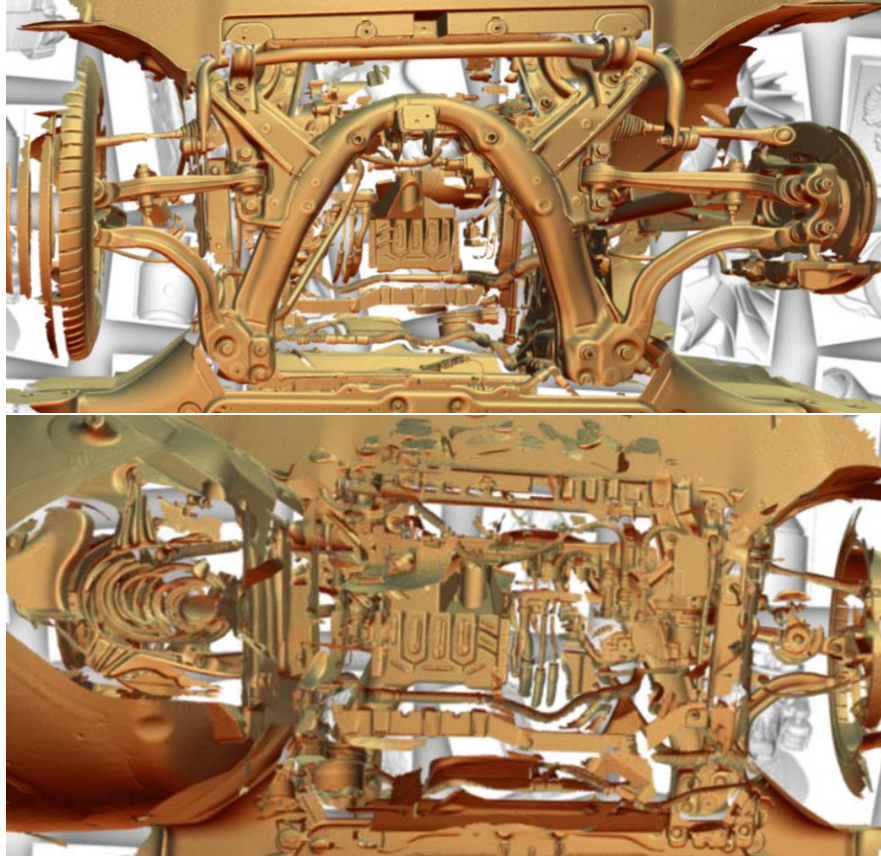


Figure 28. 3D Scan result from a Tesla model S front suspension

From this cloud of points, the area that belong to the part that was selected for this study was extracted to parametrically design it in a parametric cad software. This process resulted in obtaining a digital copy of the lower control arm from the suspension of this vehicle. (Figure 28), this model has accurate dimensions and geometry and surface dimensions that make the part reproducible. The result obtained after using the cloud point generated by the 3D scanner as a template for accurately creating the parametric elements of the suspension can be seen in models obtained from 3D Molier® (3D Molier, 2021), on Figure 29, the same model which was used as a base parametric setup for this study.

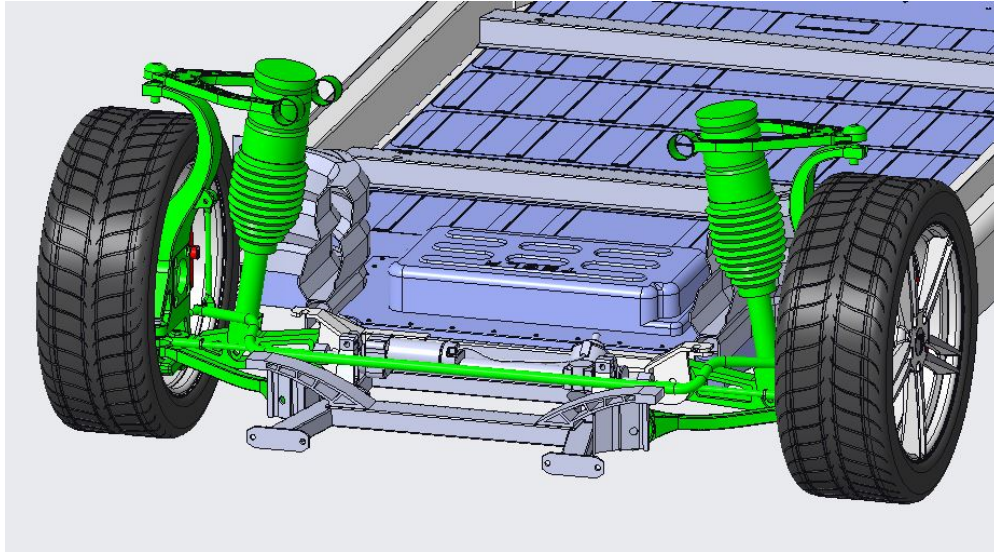


Figure 29. Tesla Model S Front Suspension 3D parametric model

To find out the areas to focus on this project, the IDES method was taken as a starting point, as the tools inside it can help to unleash the main product characteristics and areas to put the effort on. The summary of methods and tools needed to develop this study are the following as seen on Figure 10. The QFD method defined, through the what/how matrix, the technical requirements necessary for the realization of the product according to the best characteristics of an innovative product. It was necessary to study dependency relationships existing between the customer requirements. The QFD method was used to achieve this goal. This method makes use of matrices of interrelation, which provide the tools to create a unique ranking between the requirements.

IDeS



Figure 10. IDES Approach for the study

A) QFD – To find out technical characteristics.

To evaluate the best characteristics of an innovative product, it is necessary to study dependency relationships existing between the customer requirements. The QFD method was used to achieve this goal. This method makes use of matrices of interrelation, which provide the tools to create a unique ranking between the requirements. The first step is the individuation of these requirements using six basic questions: who, what, where, when, why, and how. Having obtained all the requirements, it is then possible to move on to the interrelation matrices.

The analyses were carried out using the QFD method. Moreover, the methods of QFD analysis used while carrying out this project were: the six questions, the relative importance matrix, the independence matrix, and the what-how matrix, in addition to the benchmark and the top-flop analysis. They are analyzed individually.

A1) Six Questions and Overall Requirements

The six questions of the QFD were applied to the case study in the first design phase of the innovative product. The answers, which allow the requirements from analyses with the interrelation matrix to be found, are crucial in the next analyses. From the preceding analysis and the research carried out, key words are extrapolated for the product to be designed, which serve as a guideline in the subsequent matrix analysis and design phases.

Answers to the six-question analysis made it possible to find some key words that were used to narrow the field in the next analyses on Table 1:

Table 1. Six Questions and Overall Requirements

SIX QUESTIONS		
WHO	What specific sections of the upper and lower wishbones are most subject to stress or wear during normal operation and how do these parts interact and affect the other components of the double wishbone suspension under various loads?	<i>Joints and small sections (NETWORK STRUCTURES) INNOVATION, CUSTOMIZATION</i>
WHAT	What exactly do the upper and lower wishbones represent in a double wishbone suspension and what are the technical specifications, performance and strength expectations needed for these components in the context of the overall functioning of the vehicle?	<i>Upper arm - COMPRESSION (buckling-> flexion); lower arm - FLEXION MECHANICAL STRENGTH, FATIGUE LIFE</i>
WHERE	Where are the maximum loads concentrated on the upper and lower suspension arms during normal driving situations such as braking, cornering, acceleration?	<i>The applied loads as remote points in the joint centroids > Considered for modelling</i>
WHEN	When during the various phases of vehicle operation (acceleration, braking, braking downhill, cornering) do the upper and lower arms of the	<i>When cornering (conditions explained in 8.2) MECHANICAL STRENGTH, DESIGN</i>

	double wishbone suspension undergo the maximum stress and the heaviest loads?	
WHY	Why is it important to optimize the upper and lower wishbones of the suspension considering aspects such as ride comfort and durability?	<i>Component Weight Reduction (consequent reduction of inertia)</i> <i>MECHANICAL STRENGTH, LIGHTWEIGHT, VERSATILITY</i>
HOW	How are we going to optimize the design of the upper and lower wishbones, in terms of materials, construction techniques or design, to improve their performance, strength and durability in the context of overall vehicle operation?	<i>Implementation of AM-Optimized design to reduce part density - lattice structures inside the components</i> <i>LIGHTWEIGHT, COST, SPEED, EASE, GREEN, AESTHETICS</i>

A2) Independence Matrix

The independence matrix is built by placing all the Overall Requirements items, obtained from the six questions, both in column and in line. The goal is to determine the cause-and-effect relationships for each parameter by asking the question: how does the element on the row depend on the elements on the columns?

Numeric values, distinguishing between null link (empty box), weak (1), medium (3), or strong (9), are entered in the matrix to quantify the dependence relationship between each column and row element. The independence matrix (Table 2) puts requirements found in the previous analysis into a scale of importance. The most important elements for the designer in the preliminary stages of design are summarized in the characteristics stated in the rows and columns of the chart. Then an interpolation of these features is performed based on the factual needs regarding the internal system and the final user, the values in the chart are identified through a scoring system agreed upon upstream of the analysis.

Therefore, the proper characteristics of rows and columns were identified after answering the six questions, which identified the most important characteristics to be used for this project.

Table 2. Independence Matrix

Independence Matrix	LIGHTENING	COST	SPEED OF REALIZATION	EASE OF REALIZATION	INNOVATION	MECHANICAL STRENGTH	FATIGUE LIFE	AESTHETICS	DESIGN	GREEN	VERSATILITY	CUSTOMIZATION	TOTAL
LIGHTENING	0	1	1	1	0	9	9	0	0	0	0	0	21
COST	3	0	9	3	3	1	1	3	3	1	1	9	37

SPEED OF REALIZATION	1	1	0	9	0	0	0	1	9	0	0	0	21
EASE OF REALIZATION	0	0	3	0	0	0	0	1	9	0	0	3	16
INNOVATION	0	1	3	3	0	0	0	0	3	3	3	1	17
MECHANICAL STRENGTH	9	1	0	0	1	0	9	3	3	0	0	0	26
FATIGUE LIFE	9	1	0	0	0	9	0	9	9	0	0	0	37
AESTHETICS	0	1	3	0	1	3	3	0	9	0	0	9	29
DESIGN	9	3	3	3	9	9	9	3	0	1	9	3	61
GREEN	3	9	1	0	1	0	0	0	3	0	1	0	18
VERSATILITY	1	1	1	3	1	0	0	0	9	0	0	0	16
CUSTOMIZATION	0	0	0	0	3	0	0	9	1	0	0	0	13
TOTAL	35	19	24	22	19	31	31	29	58	5	14	25	

A3) Importance Matrix

While the construction is similar to the previous matrix, a different question is analyzed: is the element in the row more important than the element in the column?

As in the matrix described above, the numerical values are distinguished in:

- **1**: the row element and the column element have the same importance,
- **0**: the row element is less important than the column element,
- **2**: the row element is more important than the column element.

The importance matrix (Table 3) narrows the field even more to reach more precise innovative characteristics.

Table 3. Importance Matrix

Importance Matrix	LIGHTENING	COST	SPEED OF REALIZATION	EASE OF REALIZATION	INNOVATION	MECHANICAL STRENGTH	FATIGUE LIFE	AESTHETICS	DESIGN	GREEN	VERSATILITY	CUSTOMIZATION	TOTAL
	LIGHTENING	1	2	2	2	2	0	0	2	2	2	2	2

COST	0	1	1	1	0	0	0	2	1	0	2	2	10
SPEED OF REALIZATION	0	1	1	0	2	0	0	2	1	1	1	2	11
EASE OF REALIZATION	0	1	2	1	2	0	0	2	1	2	2	2	15
INNOVATION	0	0	1	0	1	0	0	1	1	1	2	2	9
MECHANICAL STRENGTH	2	2	2	2	2	1	1	2	2	2	2	2	22
FATIGUE LIFE	2	2	2	2	2	1	1	2	2	2	2	2	22
AESTHETICS	0	0	1	0	1	0	0	1	0	1	2	2	8
DESIGN	0	1	1	0	1	0	0	1	1	2	2	2	11
GREEN	0	0	0	0	0	0	0	0	0	1	2	2	5
VERSATILITY	0	0	0	0	0	0	0	1	0	1	1	1	4
CUSTOMIZATION	0	1	0	0	0	0	0	0	0	1	1	1	4

A4) What–How Matrix

Through what/how matrix, the customer’s requirements are compared with the technical requirements necessary for the realization of the product.

In this case numerical evaluations are used to identify the type of relationship:

- Nothing (empty box, equivalent to 0),
- Weak (1),
- Medium (3),
- Strong (9).

The what–how matrix (Table 4) is a very useful tool to understand the most influential spec that meets the requirements.

Table 4. What-How Matrix

WHAT-HOW MATRIX	Lightweight Material	AM Polymer-based	AM metallic	Composite Materials	Lattice Structures	Post-Process Treatment	Good Manufacture Practices	TOTAL

LIGHTENING	9	9	0	9	9	0	0	36
COST	3	1	9	9	3	9	1	35
SPEED OF PRODUCTION	0	1	1	3	9	9	1	24
EASE OF PRODUCTION	0	9	9	3	3	1	3	28
MECHANICAL STRENGTH	3	9	9	9	3	9	3	45
FATIGUE LIFE	3	3	3	9	3	9	3	33
TOTAL	18	32	31	42	30	37	11	

Finally, the functions obtained from the QFD analysis:

Lightweight Material AM Polymer-based AM metallic Composite Materials
Lattice Structures Post-Process Treatment Good Manufacture Practices

B) Benchmarking – to find out market solutions to the issue.

To design an innovative product, it is fundamental to analyze the models already existing on the market. Benchmarking is the process to study and systematically compare the various products and avoid subsequent change requests due to re-processing or mistaken decisions made during the design process (Piancastelli et al., 2014).

Moreover, to have a clear idea of the competitors' proposals, a benchmark analysis was carried out, comprising all the important characteristics of both products to design (Table 5). This arrived at the benchmark overall score with the top flop analysis.

Table 5. Benchmarking Analysis for a) Lower Arm; b) Upper Arm

a) Lower Arm						
Model	Bmw 5 Series	Mercedes Benz S Class	Alfa Romeo Stelvio	Range Rover Sport 2017	Mitsubishi Lancer Evolution 7	
						
Top/flop analysis						Innovations
Material	Aluminum alloy	Aluminum alloy	Aluminum alloy	Aluminum alloy	Aa 7075	-
Technology	Foundry	Forging	Foundry	Foundry	Forging	-
Weight kg]	4	3	2	3	1.5	1.5
Symmetries	1	2	1	1	1	2
Single component	Yes	Yes	Yes	Yes	No	Yes
Lattice structures	No	No	No	No	Yes	Yes
Quarries	Yes	Yes	Yes	Yes	Yes	Yes
Top	2	3	2	2	3	
Flop	2	1	2	1	1	
Delta	0	2	0	1	2	
b) Upper Arm						

Model	Toyota Supra Mk4 1995	Nissan R35 Gtr	Mclaren F1 Gtr	Toyota Tf104b	Dodge Viper 2002	
						
Top/flop analysis						Innovations
Material	Aluminum alloy	Aa 6061-t6	Titanium alloy	Epoxy carbon fiber	Aluminum alloy	-
Technology	Forging	Cnc machines	Cnc machines	Autoclave lamination	Forging	Lamination
Weight kg]	3	2.8	1.8	0.2	2	0.2
Symmetries	2	1	2	0	1	2
Single component	Yes	No	Yes	Yes	No	Yes
Lattice structures	No	Yes	No	No	No	Yes
Quarries	No	Yes	Yes	No	Yes	Yes
Top	2	2	3	2	1	
Flop	3	1	1	3	2	
Delta	-1	1	2	-1	-1	

C) TRIZ method application

TRIZ methodology will be applied to the case study, in order to find out, in a first glampse, the Inventive Principles to conduct the project with, for this purpose, the Altshuller Matrix, also known as the Contradiction Matrix or the 40 Principles Matrix, is a central tool in the TRIZ method. It was developed by Genrich Altshuller (Bolaños-Ruiz, 2023), the founder of TRIZ, as a means to systematically identify inventive principles to resolve contradictions in problem-solving.

The matrix consists of a table with rows and columns, where each row represents a specific engineering parameter to be improved, and each column represents a specific parameter that might be in conflict with the improvement. The matrix aims to address technical contradictions, which occur when improving one aspect of a system leads to a worsening of another aspect. This matrix works by analyzing the problem and Identifying the Contradiction; then Locating the Cells in their corresponding Altshuller Matrix where the row and column intersect; then identifying the 40 Inventive Principles, as each cell corresponds to an inventive principle. These principles are general techniques or strategies that have been successfully applied to resolve technical contradictions in various engineering problems.

Afterwards, a selection of the Inventive Principle is performed, based on the cell in which the two conflicting parameters intersect, the corresponding inventive principle is selected from the matrix. This principle provides guidance on how to overcome contradiction and find a creative solution. Later we can Generating Ideas, as it serves as a guide for generating potential solutions to the problem. It helps trigger creative thinking and provides a systematic approach to exploring innovative ideas.

C1) Matrix Inputs: exercise contradictions:

- A) **Objectives of the design:** Lower part inertia, but High resistance; this contradiction stands because usually the highest Resistance materials have a higher density, so its inertia then would be higher.

In this same case, we will have a higher load condition but at the same time we want a light design with less possible material quantity. When we analyze this basic objective into the Altshuler Matrix, the inventive principles to use, given the basic nature of this study, are:

- To portray preventive actions, preliminary assessment and feasibility.
- Use of composite materials
- Local quality, local characteristics.
- Optimization, Dynamizing
- Replacement of mechanical systems
- Sphericity, Curvilinearity, Sphericity

Finally, the best Inventive ideas suggested by the matrix are summarized in Table 6.

Table 6. Inventive Ideas from Contradictions assessment via Altshuler Matrix

CONTRADICTIONS			Inventive Ideas Suggested
Improvement	Worsening	Ideas from Matrix	
2-weight of a stationary object	8-volume of a stationary object	5, 35, 14, 2	
2-weight of a stationary object	34-reparability	2, 27, 28, 11	27 - use of short-lived objects (CHEAP)
2-weight of a stationary object	32-ease of implementation	28, 1, 9	
2-weight of a stationary object	36-device complexity	19, 15, 29	
13-stability/integrity of the object	8-volume of a stationary object	34, 28, 35, 40	40-composite; 35 parameter change (density)
13-stability/integrity of the object	34-reparability	2, 35, 10, 16	35-change parameters (density); 16-partial actions
13-stability/integrity of the object	32-ease of implementation	35, 19	
13-stability/integrity of the object	36-device complexity	2, 35, 22, 26	
14-resistance	32-ease of implementation	11, 3, 10, 32	
14-resistance	26-amount of substance	29, 10, 27	27-cheap items (polymer)
14-resistance	36-device complexity	2, 13, 25, 28	
27-reliability	34-reparability	1, 11	
27-reliability	26-amount of substance	21, 28, 40, 3	40-composite materials
11-effort/pressure	10-strength	36, 35, 21	35-change parameters (density);
10-strength	23-loss of substance	40; 31	31-porous materials; 40-composite materials
35-adaptability	32-ease of implementation	1, 13, 31	31-porous materials

B) Technologies selection to implement from TRIZ method:

The tools for product design will be chosen by following the findings of the TRIZ analysis, going in line with the main project objectives. The chosen tools would be originated by manufacturing 4.0 principles outlined in Figure 2. The overall selection can be obtained in the final version of the What – How Matrix from Table 4.

For ease the application and analysis of composite materials, as well as arriving to preventive actions, preliminary assessment and achieve a first-hand design feasibility, that allow us to optimize the design straightforwardly, the use of state-of-the-art CAD, CAE, FEM applications is mandatory. The achievement of curvilinearity is also achieved by arriving to a proper Design for additive manufacturing (DfAM) in section 8; Guidelines for the application of DfAM are in Figure 30.

1) General machine/material info gathering**2) Feature element optimization (Design strategy)**

- Element redesign for weight reduction and high performance (Nesting, Lattice, Topological Optimization)

3) DfAM guidelines (Manufacturing strategy)

- Accurate G-coding – Layering, slicing
- Print orientation
- CAD to STL conversion
- Parameters for lower material anisotropy

4) Steps to Achieve Engineering design freeze

- *Various design strategies comparison*
- *FEM simulations*
- *Right Dimensional tolerancing*
- *Process guidelines*

Figure 30. Design for Additive Manufacturing Guidelines

Moreover, IDEs method enables organizations to practically implement proper industry 4.0 technological tooling systematically across all product development areas. This process allows to take a lower time and resources to perform changes. This updated approach based on the systematic use of technology for product development management enables organizations to widen their product efficiency and minimize the risks.

8.2 Vehicle Dynamics forces analysis

A dedicated Vehicle dynamics force analysis is needed as a fundamental aspect of understanding how vehicles behave and respond to various driving conditions. It involves studying the forces that act on a vehicle and their effects on its motion and stability. Understanding these forces and their interactions is essential for vehicle design, performance optimization, and safety. Engineers use various tools, such as mathematical models, simulations, and physical testing, to analyze and fine-tune vehicle dynamics for specific applications, such as sports cars, trucks, or off-road vehicles. Several key forces come into play during vehicle dynamics analysis, as shown in Figure X, Data was taken from the vehicle manufacturer's official datasheet (Specs, 2020) Movements of interest to this study include acceleration, braking and change of direction while negotiating a curve. The dynamics of these movements are dictated by a series of forces acting on the vehicle, originating mainly from the tires, the force of gravity and aerodynamic effects. In the context of the present work, the vehicle and its components will be examined to discern the forces generated by each of these elements in a specific vehicle maneuver and configuration, and to understand how the vehicle responds to these forces. From this point of view, the establishment of a rigorous method for modeling the vehicle and of the conventions used to describe the movements is a fundamental step; The basic model of the vehicle and its parameters are given in Figure 31 and Table 7.

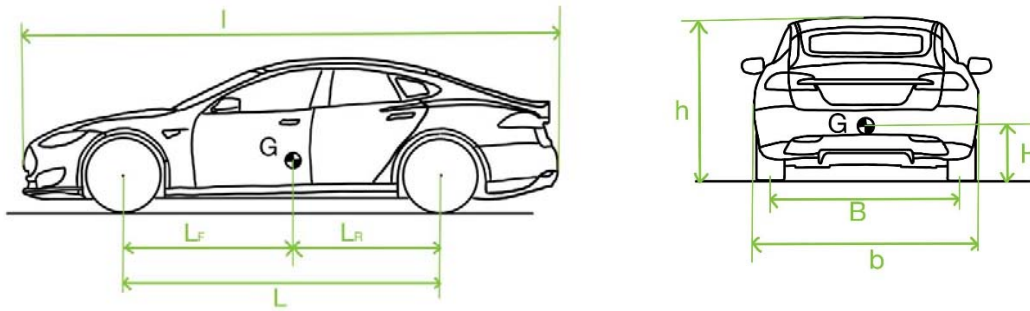


Figure 31. Source Vehicle Main dimensions

Table 7: Parameter Values for Calculations

Parameter	Symbol	Value
Vehicle length	L	4972mm
Vehicle width	b	1964mm
Vehicle height	h	1448mm
Vehicle wheelbase	L	2960mm
Axle width	b	1640mm
Height of the center of gravity from the ground	h	450mm
Distance between center of gravity and front axle	LF extension	1391.2mm
Distance between center of gravity and rear axle	LR	1568.8mm
Weight distribution between front and rear	LF/LR	47%
Unladen mass of the vehicle	m	2108kg
Passenger mass	mp	375kg

For simplicity, it has been assumed that the center of gravity is positioned in the center line of the vehicle with respect to a front view of the vehicle.

The total mass of the vehicle takes into account both the unladen mass of the vehicle and the mass that the probable passengers could have. For this study it was assumed to have 5 passengers each with a mass of 75 kg.

Therefore, considering the data reported in Table 7, the weight force of the vehicle (indicated with P) with which the constraint reactions on the wheel are calculated in the various cases takes into account both the empty mass of the vehicle and the mass of 5 passengers (maximum capacity of the considered vehicle):

$$P = (m + m_p)g = (2108 + 5 \cdot 75) \cdot 9.81 = 24358 \text{ N}$$

In this study two cases will be analyzed: the static case and the dynamic cases. The static case examines the constraint reactions that are unloaded on the wheel deriving from the vehicle's own weight, providing an essential view of the forces that constantly act on the system. Dynamic cases, on the other hand, involve specific driving conditions that are representative of common real-life situations. In particular, braking, acceleration and cornering situations will be taken into consideration. These analyzes will allow us to gain an in-depth understanding of the behavior of the suspension under various stresses.

8.1.1 Static Case

In this case the vehicle is considered stationary on a level road. For simplicity, both the car chassis and the tires are considered as a rigid body, therefore, the wheel touches the road along a segment which, seen from the side, can be traced back to a point. The constraint reactions, due exclusively to the weight force of the vehicle, are calculated at this contact point, as shown in figure X.

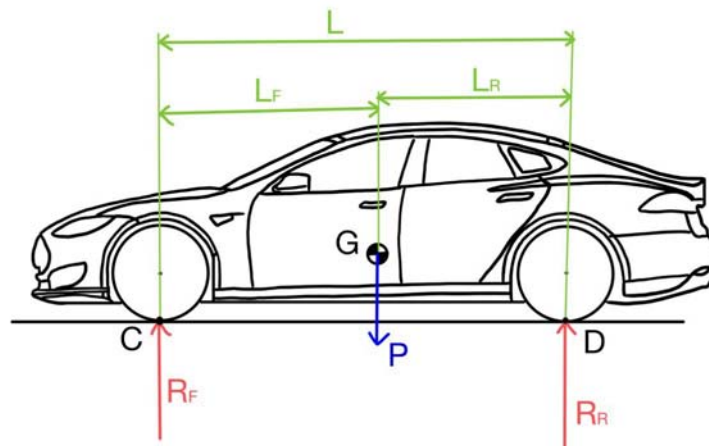


Figure 32. Forces Acting on the Vehicle in a Static Case

Points C and D represent the point of contact between the tire and the road. To find the constraining reactions e, rotational equilibria centered in the two contact points can be performed, in particular, to calculate the anterior reaction, a rotational equilibrium centered in point D is performed and similarly the rear reaction is calculated with a centered equilibrium in c. $R_F R_R$

Finally, since we are interested in the front left suspension, assuming that the vehicle has a geometric and dynamic symmetry between the right and left side, we find the front left reaction simply by dividing the force of the front reaction by two. R_F^{Sx}

$$R_F = P \frac{L_R}{L} = 12910 \text{ N}$$

$$R_R = P \frac{L_F}{L} = 11448 \text{ N}$$

$$R_F^{sx} = \frac{1}{2} R_F = 6455 \text{ N}$$

8.1.2 Dynamic Cases

For the study of these cases we consider the vehicle in movement in different situations for each of which through the dynamics of the vehicle the constraint reactions between the tire and the road will be calculated. These calculations differ from the static case in that in addition to the force lost, the forces of inertia and the respective friction forces will be present. To simplify the treatment for each of the situations analyzed below, some simplifying hypotheses will be made.

8.1.3 Braking on The Flat

For this situation, the hypotheses that have been considered are the following:

- The road is smooth, so the vehicle is not affected by vibrations due to the roughness of the ground.
- The car frame is considered rigid along with the wheels.
- The vehicle has a symmetry between the right and left side, therefore, the forces are equal between the two sides.
- The acceleration due to vehicle braking is considered constant.

The acceleration due to sudden braking (indicated with) in this case was considered equal to 1.5 times the gravitational acceleration (as also reported in the owner's manual), which generates an inertia force equal to: $a_F F_{IN}$

$$F_{IN} = (m + m_p) a_F = 36537 \text{ N}$$

The situation in question is schematized by Figure 33:

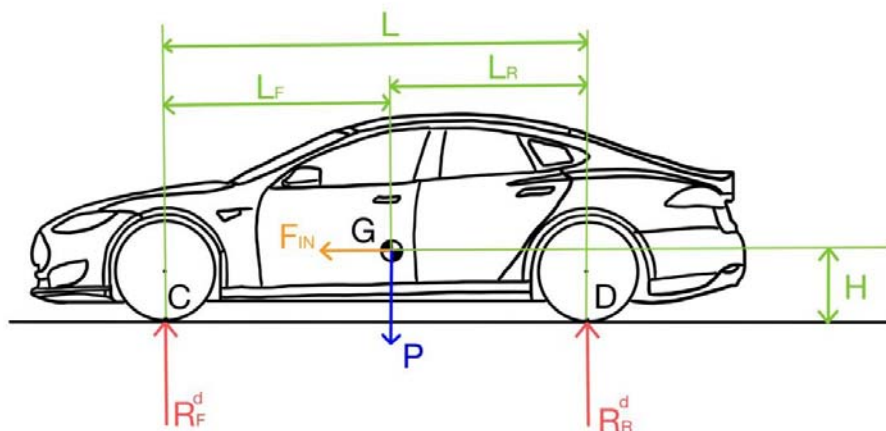


Figure 33. dynamic diagram of the car when braking

To find the constraint reactions e, rotational equilibria centered in the two contact points can be performed in the same way as for the static case, but with the addition of the inertia force. $R_F^d R_R^d$ Finally, to find the reaction that is discharged on the left front wheel, exploiting the hypothesis of symmetry between the right and left side of the car, I again divide the found front reaction by two.

The rotational equilibrium centered at point C is:

$$-R_F^d L + PL_R + F_{IN}H = 0$$

From which, replacing the values reported in Table 7 it is possible to obtain the binding reaction that is discharged on the front:

$$R_F^d = \frac{PL_R + F_{IN}H}{L} = 18465 \text{ N}$$

Similarly, the rotational equilibrium centered at point D is:

$$R_R^d L - PL_F + F_{IN}H = 0$$

By substituting the values shown in table X, the binding reaction that is discharged on the rear is obtained:

$$R_R^d = \frac{PL_F - F_{IN}H}{L} = 8641 \text{ N}$$

Dividing by two gives the left front reaction:

$$R_F^{sx} = \frac{1}{2} R_F^d = 9232 \text{ N}$$

8.1.4 Accelerated on The Flat

For this situation the hypotheses are the same as for the case of flat braking, but with the difference that this time the car in question is able to reach a maximum acceleration of 11.34 m/s², which in this case would generate a force of inertia on the vehicle equal to: $a_A 1,25g$

$$F_{IN} = (m + m_p)a_A = 30448 \text{ N}$$

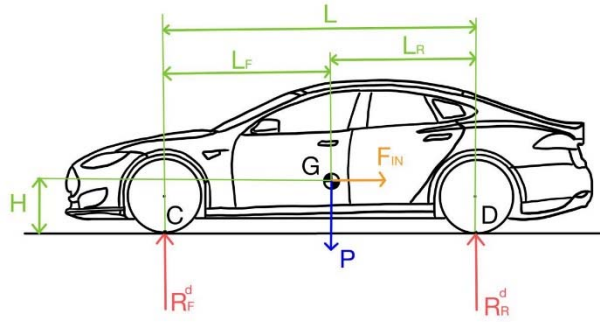


Figure 34. Schematization of the Car Acceleration Case

The constraint reactions are found again by performing rotational equilibria around the contact points between the tire and the road. Finally, the reaction that is discharged on the front left wheel is calculated by again exploiting the hypothesis of symmetry between the right and left side of the car. The previous reaction is obtained from the rotational equilibrium centered at point C:

$$-R_F^d L + P L_R - F_{IN} H = 0$$

And replacing the values shown in the table X of the parameters becomes:

$$R_F^d = \frac{P L_R - F_{IN} H}{L} = 8281 \text{ N}$$

Instead, through the rotational equilibrium centered in point D, the back reaction is found:

$$R_R^d = \frac{P L_F + F_{IN} H}{L} = 16077 \text{ N}$$

And dividing by two using the assumption of symmetry by two we obtain the left front reaction:

$$R_F^{sx} = \frac{1}{2} R_F^d = 4140 \text{ N}$$

8.1.5 Curb

In the context of vehicle dynamic analysis, particular focus will be placed on the study of cornering behavior, a common and relevant driving situation. In order to create a model that accurately reflects real conditions, we will consider a generic representative case, i.e. a parabolic curve (with slope) on a motorway traveled at constant speed. This setup was chosen for its relevance to daily driving and for its usefulness in highlighting critical aspects of the suspension system.

For the study of this case, the following hypotheses are considered:

- The road is smooth, so the vehicle is not affected by vibrations due to the roughness of the ground

- The car frame is considered rigid along with the wheels
- The vehicle has geometric symmetry between the left and right sides
- The car's speed is constant throughout the turn
- The curve considered has a constant radius of curvature, therefore the force of inertia of the vehicle is also constant
- The curve is parabolic with a constant slope

The inertia force acting on the vehicle in this case depends on the speed at which the vehicle travels around the bend and on the radius of curvature of the bend itself, as well as on the mass of the vehicle. For this case it was assumed that the vehicle takes the curve with a speed of 130 km/h (maximum speed allowed on the motorway) and that the curve has a constant curve radius equal to 100 m (curve radii below which it is not customary to build motorway curves) with a gradient of 6.5% (maximum gradient of motorway curves).

$$F_{IN} = \frac{(m + m_P)v^2}{R} = 32379 \text{ N}$$

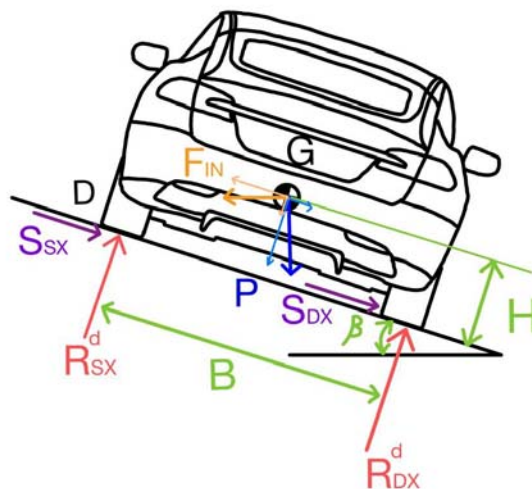


Figure 35. schematization of the forces acting on the vehicle during a curve

The slope of the curve must be converted into an angle expressed in radians in order to perform the following calculations:

$$\beta[\text{rad}] = \text{atan}\left(\frac{\beta[\%]}{100\%}\right) = 0,065 \text{ rad}$$

Furthermore, the coefficient of friction between the tire and the asphalt in standard conditions (dry asphalt and rubber in good condition) was also assumed to be $f_s = 0,95$

For the calculation of the vertical constraint reactions between the tire and the asphalt (in this case between the right and left sides of the vehicle) a rotation equilibrium centered on the

contact points is again performed. Referring to figure X, the reaction of the left side of the car is found via the rotational balance centered at point C:

$$-R_{sx}^d B + \frac{B}{2} P \cos(\beta) - P \sin(\beta) H + F_{IN} \cos(\beta) H - F_{IN} \sin(\beta) \frac{B}{2} = 0$$

And substituting the values reported In Table 7 we get:

$$R_{sx}^d = P \left[\frac{1}{2} \cos(\beta) - \frac{H}{B} \sin(\beta) \right] + F_{IN} \left[\frac{H}{B} \cos(\beta) + \frac{1}{2} \sin(\beta) \right] = 21636 \text{ N}$$

Analogously with a rotational equilibrium centered on point D, the reaction is found on the right side of the car: (point on the left)

$$R_{dx}^d B - P \sin(\beta) H - P \cos(\beta) \frac{B}{2} + F_{IN} \cos(\beta) H - F_{IN} \sin(\beta) \frac{B}{2} = 0$$

And by replacing the parameters with the values shown in table X, we obtain:

$$R_{dx}^d = P \left[\frac{H}{B} \sin(\beta) + \frac{1}{2} \cos(\beta) \right] + F_{IN} \left[\frac{1}{2} \sin(\beta) - \frac{H}{B} \cos(\beta) \right] = 4771 \text{ N}$$

Once the vertical reactions are known, the friction forces can be calculated, which can be considered as constraint reactions acting on the tire and acting in a horizontal direction:

$$S = S_{sx} + S_{dx} = f_s (R_{dx}^d + R_{sx}^d)$$

$$S_{sx} = 20554 \text{ N}$$

$$S_{dx} = 4533 \text{ N}$$

$$S_F^{sx} = 47\% \cdot S_{sx} = 9660 \text{ N}$$

Considering the left front wheel, the forces to be considered are obtained by considering only the portion that is discharged on the front (53% unbalance between front and rear) both for the vertical constraint reaction and for the horizontal friction force:

$$R_F^{sx} = 47\% \cdot R_{sx}^d = 10169 \text{ N}$$

8.1.6 Downward Braking

In the context of dynamic analysis, another case that deserves detailed examination is that of braking in a downhill situation. This scenario introduces a further complexity, since in addition to the forces considered for the case of flat braking, one must also take into account the gravitational force acting in the direction of the slope and the aerodynamic resistance which opposes

resistance to the movement of the vehicle. The interaction between these elements can have a significant impact on the binding reaction that is discharged on the wheel.

For the study of this case, the following hypotheses are considered:

- The road is smooth, so the vehicle is not affected by vibrations due to the roughness of the ground
- The car frame is considered rigid along with the wheels
- The vehicle has geometric symmetry between the left and right sides
- The descent has a constant slope

Again in relation to this case, it was also considered that the vehicle starts at a speed of and that the descent has a slope of, which corresponds to a slope of $v = 90 \text{ km/h}$ 15% $\alpha = 0.149 \text{ rad}$

To this end, the model that schematizes this situation is represented in Figure 36:

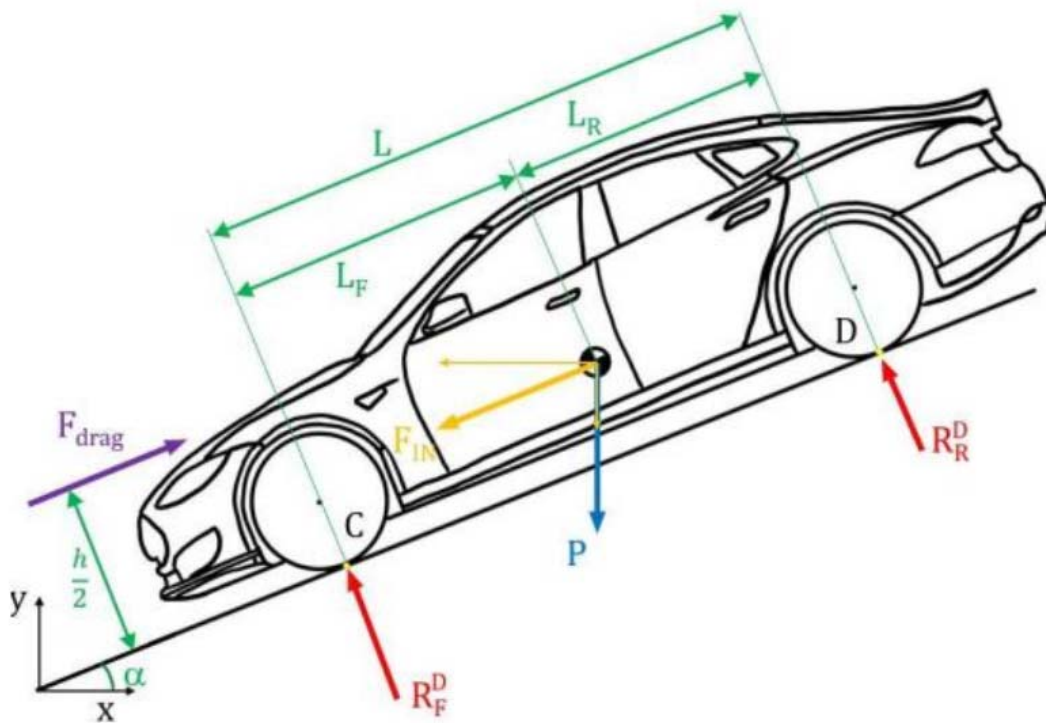


Figure 36. model of the forces acting on the vehicle in the event of braking downhill also considering the aerodynamic resistance

The acceleration due to braking as in the case of braking on level ground is considered equal to 1.5 times the gravitational acceleration; Therefore, the force of inertia is equal to: F_{IN}

$$F_{IN} = (m + m_p)a_F = 36537 \text{ N}$$

As far as aerodynamic resistance is concerned, for the calculations reference is made to the following data:

- $\rho = 1.225 \text{ kg/m}^3$ air density under standard conditions (e) $p = 1 \text{ atm}$ $T = 15^\circ\text{C}$
- $c_D = 0.24$ drag coefficient of the Tesla Model S (as listed in the owner's manual)
- $A = 0.8 \cdot h \cdot b = 2.275 \text{ m}^2$ frontal resistant section of the vehicle (approximately equal to 80% of the product between the height and the width of the vehicle)

For simplicity, the aerodynamic drag is assumed to act at half the height of the vehicle ($h/2$) and is calculated as:

$$F_{drag} = \frac{1}{2} \rho A c_D v^2$$

Substituting the previously defined values, we obtain:

$$F_{drag} = \frac{1}{2} \rho A c_D v^2 = 209 \text{ N}$$

Despite its potential impact on vehicle dynamics, the analysis revealed that at a speed of 90 km/h, the air resistance on the Tesla Model S is only 209 N. This surprisingly low value is attributed to the coefficient of exceptionally low drag of the model, which is a hallmark of Tesla's advanced aerodynamic design. This low coefficient is the result of an accurate design that aims to reduce friction with the air by optimizing the shape and surfaces of the vehicle. Despite its small entity, aerodynamic resistance will be included in the calculations, since even minimal variations in this parameter can influence the overall analysis of the binding reactions on the suspension.

For the calculation of the vertical constraint reactions between the tire and the asphalt, a rotation equilibrium centered on the contact points is performed. Referring to Figure 36, by means of the rotational equilibrium centered at point C, the front support reaction of the car is found:

$$-R_F^D L + P \cos(\alpha) L_R + P \sin(\alpha) H + F_{IN} H - F_{drag} \frac{h}{2} = 0$$

Substituting the numerical values of the aerodynamic resistance and of the parameters reported in Table 7 we get:

$$R_F^D = \frac{P}{L} [L_R \cos(\alpha) + H \sin(\alpha)] + \frac{1}{L} \left(H F_{IN} - F_{drag} \frac{h}{2} \right) = 18820 \text{ N}$$

Taking advantage of the symmetry hypothesis, to obtain the part of the force that is discharged on the left side, it is sufficient to divide it by two:

$$R_F^{sx} = \frac{1}{2} R_F^d = 9410 \text{ N}$$

Similarly, for the reaction on the rear, it can be calculated by setting a rotation equilibrium around point D:

$$R_R^D L - P \cos(\alpha) L_F + P \sin(\alpha) H + F_{IN} H - F_{drag} \frac{h}{2} = 0$$

Also, in this case replacing the numerical values obtained from the calculation of the aerodynamic resistance of the vehicle and the parameters reported in Table 7 we get:

$$R_R^D = \frac{1}{L} \left[P(L_F \cos(\alpha) - H \sin(\alpha)) + F_{drag} \frac{h}{2} - F_{IN} H \right] = 5269 \text{ N}$$

In the previous calculations of the binding reactions between the tire and the asphalt in the various driving conditions, a model was adopted which does not consider the deformability of the tire rubber. This choice was motivated by the need to simplify the analysis, but it is important to recognize that the tire actually deforms under load, influencing the transmitted forces. To account for this effect, an approximation has been introduced in which it is assumed that the tire absorbs approximately 20% of the applied load. This approximation is based on existing studies in the field of vehicle dynamics and material mechanics (Modeling and experimental study of tire deformation characteristics under high-speed rolling condition) and represents a realistic estimate of the tire's ability to dissipate forces through its deformation. While this approximation introduces a certain degree of uncertainty into the analysis, it was found to be an acceptable compromise to balance the complexity of the model with the need to provide an accurate representation of tire-road interactions.

In Table 8 can be seen the results deriving from the analysis carried out on the binding reactions between the tire and the asphalt are presented. The data are distinctly separated into two categories: the first value is the one that has been calculated previously for each case and represents the binding reaction between the tire and the asphalt calculated without considering the effect of the tire deformability. The second value, on the other hand, considers the reduction in the load transmitted to the wheel hub, attributable to the intrinsic deformation of the tire. This correction assumes that the tire deformability absorbs about 20% of the load as explained above.

Table 8. Forces at Play for Each Case Analysed

Summary of the Acting Forces	direction of force	reaction on the tire [N]	wheel hub reaction [N]
Case A) Static	vertical	6445	5156
Case B) Downward Braking	vertical	9232	7386
Case C) accelerated smoothly	vertical	4140	3312
Case D) curb	vertical	10169	8135
	horizontal	9660	7728

Case E) downhill braking	vertical	9410	7528
---------------------------------	----------	------	-------------

Case A) Static: The constraint reaction that is discharged on any of the front wheels is calculated if the car is stationary subject only to its own weight:

Case B) Dynamic 1: Downward Braking – The reaction generated on a front wheel by means of a sudden braking in a downhill. In this case the worst-case scenario is considered, given that the slope in the hill is very steep.

Case C) Dynamic 2: Acceleration - The binding reaction that is generated on any front wheel in case of acceleration (inertias) is calculated.

Case D) Dynamic 3: Curb: The constraint reaction that is generated on any front wheel in the event that the car curves at constant speed while maintaining the same curve radius is calculated.

Case E) Dynamic 4: Normal Braking - The binding reaction that is generated on a front wheel in the event of sudden braking (inertia) is calculated.

8.3 Vehicle Dynamics Simulation analysis in FEM software – ANSYS

A Proper Vehicle Dynamics Simulation exercise was performed in the suspension model using ANSYS® 2019 R3 software. Firstly, an optimization of the model had to be performed in order to obtain the best results from CAE software to be used, this passage was done in CREO™, as the obtained model was intended for visualization purposes only. In this process the joints between sub-elements were reassessed and several analyses were done in order to secure consistent results. The obtained model shown in Figure 37 shows the left side of the suspension and the 3 parts selected for optimization analysis, by following the guidelines of the function’s deployment from QFD analysis of Section 8.1A. The analysis was performed in order to realize the maximum values that the suspension elements must sustain given the 4 cases seen in 8.1-A1 part. The summary of this exercise in ANSYS can be seen in Figure 39. The model of the suspension on which the finite element analyzes will be carried out is represented in Figure 37 and is composed of the elements represented in Table 9:



Figure 37. model of the left suspension (in brown the aluminum components and in gray the steel components)

Table 9: data relating to the components present in figure X of the left suspension model

Component	Material	Weight Kg]	Suppressed
Pins X5	steel	0.32	Yes
Upper Arm	steel	2.278	no
Lower-Arm	aluminum	1,764	no
Tie Rod	aluminum	0.14	no
Steering Arm	aluminum	1.194	no
Spindle	aluminum	9,448	no
Wheel's Hub	steel	5,347	no
Disc Brake	steel	12,759	Yes
Wheel Rim	aluminum	9	Yes
Anti Roll Bar	steel	6	no
Brake Caliper	steel	7	Yes
Mass of Suppressed Elements [kg]		30	

The same cases analyzed previously will be analyzed through FEM to understand the internal reactions between the various components of the suspension. The components to be analyzed will focus in both arms (highlighted in Figure 38), therefore immediately excluding the spindle given its size and complexity of manufacturing through Additive Manufacturing, especially from an economic point of view.

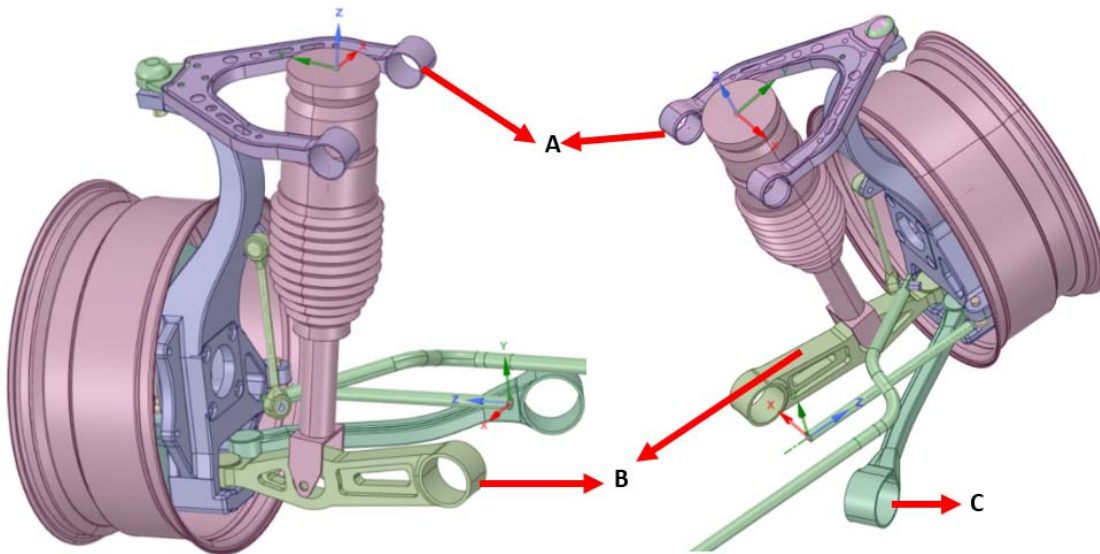


Figure 38. Vehicle suspension for analysis: A: Upper Arm; B: Lower Arm 1; C: Steering, Lower Arm 2

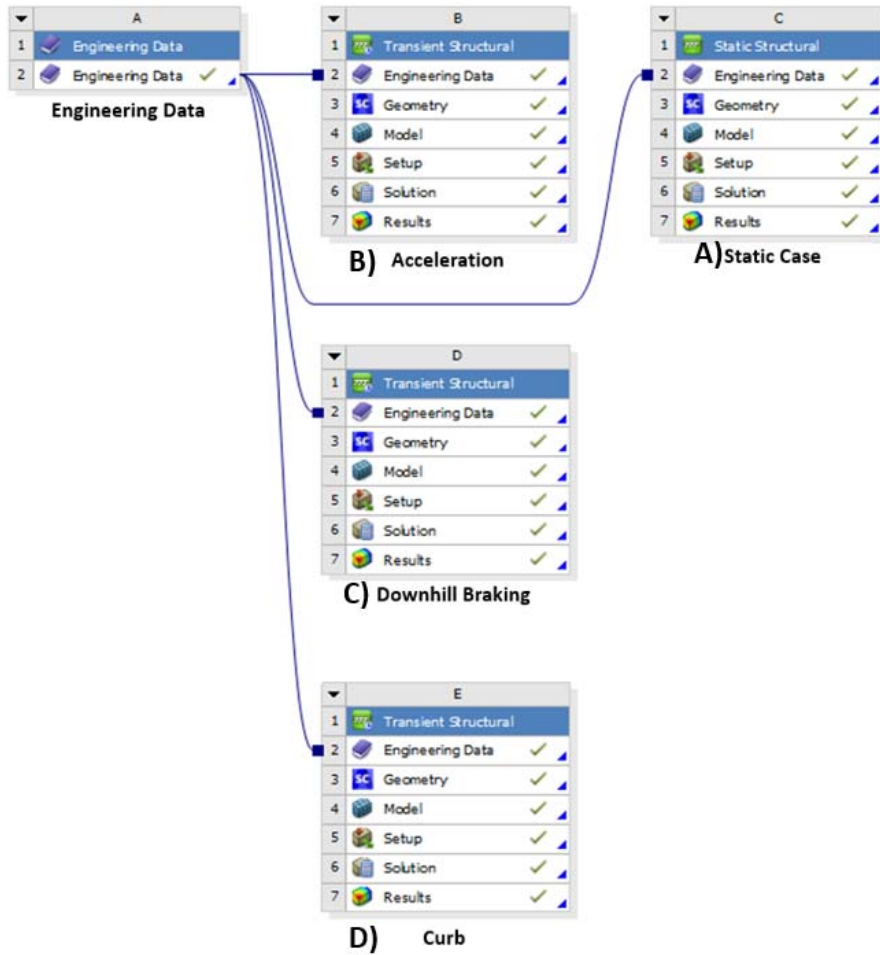


Figure 39. Simulation Project Schematic for Vehicle Dynamics

Engineering Data, data input from Structural steel and Aluminum were used to include parameters for fatigue, Temperature and mean Stress (Figure 40).

Outline of Schematic A2, B2, C2, D2, E2: Engineering Data					
	A	B	C	D	E
1	Contents of Engineering Data			Source	Description
2	Material				
3	Aluminum Alloy				General aluminum alloy. Fatigue properties come from MIL-HDBK -SH, page 3-277.
4	Structural Steel				Fatigue Data at zero mean stress comes from 1998 ASME BPV Code, Section 8, Div 2, Table 5 -110.1
*	Click here to add a new material				

Properties of Outline Row 3: Aluminum Alloy					
	A	B	C	D	E
1	Property	Value	Unit		
2	Material Field Variables	Table			
3	Density	2770	kg m^-3		
4	Isotropic Secant Coefficient of Thermal Expansion				
6	Isotropic Elasticity				
12	S-N Curve	Tabular			
16	Tensile Yield Strength	2.8E+08	Pa		
17	Compressive Yield Strength	2.8E+08	Pa		
18	Tensile Ultimate Strength	3.1E+08	Pa		
19	Compressive Ultimate Strength	0	Pa		
20	Isotropic Thermal Conductivity	Tabular			
23	Specific Heat, C _p	875	J kg^-1 ...		
24	Isotropic Relative Permeability	1			
25	Isotropic Resistivity	Tabular			

Table of Properties Row 2: Aluminum Alloy Field Variables					
	A	B	C	D	E
1	Variable Name	Unit	Default Data	Lower Limit	Upper Limit
2	Temperature	C	22	Program Controlled	Program Controlled
3	R-Ratio		-1	Program Controlled	Program Controlled

Outline of Schematic A2, B2, C2, D2, E2: Engineering Data					
	A	B	C	D	E
1	Contents of Engineering Data			Source	Description
2	Material				
3	Aluminum Alloy				General aluminum alloy. Fatigue properties come from MIL-HDBK -SH, page 3-277.
4	Structural Steel				Fatigue Data at zero mean stress comes from 1998 ASME BPV Code, Section 8, Div 2, Table 5 -110.1
*	Click here to add a new material				

Properties of Outline Row 4: Structural Steel					
	A	B	C	D	E
1	Property	Value	Unit		
2	Material Field Variables	Table			
3	Density	7850	kg m^-3		
4	Isotropic Secant Coefficient of Thermal Expansion				
6	Isotropic Elasticity				
12	Strain-Life Parameters				
20	S-N Curve	Tabular			
24	Tensile Yield Strength	2.5E+08	Pa		
25	Compressive Yield Strength	2.5E+08	Pa		
26	Tensile Ultimate Strength	4.6E+08	Pa		
27	Compressive Ultimate Strength	0	Pa		
28	Isotropic Thermal Conductivity	60.5	W m^-1...		
29	Specific Heat, C _p	434	J kg^-1 ...		
30	Isotropic Relative Permeability	10000			

Table of Properties Row 2: Structural Steel Field Variables					
	A	B	C	D	E
1	Variable Name	Unit	Default Data	Lower Limit	Upper Limit
2	Temperature	C	22	Program Controlled	Program Controlled
3	Mean Stress	Pa	0	Program Controlled	Program Controlled

Figure 40. Engineering Data Input and Material details for Aluminum Alloy (left) and Structural Steel (right).

As a result, the following Figures 41, 42, 43 show the results of the analysis of the cases summarized in Table 8 and applied to the Upper Arm (Figure 41); Lower Arm (Figure 42); and Steering Arm (Figure 43).

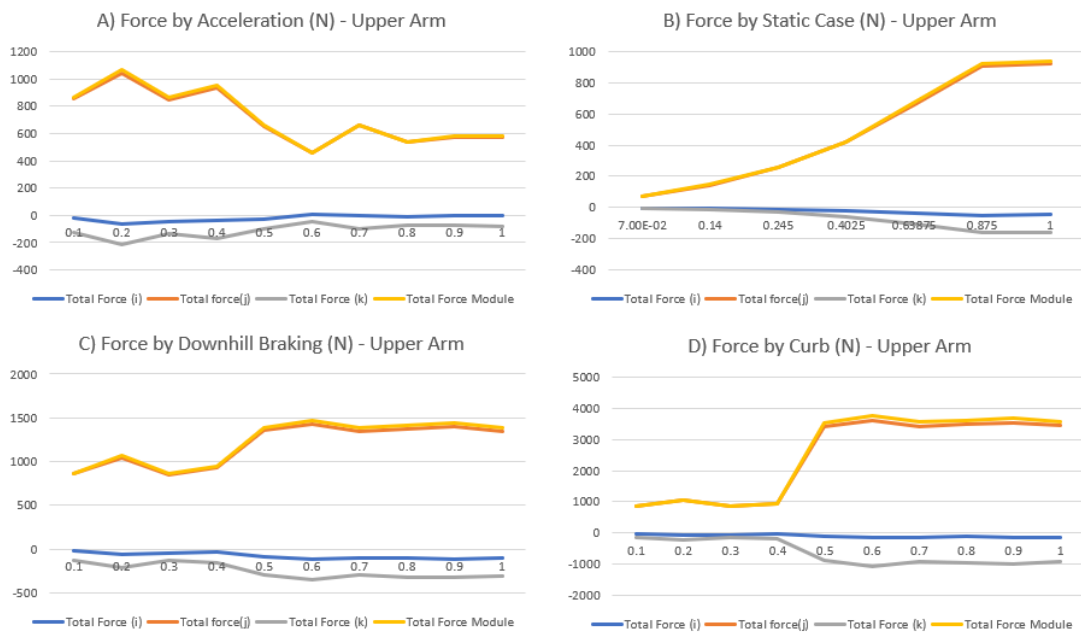


Figure 41. Results on Dynamic 4 cases analysis on: Upper arm and stub axle

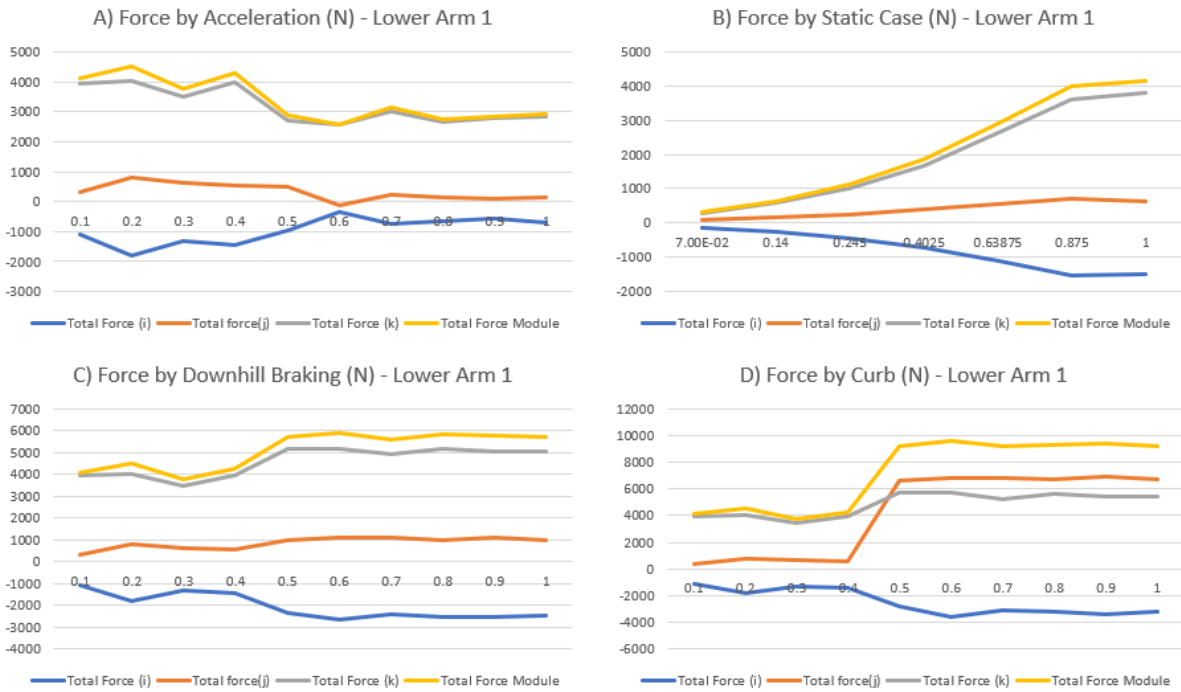


Figure 42. Results on Dynamic 4 cases analysis on: reactions between the lower arm and stub axle

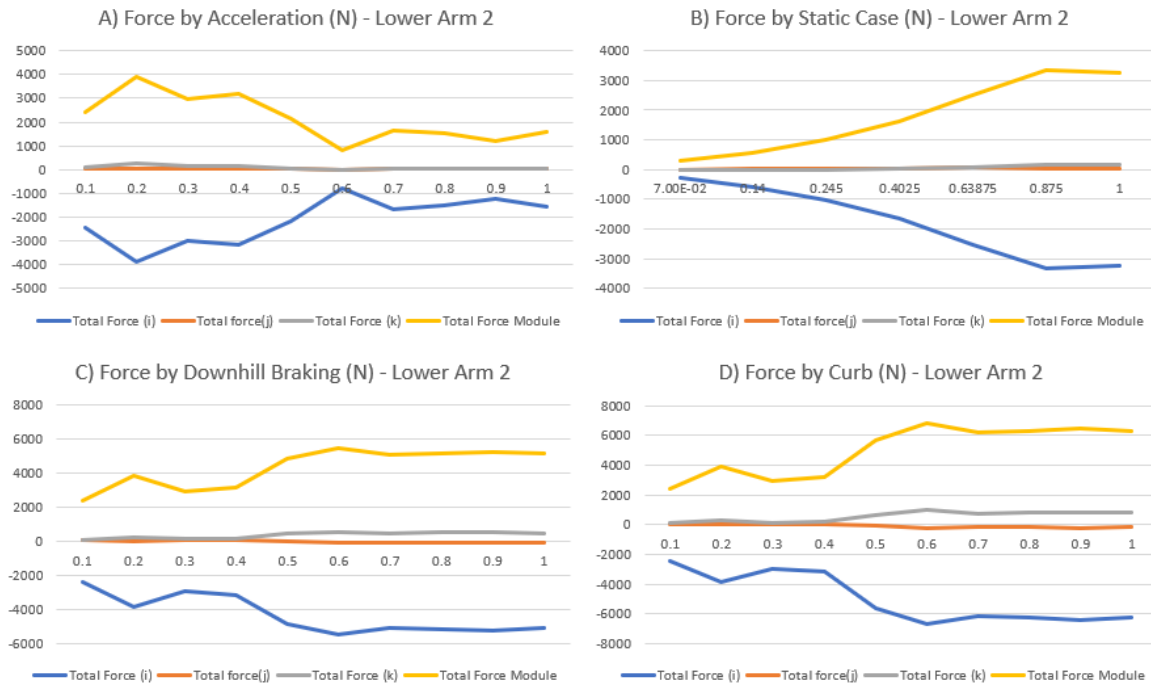


Figure 43. Results on Dynamic 4 cases analysis on: Lower Arm 2 - steering arm and the spindle.

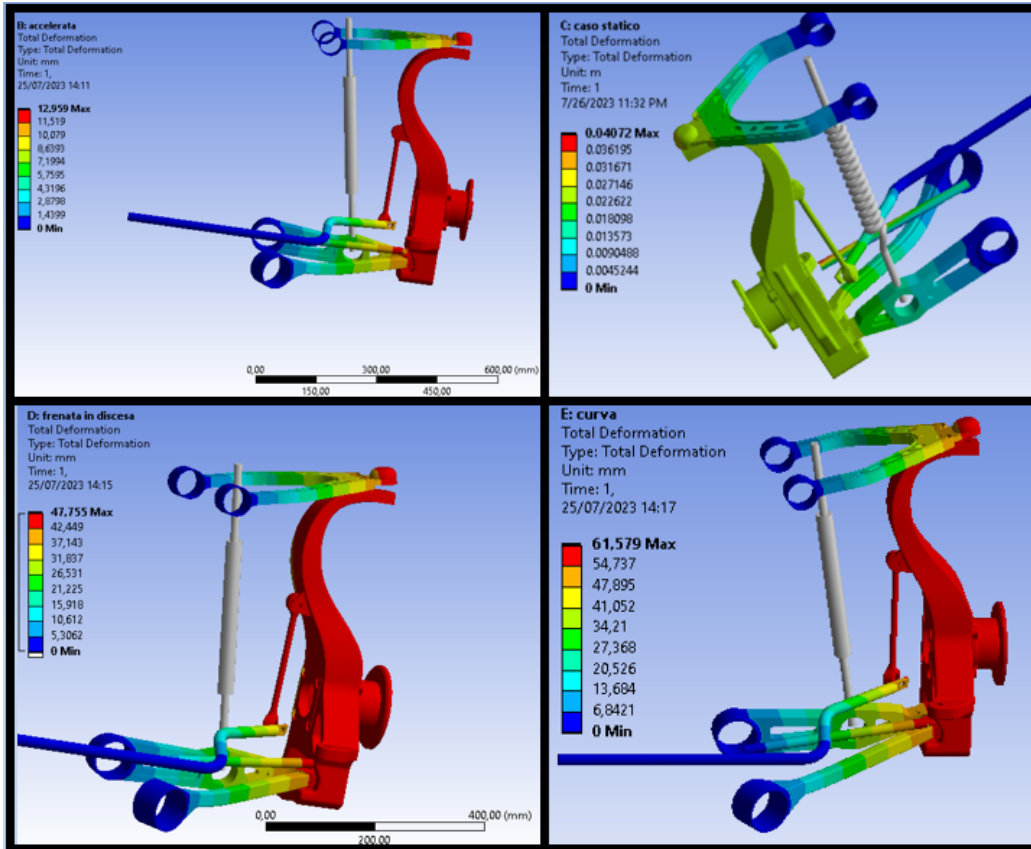


Figure 44. Maximum deformation results on the entire suspension for 4 different Dynamic cases.

Nevertheless, by concluding on the data collected in relation to the loads that the various components of the system undergo, it is possible to make a significant consideration regarding the optimization of the steering arm. Being the arm made of aluminum alloy and boasting an already light structure (about 1.2 kg as shown in Table 9), the loads to which it is subjected are within reasonable limits: further attempts at optimization, while being able to make some marginal improvements, would not be justifiable from an economic point of view. The gain in weight or strength would be minimal and the expense associated with such optimization would be disproportionate to the benefits gained. Therefore, it is concluded that the current steering arm configuration represents a near-optimal solution and further interventions in this area would not represent an effective investment.

Therefore, the optimization will be carried out on the upper arm and on the lower arm of the suspension, which compared to the steering arm would have more room for improvement.

8.4 Results from Dynamic Analysis and Topological Analysis Set Up

From the accurate data from the dynamic analysis of the suspension, we proceeded to identify the heaviest loads acting on the two components chosen for system optimization, i.e. the upper arm and the lower arm. The loads chosen would be those of the most severe situations (the greatest loads) of the set of all loads obtained from the previous analysis for each of the two components. These loads will then be used as input to perform a topological optimization on both components. The goal of this optimization is

to provide an idea of the ideal geometry that these components should have, evaluating any differences with respect to the original configuration. This step represents a critical phase in the evolution of the project,

Analyzing the graphs, it can be seen that the most critical case is the one in curves since it presents the highest force values for both components. Therefore, for both components, the loads considered for topological optimization are summarized in Table 10 according to the references in Figure 45.

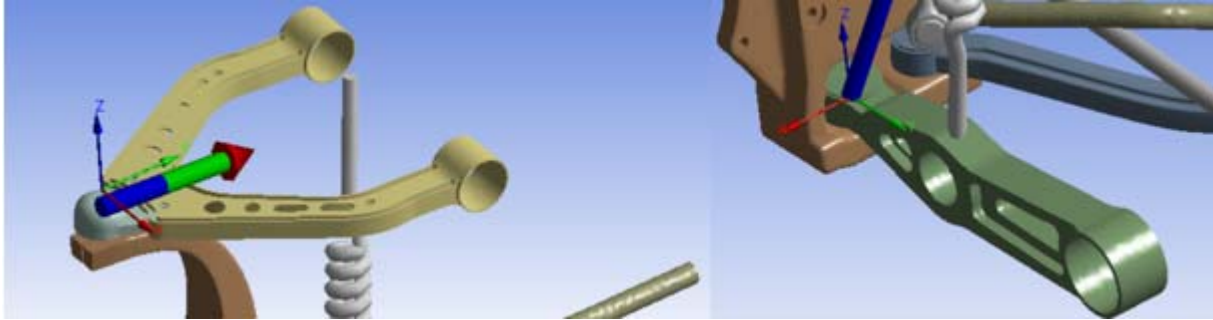


Figure 45. Reference Systems of The Upper and Lower Arm

Table 10. Load Values To Set The Topological Optimization According To The Respective Reference Systems

Upper arm		Lower-arm	
fx	-173 N	fx	-3563 N
fy	3681 N	fy	7119 N
Fz	-75 N	Fz	5030 N

8.5 Product Design for Additive Manufacturing (DfAM) > Topological Optimization (TO)

Topological Optimization: Reticular and Lattice Structural Deployment.

Topological optimization is a design approach used in engineering to optimize the material distribution within a given design space (Maute & Ramm, 1995). It is a mathematical optimization method that often uses algorithms like finite element analysis to analyze the structural behavior and iteratively adjust the material distribution (Munk et al., 2015).

The goal is to find the most efficient arrangement of material in a structure to meet certain performance criteria, such as minimizing weight, maximizing stiffness, or improving heat dissipation. This optimization process often involves the use of computational algorithms to iteratively adjust the material layout based on the specified criteria.

Key Aspects for implementation of Topological Implementation in today's industry:

Computational Power: Advances in computing power and simulation techniques enable faster and more complex analyses, making topological optimization more practical (Mukherjee et al., 2021).

3D Printing and Advanced Manufacturing: With the rise of 3D printing and other advanced manufacturing technologies, it has become feasible to produce intricate structures that topological optimization may suggest (S. Li et al., 2020).

Lightweighting: In industries such as aerospace and automotive, there is a continuous push for lightweight structures to improve fuel efficiency and overall performance. Topological optimization helps in achieving lightweight designs without compromising structural integrity (Plocher & Panesar, 2019) .

Material Efficiency: By optimizing material distribution, industries can make more efficient use of materials, potentially reducing costs and waste.

Performance Enhancement: The approach can enhance the performance of structures by tailoring the material distribution to meet specific performance criteria, such as stiffness, strength, or thermal conductivity (Y. Li et al., 2020).

Customization: In the medical field, topological optimization can be applied to design patient-specific implants or prosthetics, taking into account individual anatomy and load conditions, (Dalpadulo et al., 2020), (Minnoye et al., 2022).

Overall, topological optimization is gaining traction due to advancements in computational capabilities and the increasing importance of lightweight and efficient designs across various industries. It allows engineers to explore innovative and unconventional designs that may not be apparent through traditional methods, leading to more optimized and high-performing structures. Volkswagen AG's take on TO assessed the Future challenges for this method (Fiebig et al., 2015) that involve becoming the top design proposal of casting parts; and the integration of manufacturing simulation. until a final continuous and integrated development process, in line with IDES method tools used in this exercise. Whilst crashworthiness and acoustic (Gonçalves et al., 2020) requirements cannot be completely supported by optimization methods (Yousaf et al., 2023).

Finally, the synergy between topological optimization and lattice structures (Pan et al., 2020) enables engineers to create lightweight, strong, and efficient designs across various industries. This combination is particularly powerful in the context of advanced manufacturing technologies, where intricate lattice structures can be faithfully reproduced.

8.5.1 Lattice Structures

A reticular structure, ie. a structure created with interconnected bars in the form of triangles to create a network. The joints of the bars are called nodes, and they can be rigid or articulated. These are also called reticulated or bar structures. Reticular structures have evolved during time thanks to the manufacturing and product design technology until becoming a 3D – oriented pattern which is called a Lattice Structure.

Lattice structures are becoming increasingly common in product design. These are repeated patterns that fill a volume or conform to a surface. In engineering design, lattices are cellular materials—often inspired

by nature—that consist of beams, surfaces, or plates that fit together following an ordered or stochastic pattern(Cucinotta et al., 2021). (Figure 46).

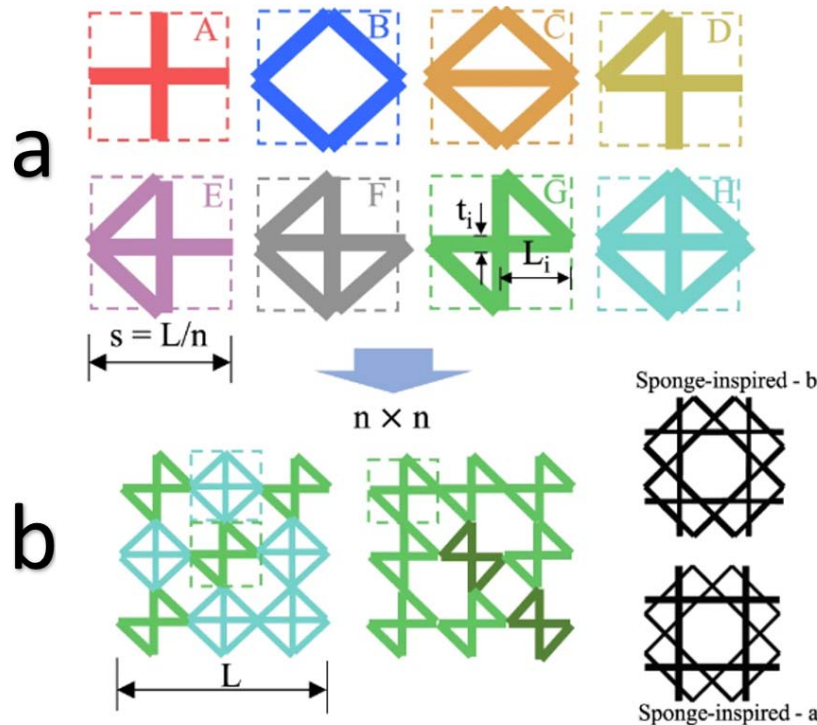


Figure 46. a) Unique beam-based building blocks generated by diverse-connected boundary nodes; b) $n \times n$ non-uniform unit cells with $n = 3$ by different combinations of building blocks, design a and its 90°-rotated version b (identified by a darker green).

There is a vast array of lattice structures and several ways to create lattices. Many popular engineering design software like ANSYS® and Creo® have developed plug-ins in order to offer the possibility to portray lattice-like structural solutions. Another software specifically designed for this purpose is nTopology®, which offers a wide range of types of lattice structures, stating that this type of multi-element pattern can be fully adapted to most design requests (Varotsis, 2022):

- Lattices can be periodic, non-periodic, or stochastic.
- They can consist of beams, plates, or Triply Periodic Minimal Surfaces (TPMS).
- They can fill a volume or be applied on a surface.
- They can be trimmed to a design space or conform to it.
- They can be generated based on a mesh, a CAD body, or directly as an implicit body.

For periodic lattice structures, the unit cell type determines most of the lattice properties. There is a wide range of unit cell types, each of which will be appropriate for different applications. As a rule of thumb:

- Beam lattices can offer high stiffness-to-weight or be elastic and compliant.
- TPMS lattices offer all-around good mechanical properties.
- Honeycombs and plate lattices offer high stiffness in a specific direction.

8.5.2 Study: Response to the Same Loads of Different Latex Structures

Different simulations were carried out by using nTopology® on a 200 mm long beam with a 25 mm side square base, made up of a 2 mm thick shell and an internal part completely filled with a lattice structure. For this purpose, the forces, the constraints, the thickness of the structures (Thickness = 1 mm) and the dimensions of the cells (single cell dimension: 5 mm x 5 mm x 5 mm) are kept constant at each simulation, while the type of lattice cell was changed.

The material inserted in the simulations also remains constant in each of them: a stainless steel has been chosen. The results will first be shown, for each type of cell, of a series of simulations on the beam, which is wedged at one end and on which, a few millimeters from the opposite end, a force of 5000N is applied perpendicular to the axis of the beam itself.

Subsequently, the results of the simulations will be shown on the same beam still fixed at one end, on the opposite base of which a traction force equal to 5000 N is applied parallel to the axis of the beam and distributed over the entire face. For each simulation the following parameters will be shown: Displacement, strain, stress and reaction forces.

N.B. for the first 19 structures, cells of the type: graph unit cell are used. For the last 6 cells of the type: walled TPMS unit cell are used.

Distortion was always shown. The results of the first two simulations (subjected to the first type of cargo) with the intention of showing a visual example of the work done and to highlight the differences in response of the various structures, the which characterize the utility of all the simulations. The details of the different types of internal lattice-elements composition can be seen in Figure 47. The results on the Mechanical Characterization on each Type of this Reticular Structures are summarized in Table 11.

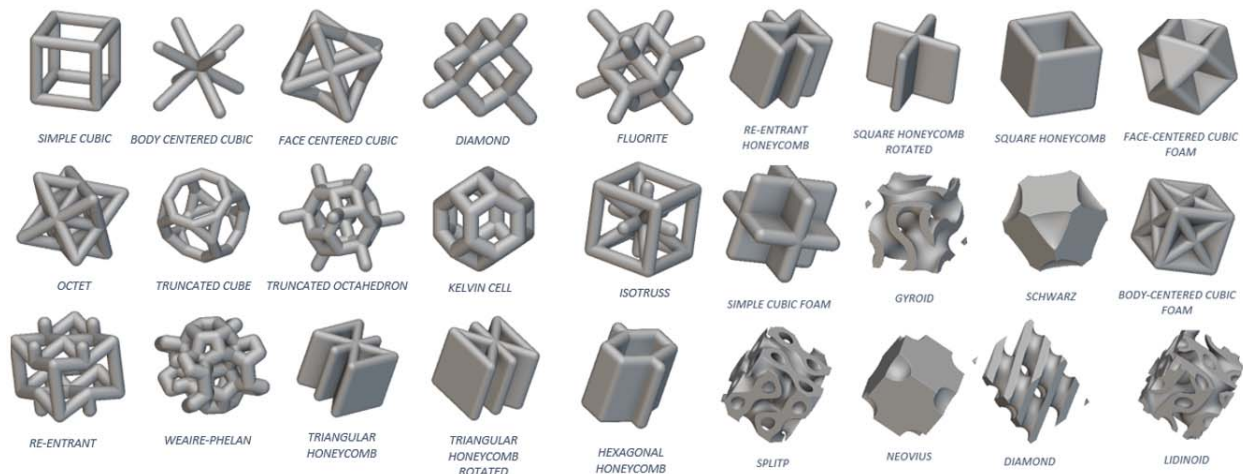


Figure 47. Reticular Structures Used in the study

Table 11. Mechanical Characterization for each Type of Reticular Structures

Lattice Structure Typology	Unit Cell Type	Simulation	Max Stress(Pa)	Max Displacement(mm)
SIMPLE CUBIC	Beam	1	1.86E+09	3.93E+00
BODY CENTERED CUBIC	Beam	1	1.91E+09	3.92E+00
FACE CENTERED CUBIC	Beam	1	9.92E+08	3.72E+00
DIAMOND	Beam	1	1.13E+09	3.89E+00
FLUORITE	Beam	1	1.08E+09	3.52E+00
OCTET	Beam	1	9.62E+08	3.21E+00
TRUNCATED CUBE	Beam	1	1.09E+09	3.85E+00
TRUNCATED OCTAHEDRON	Beam	1	1.29E+09	3.41E+00
KELVIN CELL	Beam	1	1.06E+09	3.55E+00
ISOTRUSS	Beam	1	8.43E+08	3.37E+00
RE-ENTRANT	Beam	1	1.22E+09	3.59E+00
WEAIRE- PHELAN	Beam	1	9.24E+08	2.94E+00
TRIANGULAR HONEYCOMB	Honeycomb	1	7.64E+08	2.51E+00
TRINAGULAR HONEYCOMB ROTATED	Honeycomb	1	7.43E+08	2.26E+00
HEXAGONAL HONEYCOMB	Honeycomb	1	8.79E+08	3.25E+00
RE-ENTRANT HONEYCOMB	Honeycomb	1	1.22E+09	3.09E+00

SQUARE HONEYCOMB ROTATED	Honeycomb	1	1.16E+09	3.19E+00
SQUARE HONEYCOMB	Honeycomb	1	8.18E+08	3.11E+00
FACE- CENTERED CUBIC FOAM	Plate	1	5.62E+08	1.97E+00
BODY- CENTERED CUBIC FOAM	Plate	1	5.09E+08	1.95E+00
SIMPLE CUBIC FOAM	Plate	1	8.33E+08	2.57E+00
GYROID	TPMS	1	7.55E+08	3.04E+00
SCHWARZ	TPMS	1	5.59E+08	2.54E+00
DIAMOND	TPMS	1	6.86E+08	2.54E+00
LIDINOID	TPMS	1	2.28E+09	2.27E+00
SPLITP	TPMS	1	9.58E+08	2.66E+00
NEOVIUS	TPMS	1	5.91E+08	2.11E+00
SIMPLE CUBIC	Beam	2	2.63E+08	3.75E-02
BODY CENTERED CUBIC	Beam	2	2.41E+08	3.47E-02
FACE CENTERED CUBIC	Beam	2	1.31E+08	2.77E-02
DIAMOND	Beam	2	1.48E+08	3.25E-02
FLUORITE	Beam	2	8.80E+07	2.39E-02
OCTET	Beam	2	5.52E+07	1.93E-02
TRUNCATED CUBE	Beam	2	1.84E+08	3.11E-02
TRUNCATED OCTAHEDRON	Beam	2	1.38E+08	2.30E-02
KELVIN CELL	Beam	2	1.18E+08	2.50E-02

ISOTRUSS	Beam	2	1.02E+08	2.20E-02
RE-ENTRANT	Beam	2	9.81E+08	2.32E-02
WEAIRE- PHELAN	Beam	2	8.70E+07	1.65E-02
TRINGULAR HONEYCOMB	Honeycomb	2	2.67E+07	1.20E-02
TRIANGULAR HONEYCOMB ROTATED	Honeycomb	2	2.20E+07	1.03E-02
HEXAGONAL HONEYCOMB	Honeycomb	2	4.47E+07	2.09E-02
RE-ENTRANT HONEYCOMB	Honeycomb	2	4.22E+07	1.92E-02
SQUARE HONEYCOMB ROTATED	Honeycomb	2	4.37E+07	1.95E-02
SQUARE HONEYCOMB	Honeycomb	2	3.19E+07	1.78E-02
FACE- CENTERED CUBIC FOAM	Plate	2	1.62E+07	8.25E-03
BODY- CENTERED CUBIC FOAM	Plate	2	1.48E+07	8.24E-03
SIMPLE CUBIC FOAM	Plate	2	2.71E+07	1.32E-02
GYROID	TPMS	2	4.16E+07	1.75E-02
SCHWARZ	TPMS	2	2.31E+07	1.21E-02
DIAMOND	TPMS	2	3.76E+07	1.26E-02
LIDINOID	TPMS	2	3.82E+07	1.04E-02
SPLITP	TPMS	2	5.69E+07	1.44E-02
NEOVIUS	TPMS	2	1.62E+07	9.34E-03

The results of Table 11 show the different mechanical responses for each type of reticular structure. These values are key in deciding the most feasible geometry of the internal structure of structural elements in

function of its capacity of sustain a given mechanical behavior. The typology of internal structure was also biased by other characteristics valued like manufacturability, and surface quality. From the comparison it emerges that the lattices that responded well to the load showing the lowest Von Mises stresses are those that have continuous walls:

- simple cubic foam (SCF)
- hexagonal honeycomb (HH)
- square rotated honeycomb (SRH)

Of the latter two, it can be observed that the axial orientation is by far optimal with respect to the transversal one for the type of load under examination.

Also noteworthy is the re-entrant grating, but unfortunately to be discarded given the nature of the FDM printing process which would confer greater mechanical properties on the plane on which it prints (the gratings are oriented in multiple spatial directions), effectively making the structure highly anisotropic reticulate. Furthermore, the effectiveness of continuous wall gratings can be underlined as they are oriented according to the same printing direction, which makes them more resistant along that direction.

Of the three lattices mentioned above, the influence of the parameters constituting the lattice on the displacement and equivalent stress was evaluated, obtaining Table 12, and Figure 48.

Table 12. mechanical resistance analysis results for top 3 rated internal structures from NTOP.

Hexagonal Honeycomb (Hh)				Square Honeycomb Rotated (Shr)				Simple Cubic Foam (Scf)			
		Total displacement [mm]	Von-Mises equivalent stress [MPa]			Total displacement [mm]	Von-Mises equivalent stress [MPa]			Total displacement [mm]	Von-Mises equivalent stress [MPa]
Fillet radius [mm]	2	1.49664	36	Fillet radius [mm]	2	1.45285	37	Fillet radius [mm]	2	1.53857	36
	3	1.43044	36		3	1.3913	34		3	1.48511	35
	4	1.34162	27		4	1.29702	32		4	1.40688	31
	5	1.25358	27		5	1.19291	30		5	1.31569	33
	6	1.16449	34		6	1.08999	28		6	1.21856	31
Lattice thickness [mm]	2	1.49664	36	Lattice thickness [mm]	2	1.45285	37	Lattice thickness [mm]	2	1.53857	36
	3	1.38964	33		3	1.34672	32		3	1.44103	33
	4	1.29870	33		4	1.25314	29		4	1.35477	31
	5	1.22029	30		5	1.16980	28		5	1.27318	30
	6	1.15232	27		6	1.09287	27		6	1.19667	27

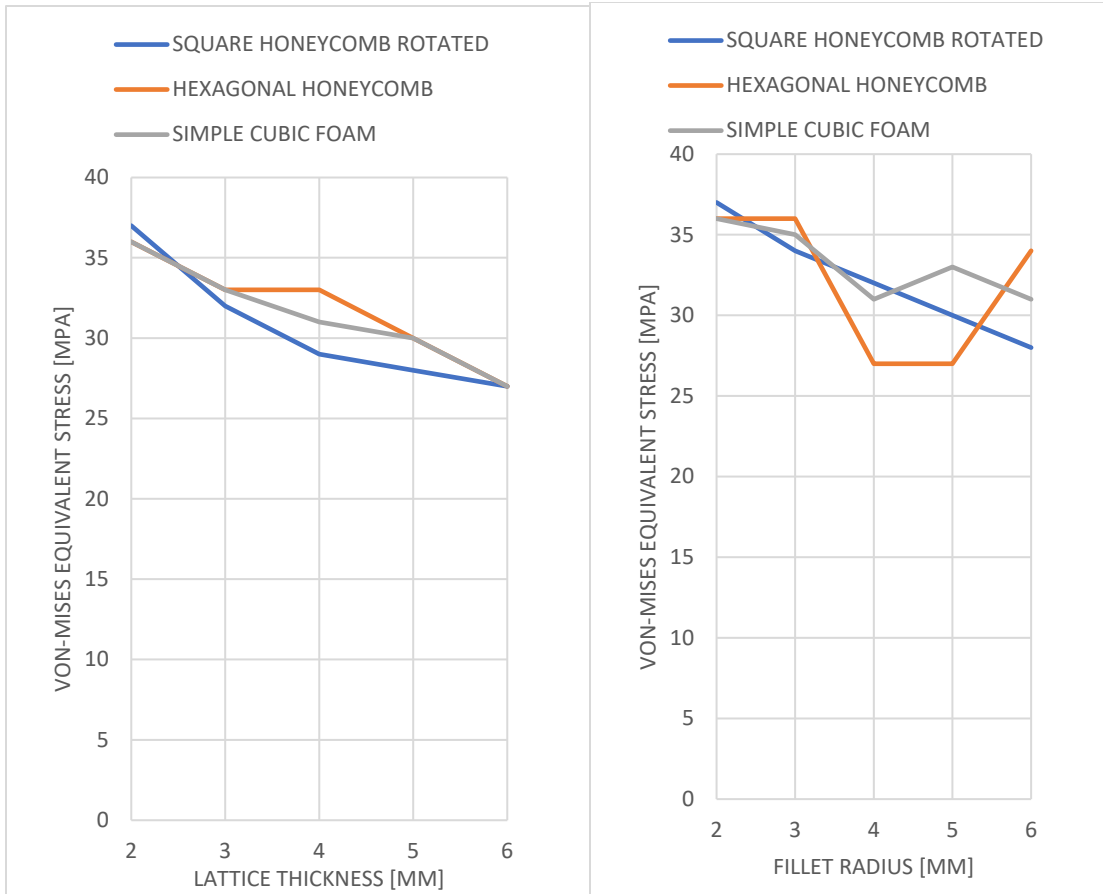


Figure 48. Von-Mises Stress vs Lattice Thickness and Fillet Radius for best scored Structure geometries.

8.5.3 Lattice Structures with Additive Manufacturing

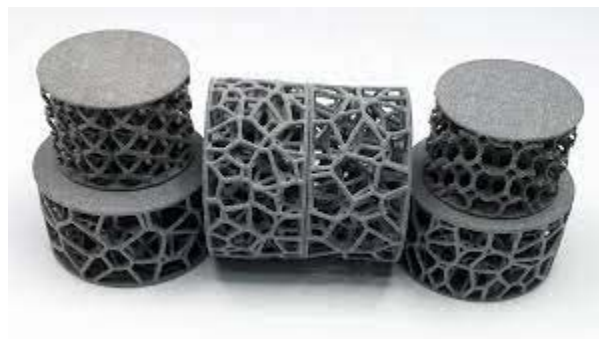


Figure 49. AM-sourced lattice structures

In 3D printing, design boundaries are no longer confined to the production process. Design for additive manufacturing (DfAM) provides numerous benefits to product development and production with the creation of complex parts with intricate geometries. These benefits are only expounded upon through the formation and use of lattice structures in additive manufacturing, resulting in improved structural optimization and functional design.

3D printed lattice structures provide many mechanical advantages. Weight reduction while retaining structural integrity is perhaps the most important benefit and the primary reason design engineers use lattice structures to optimize 3D printed parts. Lattice structures enable engineers to increase overall surface area and distribute material in the most structurally effective way possible, allowing for the production of lightweight parts with optimized weight-to-strength ratios.

The customizable nature of lattices also provides the ability to refine designs to match application requirements, leading to increased control over shock absorption and stiffness. By adjusting the thickness and position of lattice sections, engineers can distribute impact forces or employ elements that act as auxiliary features to protect critical parts of a product. Similarly, product designers can integrate characteristics to enhance vibration and noise dampening performance.

9. Material choice and Engineering approach

The material choices to take depend on some factors, starting from a given overall mechanical loading condition of the element, then thinking to the best approach according to the type of manufacture, and without any doubt, on the overall piece price.

For this exercise, as pursuing a DfAM approach, the material selection was done by overseen the most used materials for both types of AM processes to pursue in this exercise: Metal AM, Polymer / Composite AM.

In the first case, for Metal AM, the available material to use in the metal printer SISMA MySint 100 (Figure 50) is Aluminum type ALSi10, The material has good thermal and electrical conductivity, especially after heat treatment, and which powder has the following properties, in compliance with the DIN EN 1706 (EN AC—43000) standard (Tables 13 to 15).



Figure 50. SISMA® MySint 100 SLM Printer

Table 13. Powder AlSi10Mg chemical composition (EOS Metal Solutions, 2022a)

Powder AlSi10Mg	
Element	wt. %
Al	Balance
Si	10
Fe	0.55
Cu	0.05
Mn	0.45
Mg	0.35
Ni	0.05
Zn	0.1
Pb	0.05
Sn	0.05
Ti	0.015

Table 14. Typical properties (as manufactured state)
(EOS Metal Solutions, 2022b)

Mechanical Properties	Horizontal	Vertical
Yield Strength (Mpa)	250	220
Tensile Strength (Mpa)	380	360
Elongation at Break (%)	2	2

Table 15. Typical properties (heat Treated, EOS T6)
(EOS Metal Solutions, 2022b)

Mechanical Properties	Horizontal	Vertical
Yield Strength (Mpa)	250	220
Tensile Strength (Mpa)	380	360
Elongation at Break (%)	2	2

For a nonmetallic material option, a sandwich-composite layout was outlined for this exercise. A material solution which was created after having a wide research knowledge of polymer materials used for AM processes. Previous research findings made by the author, (Ferretti et al., 2021) highlighted in section 5, described the procedure suggested to arrive to best results in terms of part surface quality and mechanical behavior by reducing material anisotropy (Figure 18), by following a optimization process (Figure 19). The FDM printer to be used is the Artillery® Sidewinder X1 (Figure 51).



Figure 51. Artillery® Sidewinder X1 FDM Printer

Additionally, new material offering into the traditional polymer, FDM processes has made possible to give rise to a new type of composite material filament: Form Futura® CarbonFil®, which is a 15% carbon fiber reinforced PETG based 3D printer filament that is extremely stiff. CarbonFil 3D prints with a high dimensional accuracy and virtually no warping. The unique PETG blend of our HDglass compound and is reinforced with 15% ultra-light and relatively long stringer carbon fibers, which has resulted in an exceptionally stiff carbon fiber reinforced 3D printer filament. CarbonFil® is twice as stiff as HDglass and yet it is even 10% more impact resistant, which is a remarkable feature for carbon Fiber reinforced filament (Futura B.V., 2022) (Table 16). Additionally, another reinforced material to be tested will be the PLA, sourced from Polymaker® (Polymaker, 2022) (Table 17); a chart UTS vs number of cycles (Figure 52) was obtained after correlation from the study of (Rajeshirke et al., 2023).

Table 16. FormFutura Carbonfil™ PETG – CF Technical Data Sheet

Properties	Typical value	Test Method	Test condition
Physical			
Specific gravity	1.19 g/cc	ISO 1183	-
Melt flow rate.	3.7 cm ³ /10min	ISO 1133	200° C/5Kg
Water absorption	-	-	-
Moisture absorption	± 0.13%	-	-
Mechanical			
Impact strength	5 KJ/m ²	ISO 179	Charpy Notched @23° C
Tensile strength	92 Mpa	ISO 527	@Break
Tensile modulus	9495 Mpa	ISO 527	-
Elongation at break	3.4%	ISO 527	Strain at Break
Flexural strength	-	-	-
Flexural modulus	-	-	-
Hardness	-	-	-

Main Polymer Composition	PETG blend		
Reinforcement Fiber	Carbon Fiber 20%		
Thermal			
Print temperature	± 230 - 265° C	-	-
Melting temperature	-	- ISO 306	-
Viscat softening temp.	± 79° C		@ 0.455 Mpa (66psi)

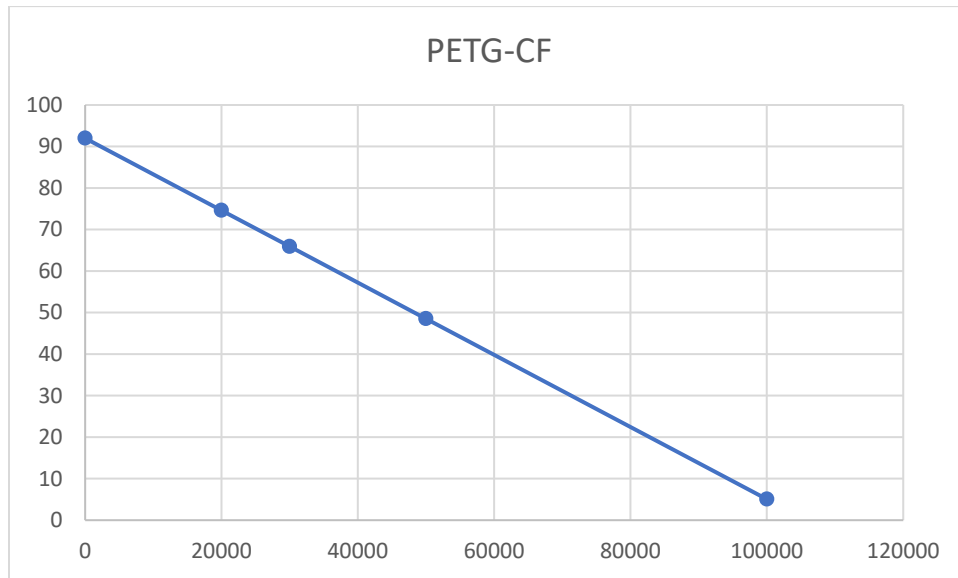


Figure 52. UTS vs number of cycles assessment for PETG material

Table 17. Mechanical Properties of Polymaker® Polylite PLA-CF

MECHANICAL PROPERTIES - Polymaker® Polylite PLA-CF		
Property	Testing Method	Typical Value
Young's modulus (X - Y) Young's modulus (Z)	ISO 527,GB /T 1040	2945±100MPa 2143+91MPa
Tensile strength (X - Y) Tensile strength (Z)	ISO 527,GB /T 1040	28.28±0.7MPa 12.54±0.7MPa
Elongation at break (X - Y) Elongation at break (Z)	ISO 527,GB /T 1040	4.2±0.12% 0.75±0.08%
Bending modulus (X - Y) Bending modulus (Z)	ISO 178,GB /T 9341	3215182MPa N /A
Bending strength (X - Y) Bending strength (Z)	ISO 178,GB /T 9341	54.2±1.4MPa N /A

Charpy impact strength (X -Y)Charpy impact strength (Z)	ISO 179,GB /T 1043	4.82±0.14kJ /m ² N /A
---	--------------------	----------------------------------

The remarkable mechanical properties of these filaments had made them probable materials to be chosen to act as a sandwich material for a 100% twill-cloth plus an adequate resin mix, laminated carbon fiber exterior. Combination of which promises to achieve sufficient mechanical characteristics to sustain higher mechanical loading conditions. As Carbon fibers have high strength (3–7 GPa), high modulus (200–500 GPa), compressive strength (1–3 GPa), shear modulus (10–15 GPa), and low density (1.75–2.00 g/cm³) (MInus & Kumar, 2005).

9.1 3-point bending test (ASTM D790)

9.1.3.1 Test probes

The composite material ought to become part of the upper suspension arm is a combination of 2 layers of carbon fiber cloth, with the right combination of epoxy resins for this application, that with the AM-sourced internal structure made with PETG+CF reinforced filament, following the optimized parameters construction. The tests were carried out in ITALSIGMA FPF100 Universal Testing Machine (UTM) 100 KN capacity with a load cell 1KN. IMETRUM U2A 101 extensometer used for measuring lateral and linear extensions of the specimen. A total of 4 different structure types (Table 18) were analyzed for best mechanical characteristics, by varying the type of internal lattice structure, and different contour characteristics, as displayed in Figures 53 and 54.

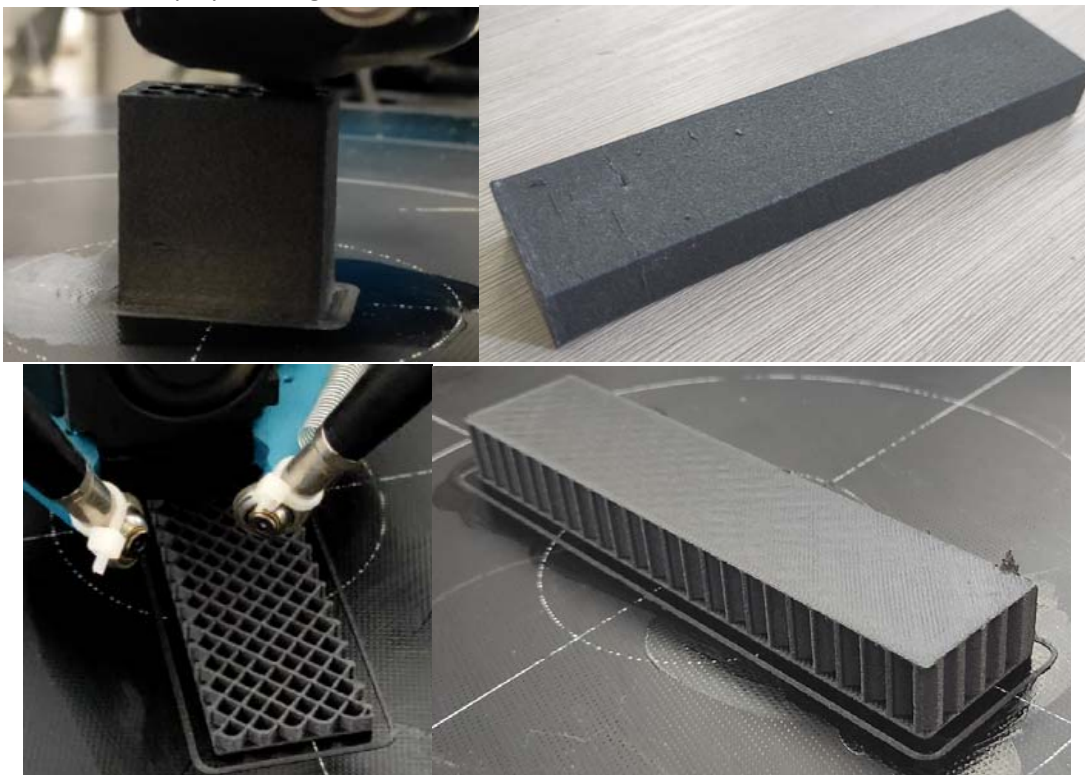


Figure 53. Probe printing with different internal structures: Honeycomb Transversal (Top) and Square Honeycomb (Down)



Figure 54. Reinforced walls Honeycomb Structure



Figure 55. Test Probes – Material: PETG + CF and 3 point bending test (ASTM D790)

The tests were performed according to ASTM D790 and were performed to test the performance of both different internal structures for the sandwich material, and the performance influence overall of manufacturing carbon fiber lamination over a PETG-reinforced material. The applied force was measured by gages located on the central application pin, which was increasing until failure.

A total of 10 probe test specimens were elaborated by following a long curing, low temperature cycle in an autoclave. The best results of CF lamination can also be achieved by following a vacuum-manual lamination process. The summary results of this exercise are shown in Table 18. Note that ideally, the flexural modulus of a material is equivalent to its Young's modulus. In practical terms, the higher the flexural modulus of a material, the harder it is to bend. Conversely, the lower the flexural modulus is, the easier it is for the material to bend under an applied force (Kwon et al., 2014).

Table 18. Test probe details for 3 bending test procedure

No	Probe Type	Weight (g)	CF Layers	Flexural Stress σ [MPa] (yield)	Flexural Strain ϵ_f (max)[MPa]	Flexural modulus E_f [GPa]	Overall Material Density (est.) (Kg/m ³)
1	Honeybomb - Transversal - 1	36.9	2	159.18	84.24	8.74	827.72
2	Honeybomb - Transversal - 2	37.2	2	127.5	99.14	7.37	827.72
3	Honeybomb - Transversal - 3	37	3	191.96	87.22	11.11	1052.19
4	Square Honeycomb (Top) + Walls - 1	26	2	96.28	106.01	4.94	687.43
5	Square Honeycomb (Top) + Walls - 2	27	3	175.27	71.79	8.94	897.87
6	Square Honeycomb (Top) - 1	18.4	2	102.64	31.23	4.97	617.28
7	Square Honeycomb (Top) - 2	18.5	2	107.77	32.79	5.22	603.25
8	Square Honeycomb (Top) - 3	19.8	3	144.75	74.09	6.57	589.23
9	Square Honeycomb (Top) - 4	19.6	2	99.56	30.29	4.82	589.23
10	Square Honeycomb (Top) - 5	19.5	2	97.57	29.69	4.72	603.25
11	Square Honeycomb (Top) - 6 - PLACF	20.3	3	135.86	31.54	7.27	827.72

Additionally, this exercise allowed to have a cost deployment for each probe, and divided by its main processes, allowing to have an estimated cost per this type of combination of materials per cm², with observed small variations between the different internal topological structures printed. Results are summarized in Table 19.

Table 19. Studied Probes Cost Deployment

No	Probe Type	Weight (g)	CF Layers	Weight (+CF) (g)	Overall Material Density (est.) (Kg/m3)	Cost AM* (€)	Cost CF (€)	Total Cost (ext) (€)	Cost per cm3 (€)/cm3	Cost AM €/cm2
1	Honeybomb - Transversal - 1	36.9	2	59	827.72	6.27	14.19	20.46	0.34	0.10
2	Honeybomb - Transversal - 2	37.2	2	59	827.72	6.29	14.19	20.48	0.34	0.10
3	Honeybomb - Transversal - 3	37	3	73	1052.19	6.28	18.54	24.82	0.41	0.10
4	Square Honeycomb (Top) + Walls - 1	26	2	49	687.43	5.45	14.19	19.64	0.32	0.09
5	Square Honeycomb (Top) + Walls - 2	27	3	64	897.87	5.53	18.54	24.07	0.40	0.09
6	Square Honeycomb (Top) - 1	18.4	2	44	617.28	4.88	14.19	19.07	0.31	0.08
7	Square Honeycomb (Top) - 2	18.5	2	43	603.25	4.89	14.19	19.08	0.31	0.08
8	Square Honeycomb (Top) - 3	19.8	3	42	589.23	4.99	18.54	23.53	0.39	0.08
9	Square Honeycomb (Top) - 4	19.6	2	42	589.23	4.97	14.19	19.16	0.32	0.08
10	Square Honeycomb (Top) - 5	19.5	2	43	603.25	4.96	14.19	19.16	0.32	0.08
11	Square Honeycomb (Top) - 6 - PLACF	20.3	3	59	827.72	5.02	18.54	23.56	0.39	0.08

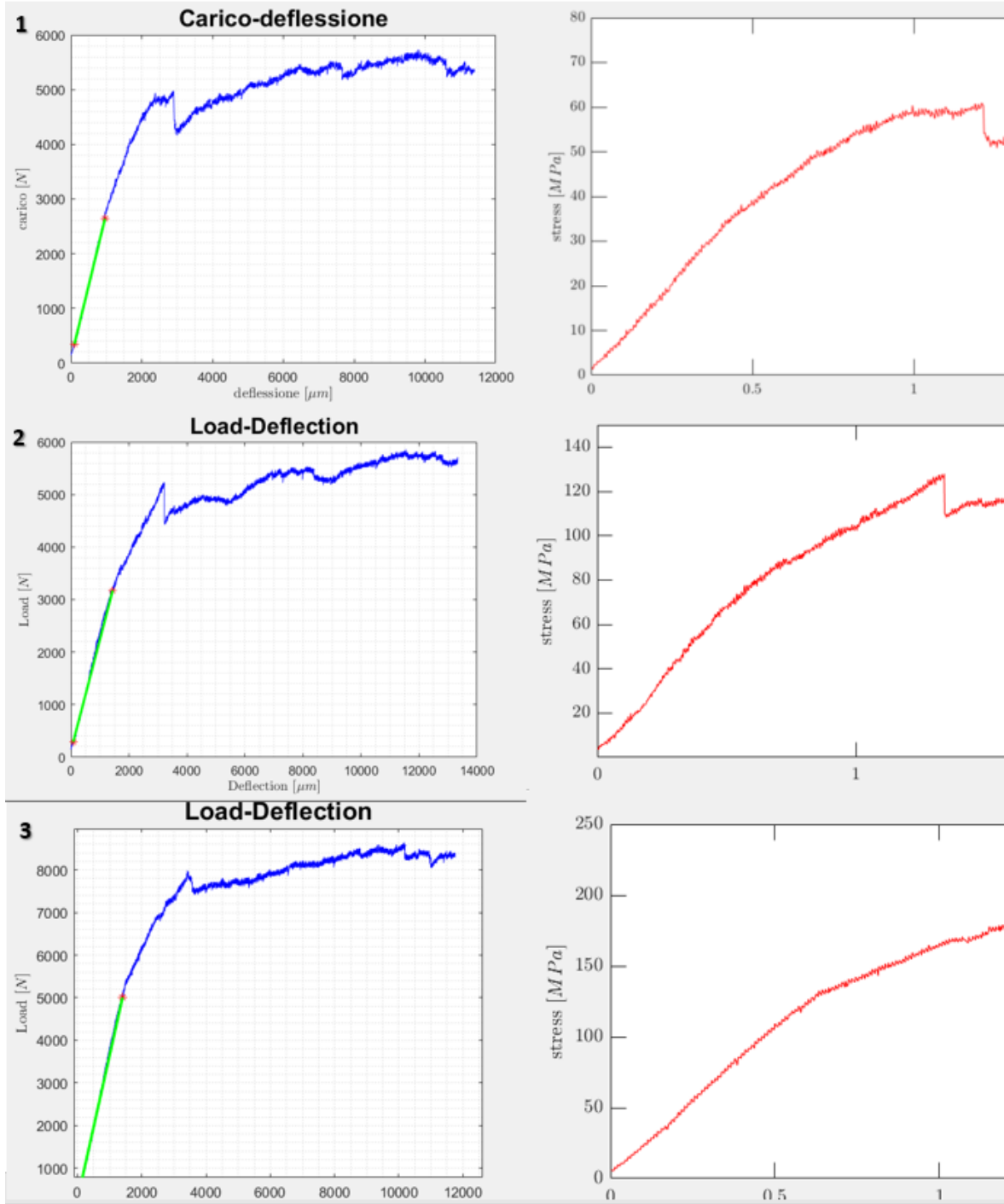


Figure 56. Test Probes 1, 2, 3 – with transversal Honeycomb structure, showed the best overall mechanical performance. Note that probe 3 has 3 layers of CF.

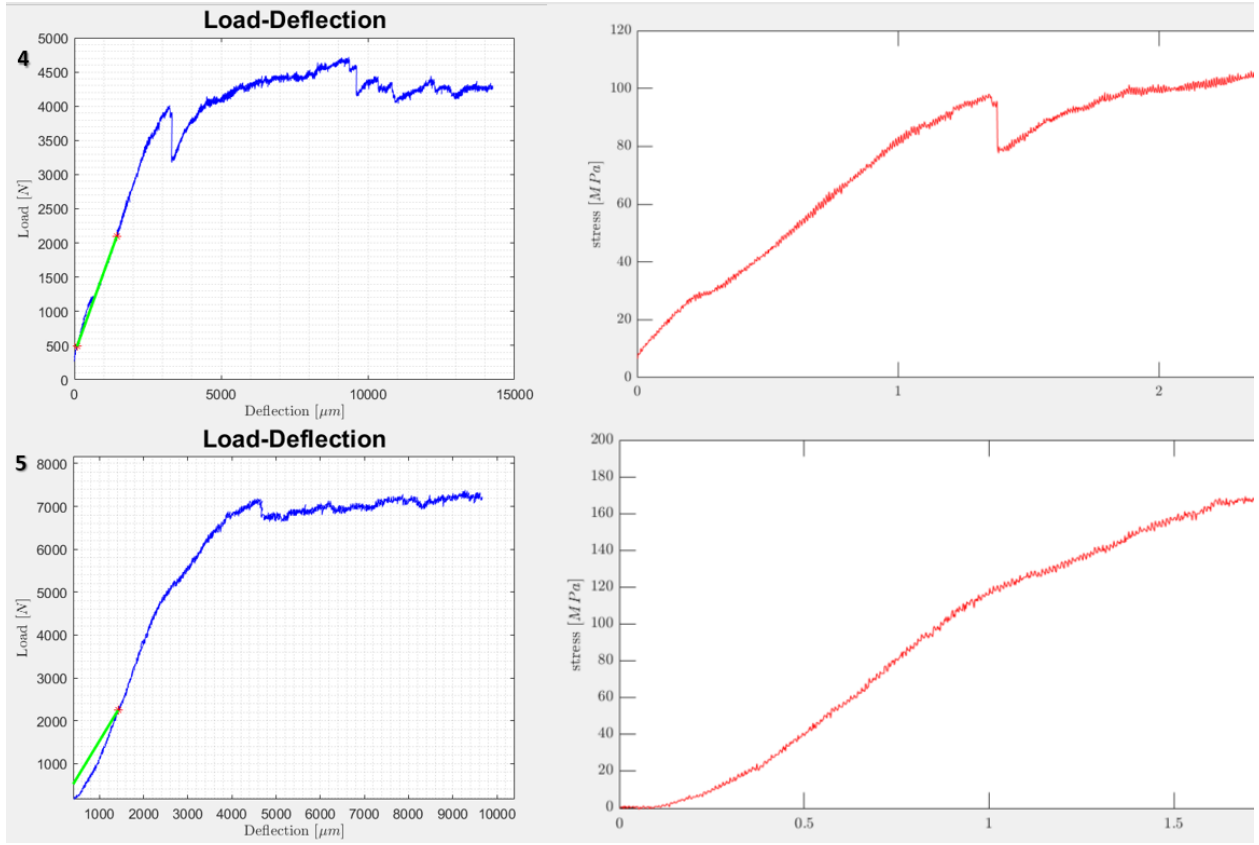


Figure 57. Test Probes 4, 5 – with Outer layer-reinforced, Square Honeycomb structure, scored second at overall mechanical performance. Note that probe 5 has 3 layers of CF.

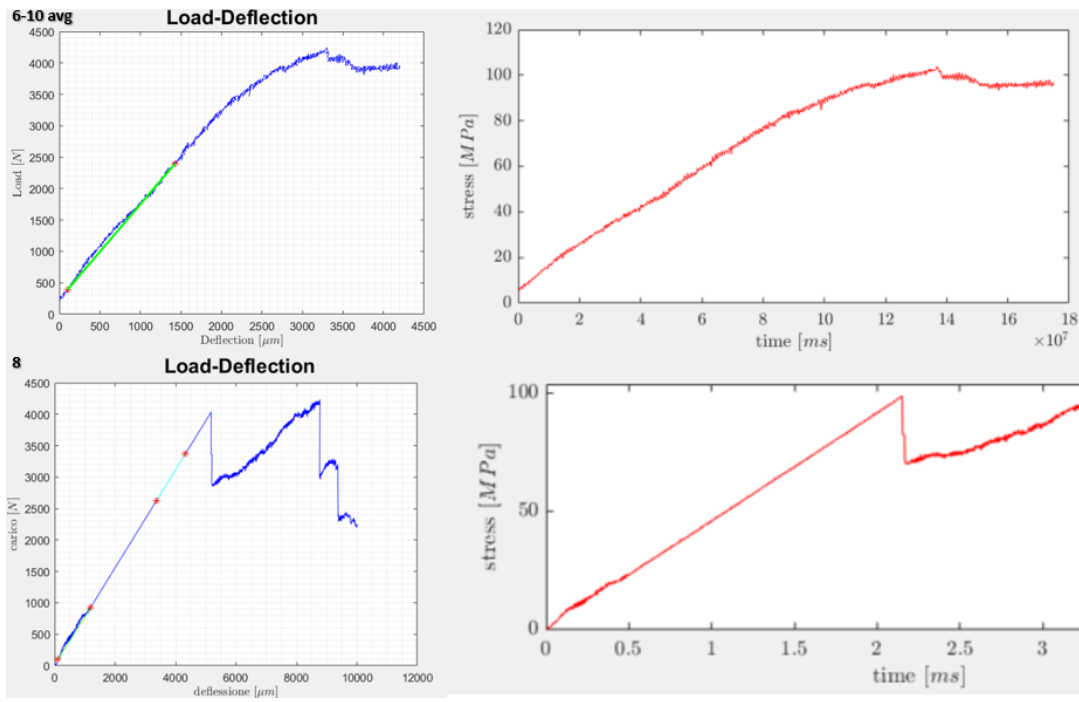


Figure 58. Average performance results of regular, square infill by Cura® in test Probes 6 to 10 with Probe 8 that has 3 layers of CF. This structure scored last overall in the test performed

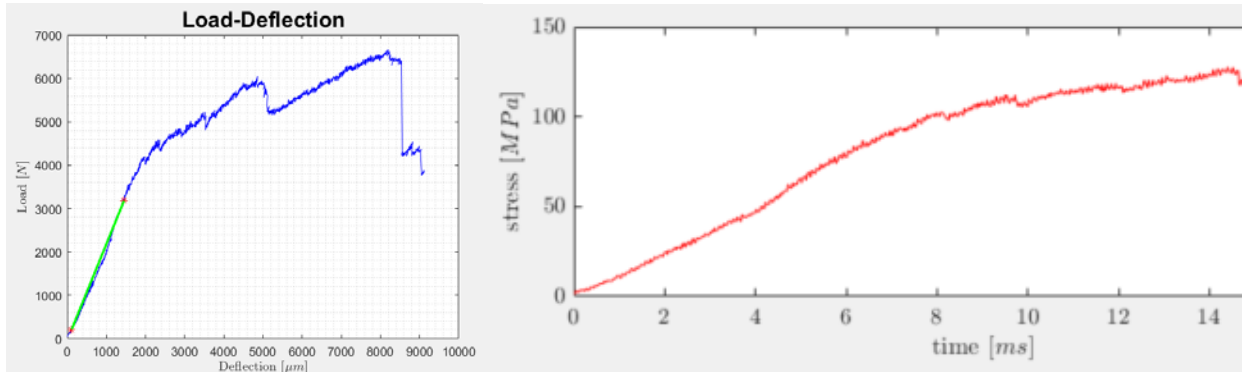


Figure 59. Test Probe 11 performance: this Probe was made with PLA-reinforced filament, and with 3 CF layers. Showed a rather elastic response behavior than the PETG counterparts.

The results of the 3-point bending test were useful to determine the adequate structural configuration for this application. Comparison of results among 3 main structural solutions were obtained (Table 20): 1) Transversal Honeycomb, 2) Regular Square Honeycomb with wall reinforcement; and a 3) Regular square Honeycomb without reinforcement. The top scored configuration was the Transversal Honeycomb with 3 layers of CF reinforcement and adding an extra layer of CF scored a further increase in a 50% increase of Avg. Flexural Stress (yield) increase and a 24% increase in Flexural Modulus.

Table 20. Results Evaluation of Analyzed Structures

Overall Structural Results from 3 Point Bend Test			
Top Scored Structure Solution	CF layers	Flexural Stress σ [MPa] (yield)	Flexural modulus E_f [GPa]
Honeycomb - Transversal - 3	3	191.96	11.11
Variations	-	Variation (%)	
Honeycomb Transversal	2	-21%	-27%
Vertical Honeycomb + Reinforced Walls	3	-9.50%	-24%
Vertical Honeycomb + Reinforced Walls	2	-50.10%	-46%
Vertical Honeycomb + No Reinforcement	3	-25%	-41%
Vertical Honeycomb + No Reinforcement	2	-47%	-55%

Nevertheless, the top-scored solution was not recommended for the final production version of the structural elements of this project, given especially due to the considerable increase of production time, materials, and hence the cost of this part in comparison to the other solutions of this study (about 3x the printing time of their counterparts, and 15% more material consumption and weight).

9.2 Carbon Fiber Lamination Strategy over PETG-CF reinforced polymer

However, the process and the quality of the end product will be different. Autoclaves are used to heat the composite material to high temperatures and pressures, which improves the properties of the carbon fiber, such as strength and stiffness. The best solution for this application would be to have a low temperature curing or if possible, an ambient temperature lamination process. Without an autoclave, other methods to cure the composite are needed, such as by using an oven, a vacuum bag, or a press. Additionally, more manual labor has to be done, such as hand-layering the carbon fiber, which can be time-consuming and challenging. Overall, building something from carbon fiber without an autoclave can be done, but it may not have the same level of quality or performance as something built with an autoclave.

9.2.1 Carbon fiber characteristics

The chosen Carbon Fiber Twill for use in this application would be a Carbon fabric of 600 g/m² for high performance applications where high strength and low weight are required. Ideal for producing epoxy, vinyl ester and urethane-acrylate composite parts or tools by hand lay-up, infusion or RTM/ RTM light; Figure 60 shows the characteristics for a Yarn-type: 12K (12000 filaments per strand of yarn) and 800 tex (both warp & weft) type of Carbon Fiber Twill Fabric.

CHARACTERISTICS		Nominal	Tolerance	Normative
Mass per unit area	g/m ²	592	± 5%	ISO 4605
Weave		2X2 Twill		ISO 2113
Width	mm	1000	± 2,5%	ISO 22198
Thickness	mm	0,6	± 2,5%	ISO 5084(**)
Other informations		Loomstate		

Nominal Construction		WARP		WEFT	
Fiber Description		HR Carbon Fiber 12K - 800 tex		HR Carbon Fiber 12K - 800 tex	
Thread Count	ends/cm	3,7	ISO 4602	3,7	ISO 4602
Weight Distribution	g/m ²	12K Carbon	296	12K Carbon	296
	%		50%		50%
Selvages		Weaving style	LENO	Type of Fiber	HM polyester 22 tex

(**) Theoretical thickness for an epoxy laminate with 40% of reinforcement in volume.

Figure 60. Twill Carbon fabric of 600 g/m²

Table 21. Mechanical Properties HT-Carbon Fiber:

Mechanical Properties HT-Carbon fiber:	
Tensile strength:	4200 MPa
Tensile modulus:	240 GPa

Fibre density:	1,78 g/cm ³
-----------------------	---------------------------

9.2.2 Epoxy Resin characteristics

The suggested epoxy Resin characteristics for this application is MasterBond® EP42HT-2LO Polymer System displayed in Figure 61, this epoxy can be used in aerospace, optical, electronic, electro-optic and specialty OEM type applications. Since EP42HT-2LO passed NASA low outgassing specifications, it can be used in special situations, such as vacuum environments where that property is obligatory. Mechanical Properties of this element are shown in Table 22.



Figure 61. MasterBond® EP42HT-2LO Polymer System

Table 22. EP42HT-2LO Technical Data Sheet

EP42HT-2LO Technical Data Sheet	
Typical Properties	
Tensile strength, 24 °C	83 - 90 Mpa
Tensile lap shear, aluminum to aluminum, 24°C	14 - 15.2 Mpa
Tensile modulus, 24°C	2760 - 3100 Mpa
Hardness, 24°C	80-90 Shore D
Hardness after 1,000 hours 85°C/85% RH	90 Shore D
Service temperature range	[-51°C to +232°C]
Mixing and Curing	
Mixing Ratio A:B	100:50 by volume
Cure Schedule	
24°C	48 - 72 h
93°C	2-3 h

Moreover, a proper epoxy component has to be chosen to guarantee the metallic Bushings to be adhered into the 3D Printed structure to guarantee the best force distribution throughout the Bushings contact surface. EP42HT-2LO Epoxy system datasheet states that is capable to perform such multi material bonding.

9.2.3 3D scanning

Another IDES tool from Industry 4.0 to be used in the study is the quality assessment of the constructed parts by means of 3D scanning. Equipment like the Faro® Quantum 3D Scanner (Figure 62) is able to accurately create a point cloud of the surfaces in contact by means of the optically superior FAROBlu Laser Line Probe or 3D color scanning present in the Prizm Laser Line Probe. The measurement speed and ergonomics of use of this device are given by an 8-Axis DOF movement of this device. The eighth axis enables rotation of what is being measured in real-time – meaning no difficulty reaching around the object, and no need to move the arm into different locations within the process. This eliminates wasted time and offers an easy-to-use measurement solution that allows users to focus on the actual measurement and not on the measurement processes.



Figure 62. Faro Quantum® 3D Scanner

The device gathered a point cloud was obtained with the aid of Geomagic® Control X software, and then compare the measured point cloud with the model, so a tolerance analysis can be performed; a correlation Histogram is generated (Figure 109) so the fit tolerance of both compared elements can be seen.

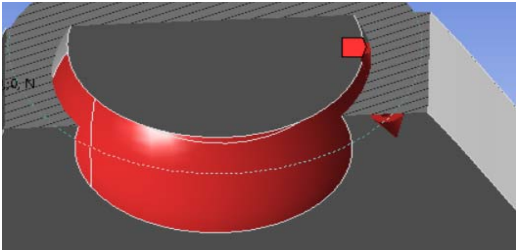
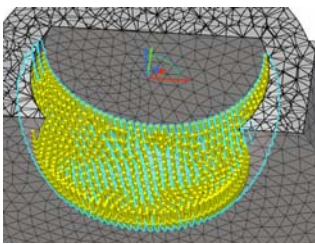
10.IDES Method Tools and Software Accuracy Exercise

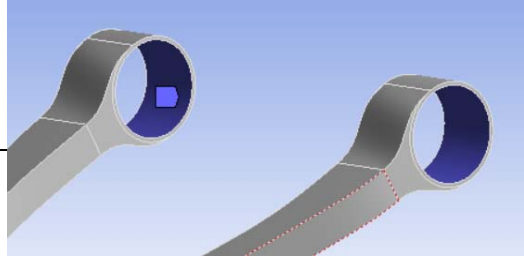
Given the description of the IDeS methods and tools to be used in this study on Figure 10, and the list of HOW ideas to execute this project on Table 4, the project will focus on the application of lightweight technologies, using state of the art approaches to this item, given by Additive Manufacturing processes and the inclusion of composite materials and also by Topological optimization, aimed to conduct

lightweight solutions to an existing component. The inclusion of post manufacturing processes are also to be taken into account depending on the material and overall mechanical requirements of each item.

It's worth noting that, the development of this study demanded a specific valuation of software capabilities for design and analysis of the solutions, ultimately needed for reaching a trustful solution. Topology optimization exercises were performed in ANSYS, CREO and NTOPOLOGY to evaluate the calculation accuracy of each software. Preliminary Structural Set-up was outlined by means of 2 FEM Software with the target: to realize the computational differences among the used software results. the same boundary conditions for each analysis were used in both ANSYS and nTopology (Table 23); This analysis resulted in very similar results from both software with correlation given in the order of 0.01.

Table 23. Preliminary FEM Software Computational Accuracy Analysis Differentiation

	ANSYS			nTopology		
Material	first name	PLA-CF		first name	PLA-CF	
	elastic module	5000	MPa	elastic module	5000	MPa
	Poisson's ratio	0.39		Poisson's ratio	0.39	
	enervation	48	MPa	enervation	-	-
	density	1.35	g/cm ³	density	1.35	g/cm ³
Mesh	form elements	tetrahedral		form elements	triangular	
	element side dimension	2	mm	size min items	2	mm
				size max items	2.25	mm
	order items	quadratic		order items	quadratic	
	grow rate	1.2		grow rate	1.2	
	span angle	coarse		span angle	30th	
	number of nodes	298190		number of nodes	292606	
number of items	179554		number of items	181228		
Boundary conditions	loaded module	7566	No	loaded module	7566	No
	component x	1000	No	component x	1000	No
	component y	-7500	No	component y	-7500	No
	component z	0	No	component z	0	No
						

	interlocking	interlocking
		
	support (avoid bending)*	support (avoid bending)*

Static Analysis	Global Displacement Results					
	Total displacement					
	maximum	1.8688	mm	maximum	1.88537	mm
	minimum	0	mm	minimum	0	mm
	Displacement x direction					
	maximum	1.6173	mm	maximum	1.63479	mm
	minimum	-0.71628	mm	minimum	-0.7098	mm
	Displacement and direction					
	maximum	0.073222	mm	maximum	0.07417	mm
	minimum	-1.6266	mm	minimum	-1.63607	mm
	Analysis results on Similar points					
	Point A					
	Total displacement	1.5967	mm	Total displacement	1.60491	mm
	Displacement x	0.73042	mm	Displacement x	0.74096	mm
	Displacement y	-1.4189	mm	Displacement y	-1.42361	mm
	Von Mises stress	3.3027	MPa	Von Mises stress	3.2533	MPa
	Point B					
Total displacement	0.093123	mm	Total displacement	0.08924	mm	

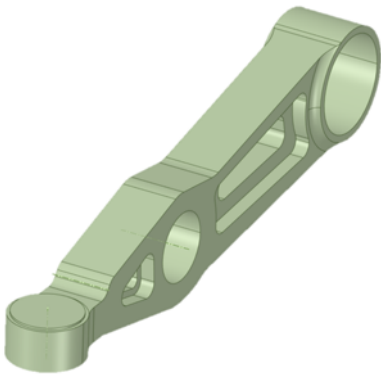
	Displacement x	-0.0505	mm	Displacement x	0.05298	7	mm
	Displacement y	0.071216	mm	Displacement y	0.06989	8	mm
	Von Mises stress	24.768	MPa	Von Mises stress	24.915		MPa

11.Product design> Topological Optimization

11.1 Lower Suspension – Steering Arm

The first component to optimize is the Suspension Lower Arm, or the “Steering” Arm of which the starting data from the CAD model is the following:

Table 24. Original Part Data – Lower Suspension Arm

	
ORIGINAL PART DATA	
Material	Al forged
Weight	1.74 Kg

The topological solution for this part was assessed in ANSYS, in which the obtained study load cases from part 8.2 were executed. The analysis started by modelling a draft, raw part that maintains just the basic geometrical constraints of the part (Figure 63). Total Deformation Distribution; and Equivalent Stress Distribution pre Optimization (Figure 64), so the result obtained after 28 iterations (Figure 65).

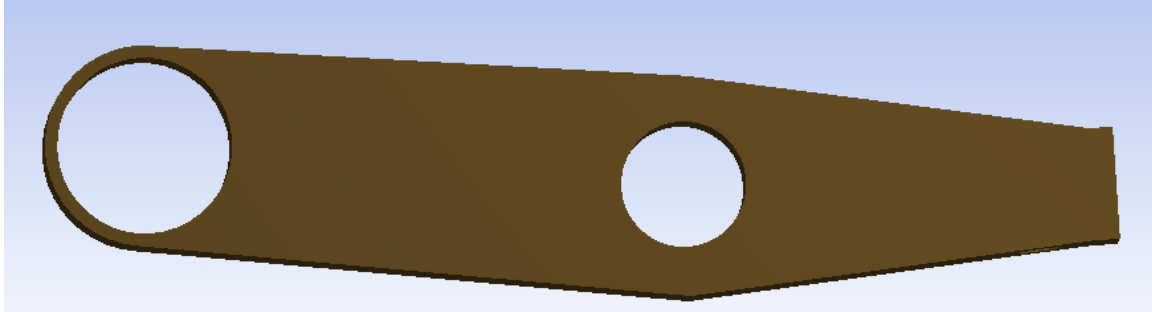


Figure 63. Raw lower arm component for Topological Optimization Exercise in Ansys

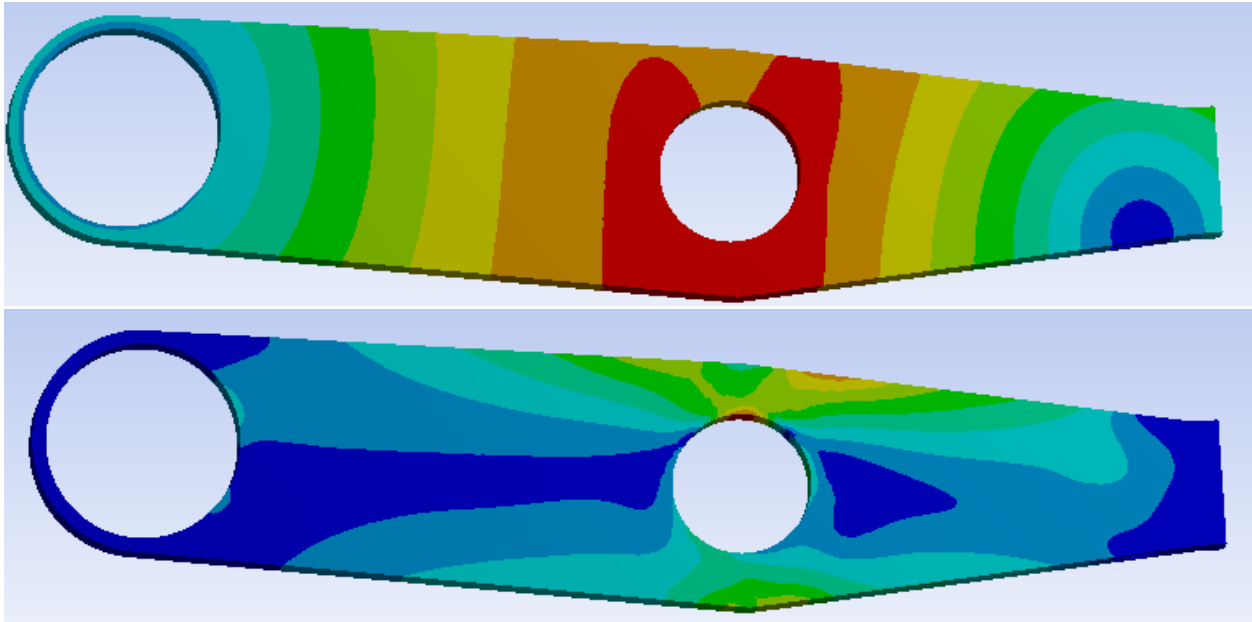


Figure 64. Top) Total Deformation Distribution; and Down) Equivalent Stress Distribution pre-Optimization

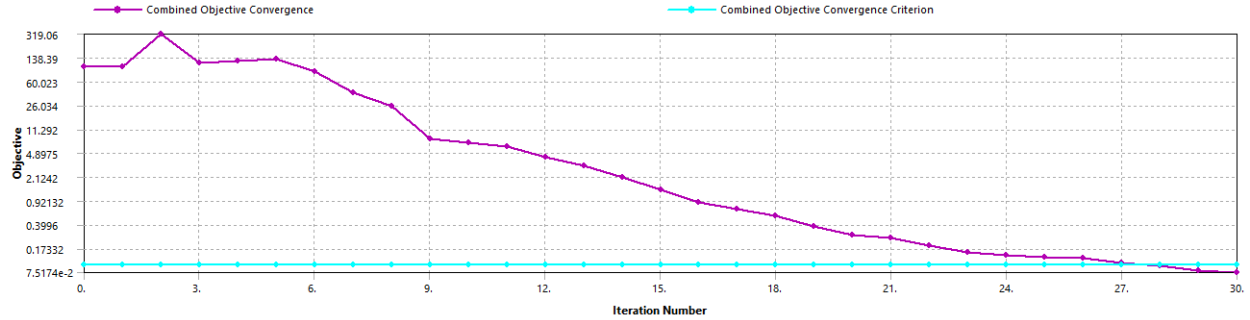


Figure 65. Optimization Solution Information, shows convergence after 28 iterations

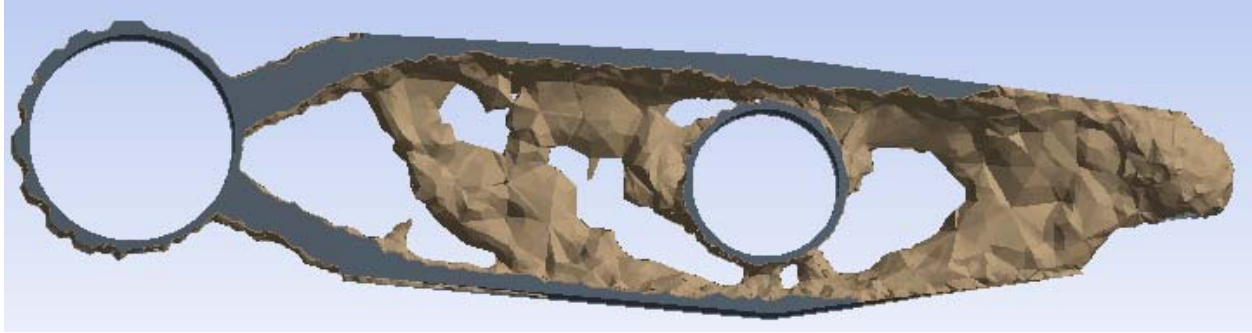


Figure 66. Obtained Part distribution density after optimization. Grey zones are to keep, and the brown zones are parts in which the material is cut up to 60%

Then the results obtained from ANSYS topological were translated into a parametric model that considers the material sections taken off by the software that denotes the areas in which the material content can be decreased an earlier iteration of this solution that was proposed with the design in Figure 67. This first iteration obtained a reduced part weight of 1.176 Kg, about 550 grams less than the original part weight. Mechanical resistance and fatigue analysis on this part (Figures 68-70) showed opportunities for further optimization.

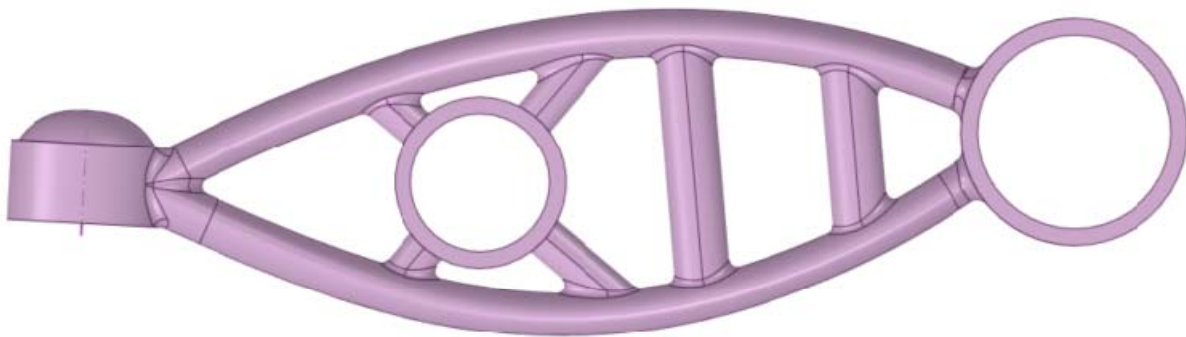


Figure 67. Early Proposal for Topological Optimized Lower Arm

This part was analyzed in ANSYS for its structural integrity, by which the max Total Deformation (Figure 68) of 0.3926 mm and max Equivalent Stress of 237.7 MPa (Figure 69). The overall results from this exercise were somewhat satisfactory, but the lifecycle assessment (Figure 70) gave a lower value of 4.69×10^4 cycles which gave the opportunity to optimize the design.

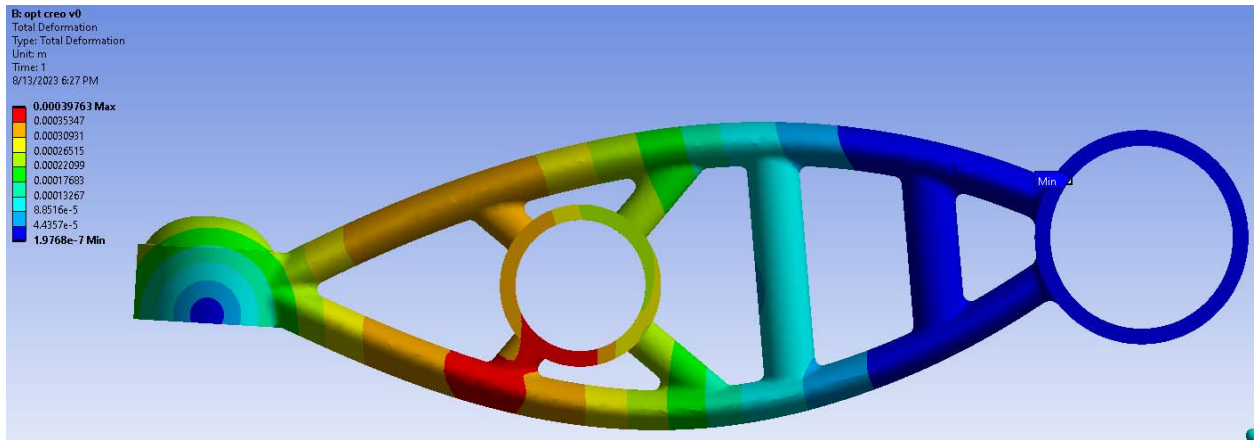


Figure 68. Total Deformation for Early Proposal – Lower Arm

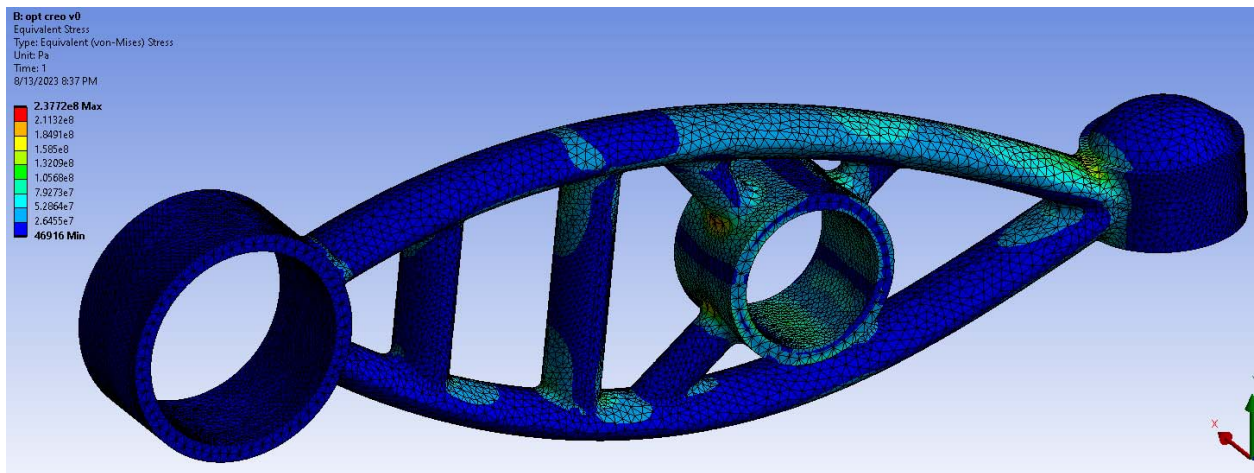


Figure 69. Equivalent Von Mises Stress – Lower Arm

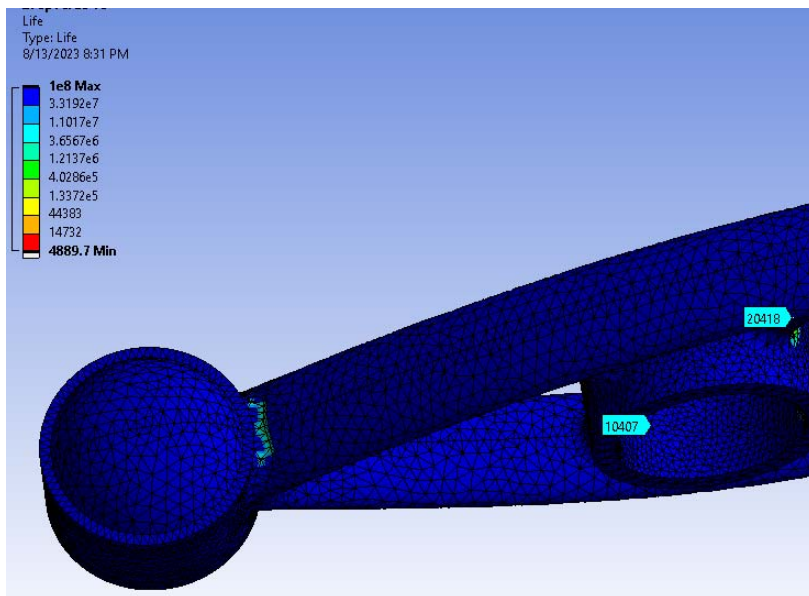


Figure 70. Fatigue assessment according to Soderberg's theory.

The optimization inputs came from the analysis of load distribution across the geometry of the part structure, there were areas in which the load was little distributed and small zones which required a better load distribution approach. Therefore, subsequent optimization iterations were performed on this part, with the aim of modifying the geometry (Figure 71) and delivering the lowest overall part Equivalent Stress, and Total Deformation, whilst delivering highest part life analysis by Fatigue. The Final iteration of this part is shown in Figure 71. Finally, the best solution on Figures 73 - 75 delivered a reduction of 42% of the max Equivalent Stress, 74% reduction in Total Deformation, and an increase in Fatigue life expectation of 3 orders of magnitude. This final iteration obtained a reduced part weight of 1.054 Kg, about 696 grams less than the original part weight. The summary specifications of the optimized part are displayed in Table 25. The overall part fabrication cost was estimated in 650 € which is 2.16 times the cost of fabrication of the stock part; it has to be outlined though, that the stock part cost is the industrialized part cost and does not include costs of tooling and subsequent costs for additional processing times that are 0 for the AM solution.

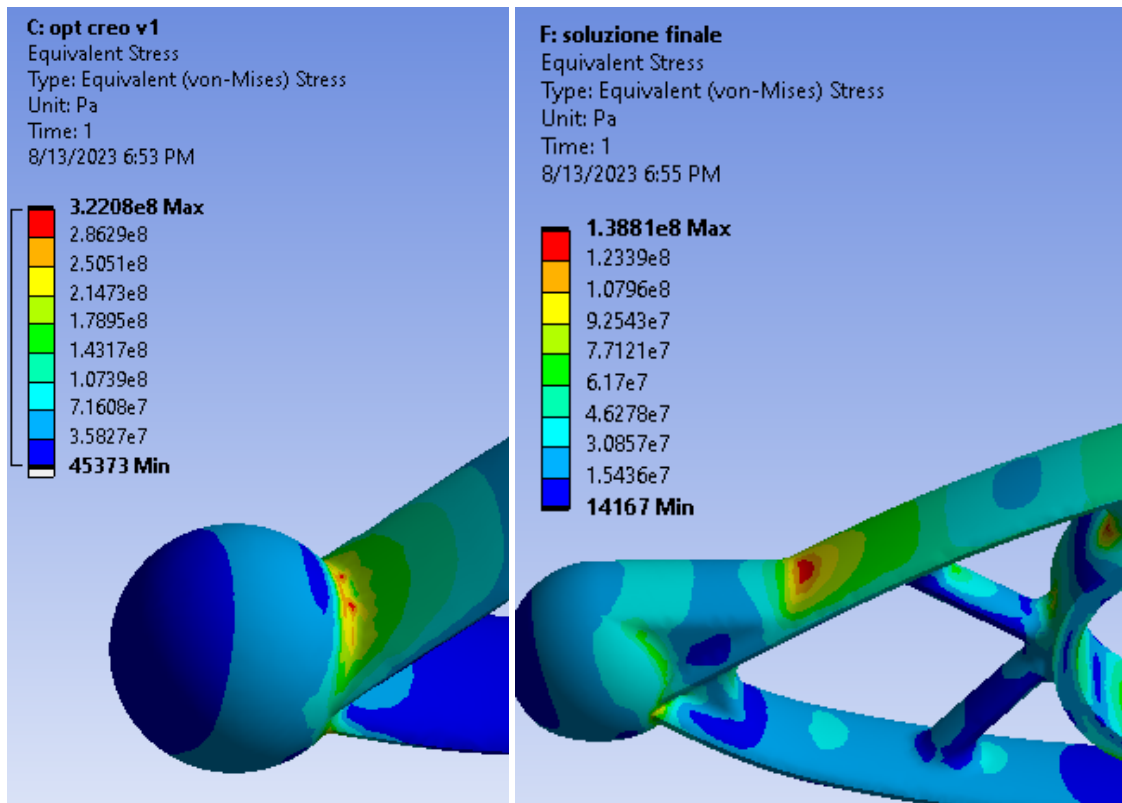


Figure 71. Geometry Optimization performed in the joint area, the best solution (right) delivered a reduction of 57% of the max Equivalent Stress.

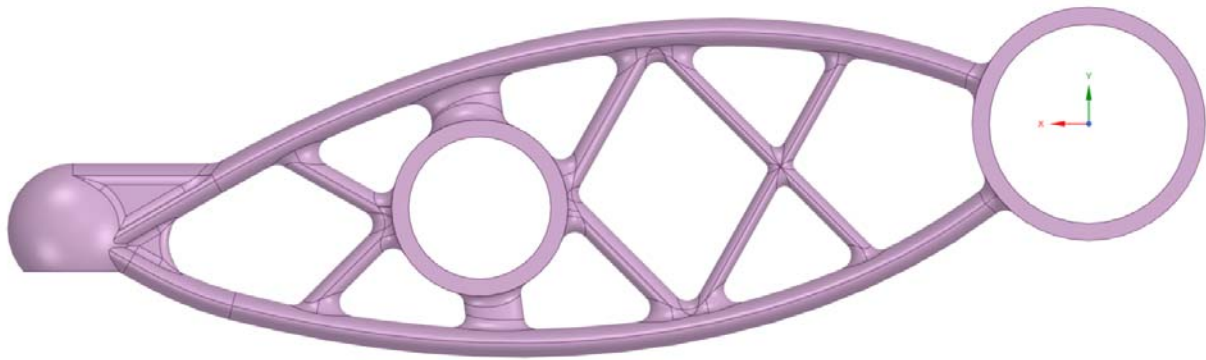


Figure 72. Optimized Lower Arm Solution.

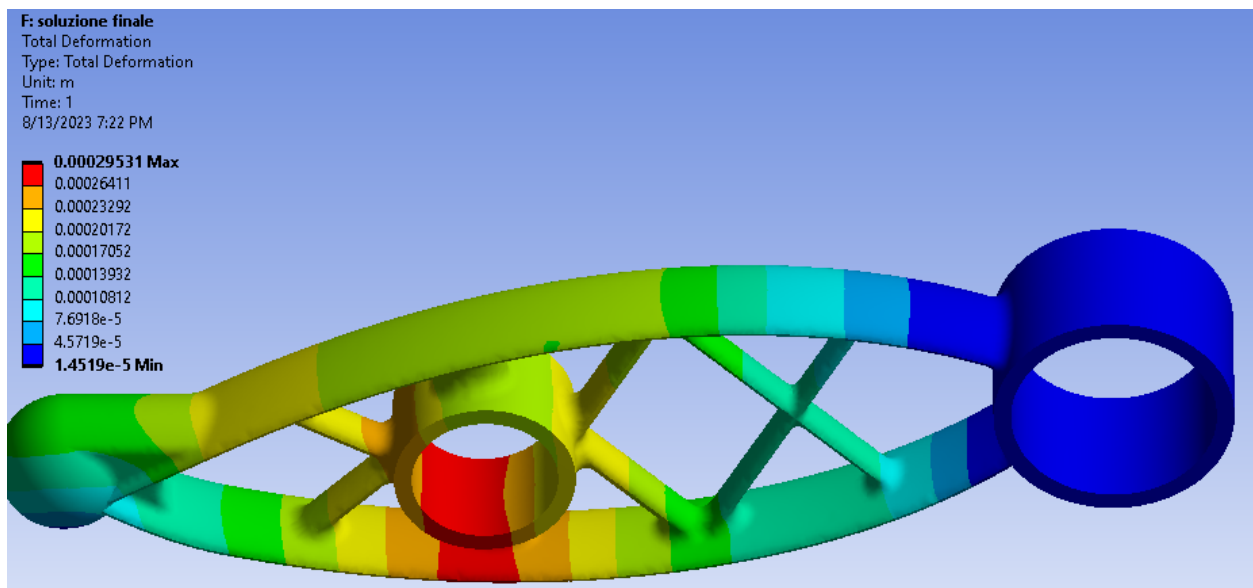


Figure 73. Geometry Optimization performed in the joint area, the best solution (right) delivered a reduction of 74% of the max total Deformation.

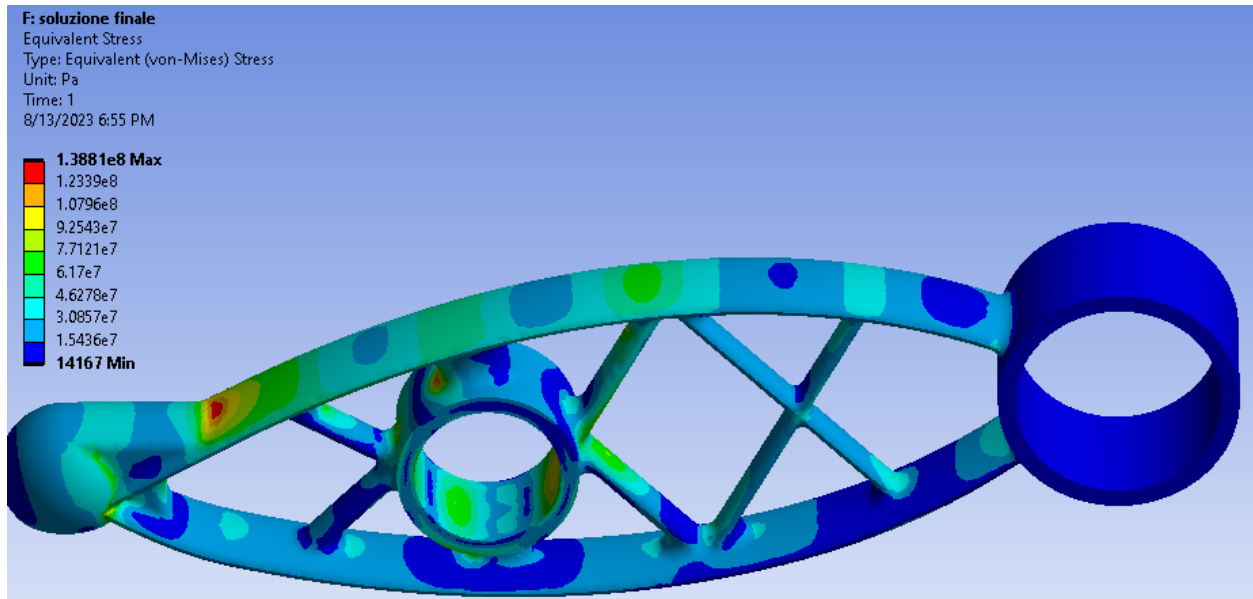


Figure 74. The best solution delivered a reduction of 42% of the max Equivalent Stress.

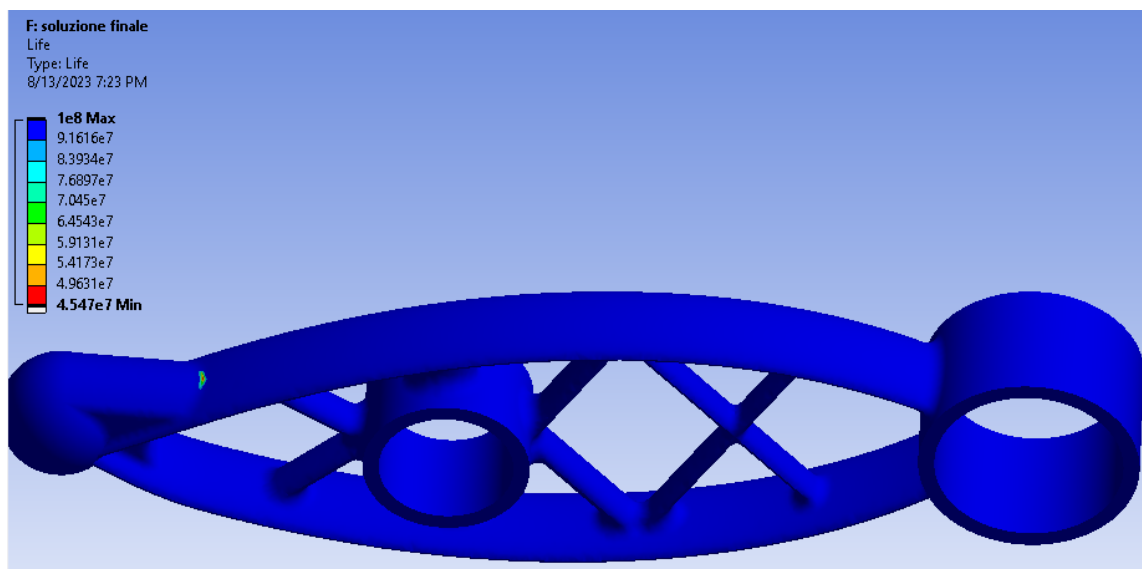


Figure 75. The best solution delivered an important increase of 3 orders of magnitude of the lowest Life Cycle expectation.

Table 25. Optimized Lower Arm Summary; *: not considering tooling costs.

SUSPENSION LOWER ARM - OPTIMIZED		
Characteristic	Value	Variation
Overall Weight	1.054 Kg	-40.25%

Material	AlSiMg10	Forged AL
Heat Treated	yes	yes
Total Part Cost (€)(est)	650	300*

11.2 Upper Suspension – Control Arm

Afterwards, the suspension Upper Arm, or the “Control” Arm of which the starting data from the CAD model is the following:

Table 26. Original Part Data – Upper Suspension Arm

ORIGINAL PART DATA	
Material	Steel forged
Weight	2.4 Kg

The topological solution for this part was first assessed in ANSYS, in which the obtained study load cases from part 8.2 were executed. The analysis started by modelling a draft, raw part that maintains just the basic geometrical constraints of the part, it was chosen to start up with a highest surface part, thought as a first instance for better results from a composite material (Figure 76).

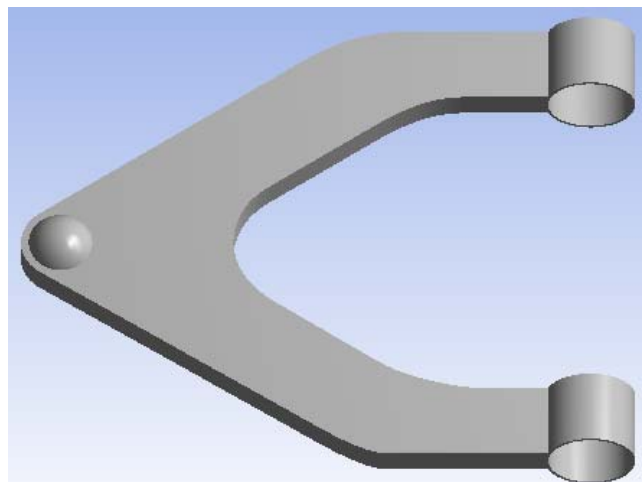


Figure 76. Raw component for Topological Optimization Exercise in Ansys

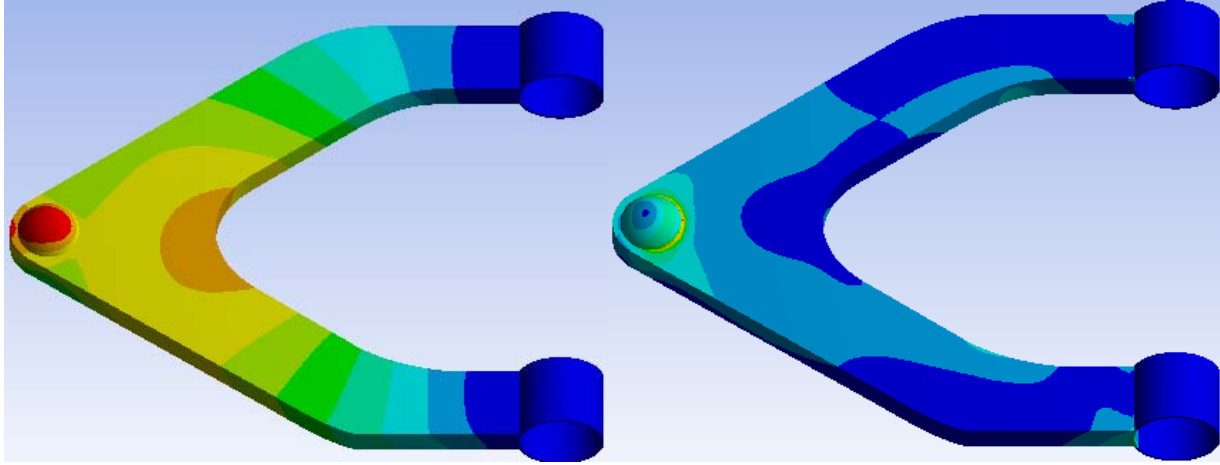


Figure 77. Left) Total Deformation Distribution; and Right) Equivalent Stress Distribution pre Optimization

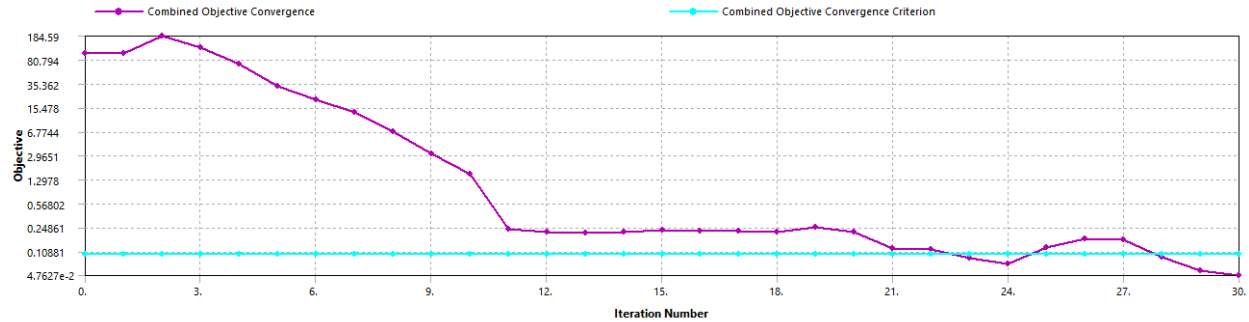


Figure 78. Optimization Solution Information, shows convergence after 22 iterations

As seen on Figures 77-78, the equivalent Stress distribution on the part’s surface showed a much lower loaded part that envisioned, so most of the surface area of this draft part was demolished for best performance, the Figure 79 shows the overall result of ANSYS topological optimization analysis.

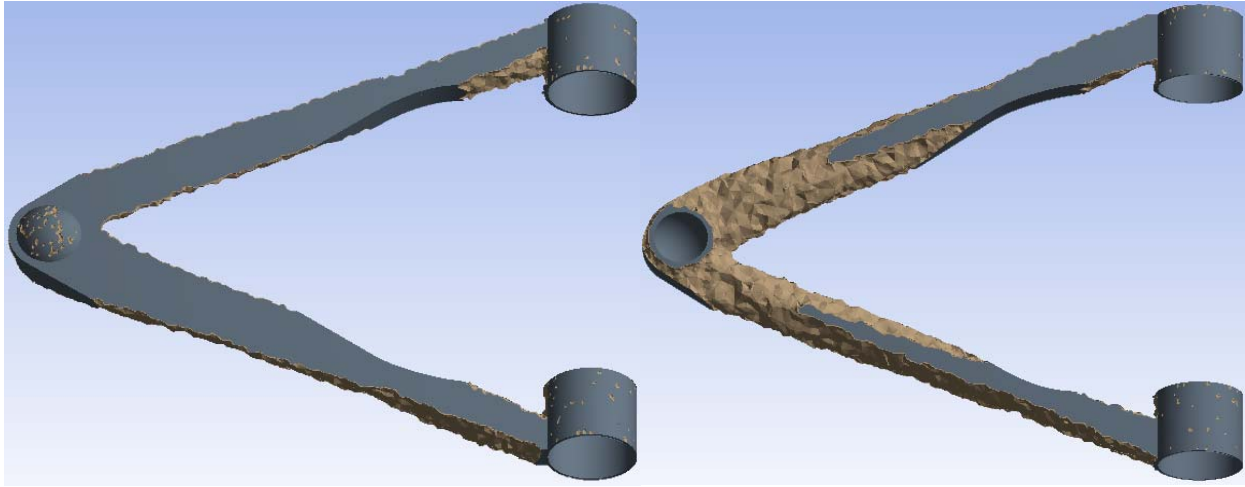


Figure 79. Upper arm distribution density after optimization. Grey zones are to keep, and the brown zones are parts in which the material is cut up to 60%

11.2.1 Optimization of internal structure:

For this case, given the forces in action, the Upper Arm optimization sequence for DfAM took 2 paths, each one of them related to a different AM method.

- 1) A Metallic SLM typology of AM was pursued as well, given the simplicity of this part to be analyzed and the overall speed of manufacturing.
- 2) A Polymer-reinforced filament FDM typology of AM was chosen driven by the overall part cost effectiveness and suitability of materials for this specific application.

11.2.1 SLM AM solution – AlSiMg10 material.

The optimization inputs came from the analysis of the FDM polymer solution, as a deliverable sourced from a traditional, metallic element was imperative to show the correlation of the Topological optimization exercise that can deliver an overall longer part life expectancy.

Therefore, subsequent optimization iterations were performed on this part, described in Figure 80 with the aim of modifying the geometry for best results (Figures 81 – 82) to deliver the lowest overall part Equivalent Stress, and Total Deformation, whilst delivering highest part life analysis by Fatigue. Then the analysis was done after including the Top-scored internal lattice structures seen in section 8.5.2 (Figures 83-84); The final iteration with optimized ball joint geometry and Honeycomb Topological Optimized structure showed in Figures 84-85 a Max Stress of 35.537 MPa, a Max Deformation of 0.15 mm, calculated Life of 1e8 cycles min, and a minimum Safety factor of 3.65. This solution delivered a reduction of 85% in Total Deformation, and a 20 % in max Stress. This final iteration (Figures 86-87) obtained a reduced part weight of 1.254 Kg, about 35% less than the original part weight. The summary specifications of the optimized part are displayed in Table 27. The overall part fabrication cost was estimated in 550 € which is 5.23 times the cost of fabrication of the stock part; but in the same manner as the lower arm stated before, the stock part cost is does not include costs of tooling and subsequent costs for additional processing times that are 0 for the AM solution.

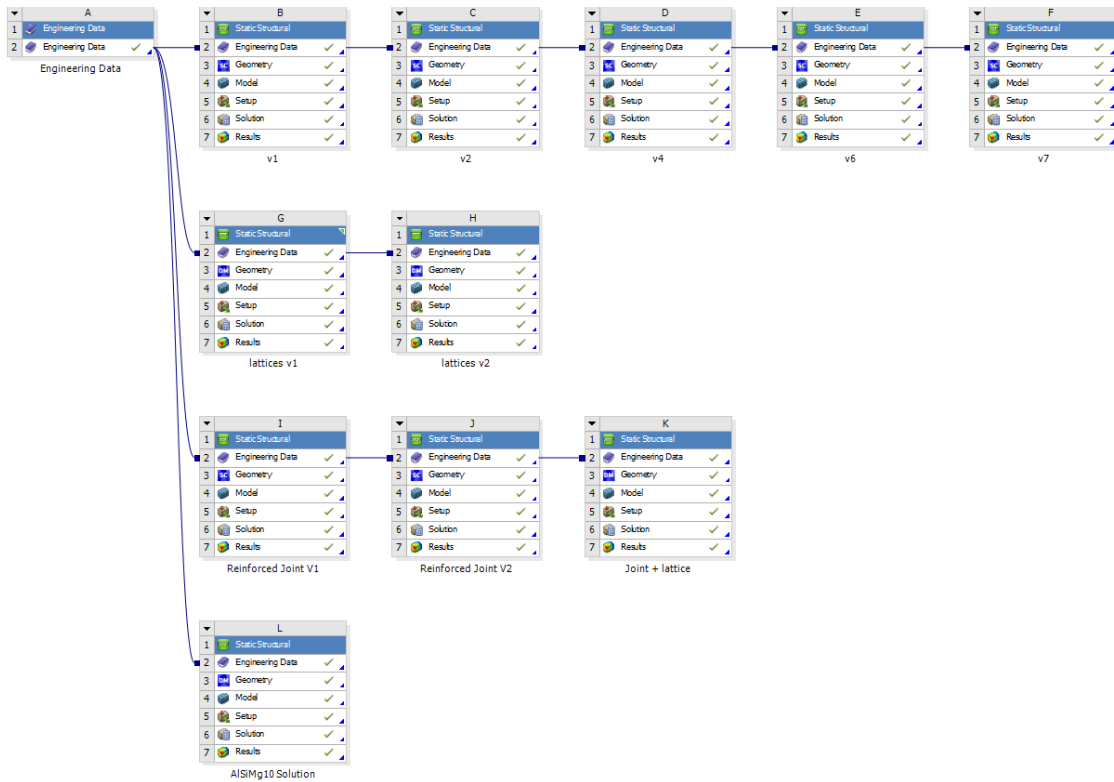


Figure 80. Project Schematic layout of the Upper Arm focused on SLM process.

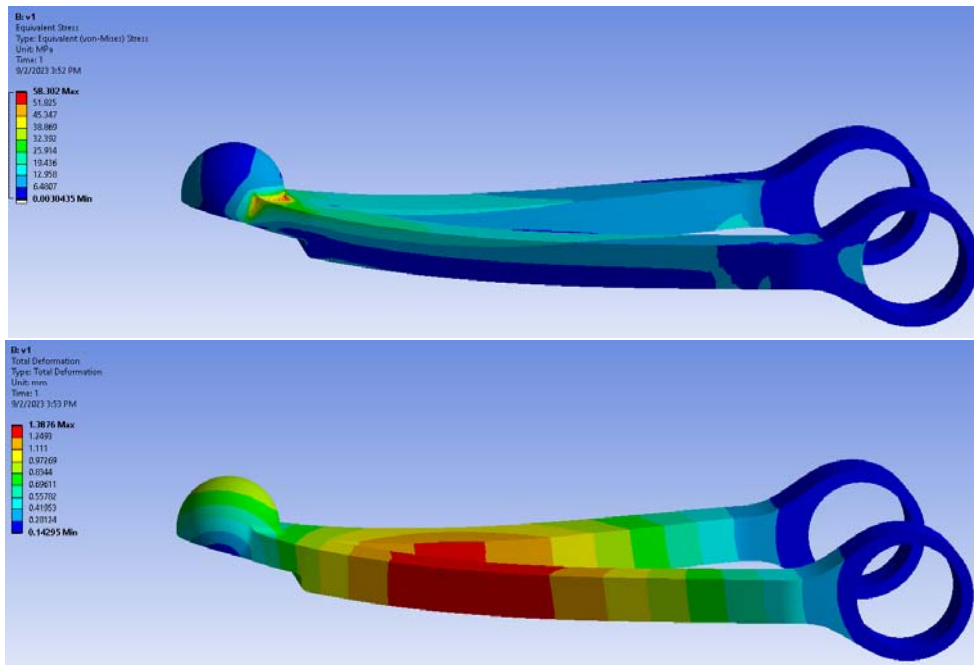


Figure 81. First Iteration with geometry V1; Max Stress= 58.302 Mpa; 1.38 mm Max deflection

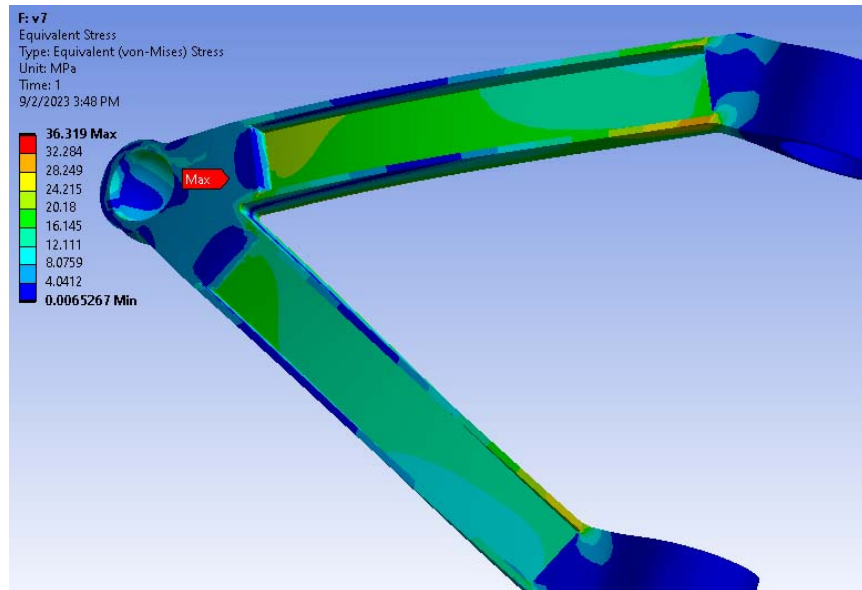
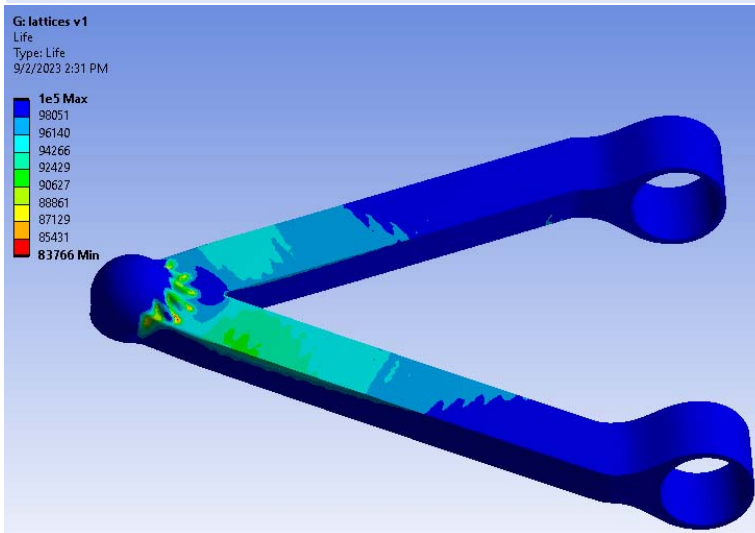
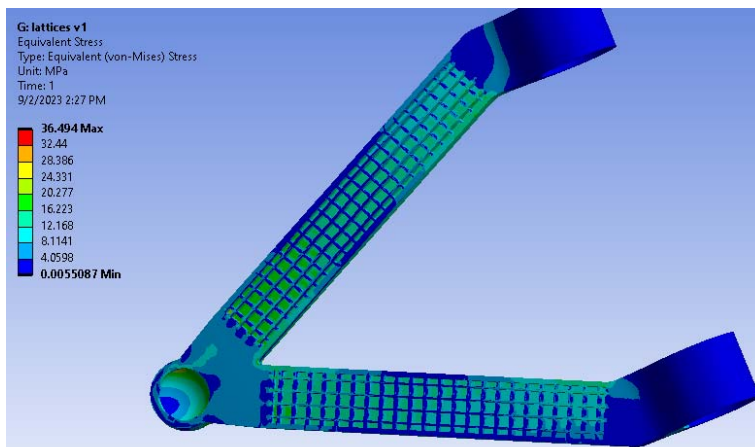


Figure 82. Iteration #7 geometry no TO- V7 Equivalent Stress distribution – part without Lattice



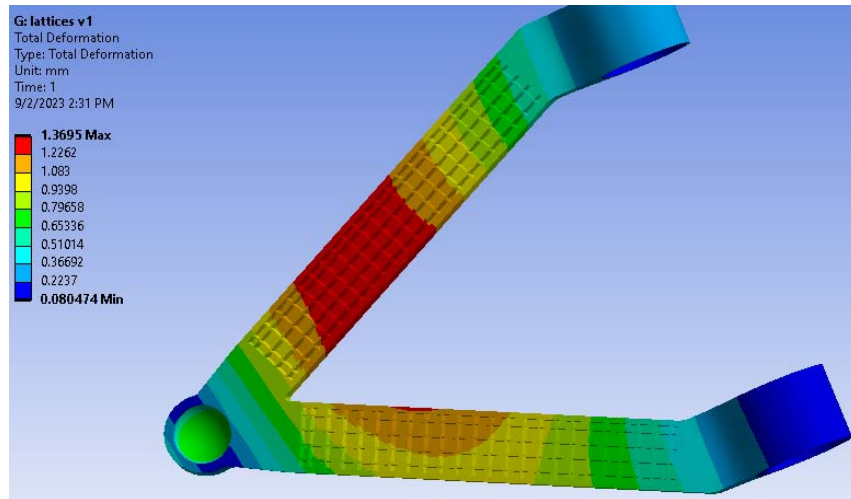


Figure 83. Results on Initial lattices Iteration: Square mesh. Note the lower Stress Distribution

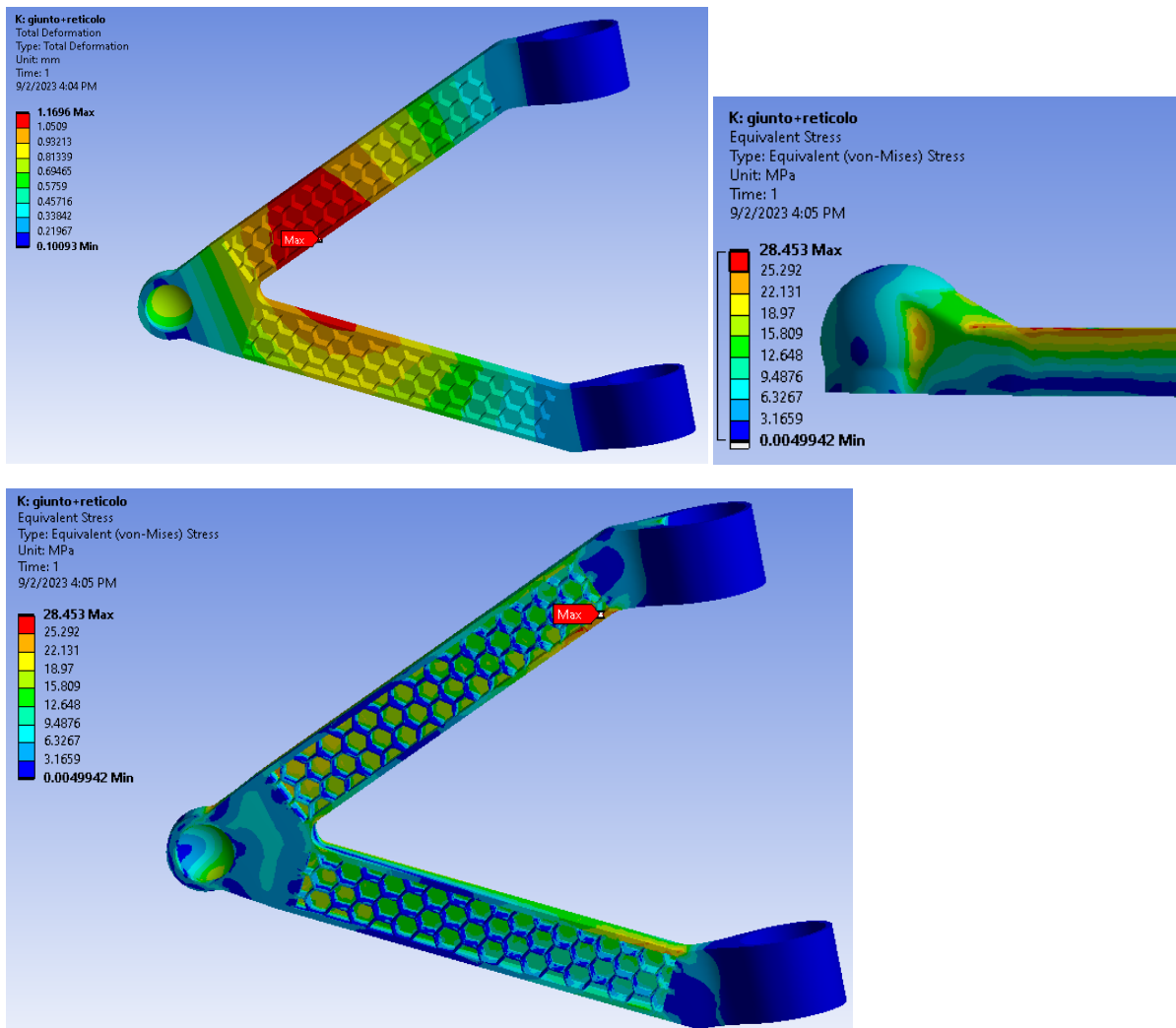


Figure 84. Iteration with optimized ball joint geometry and Honeycomb TO. Max Stress = 28.453MPa; Deformation is still high at 1.96 mm.

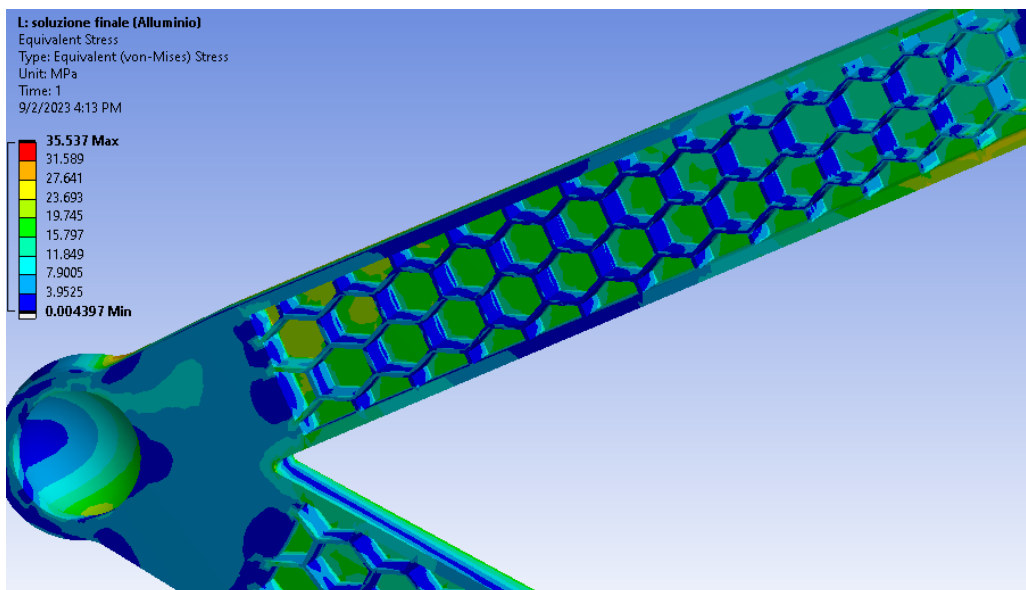
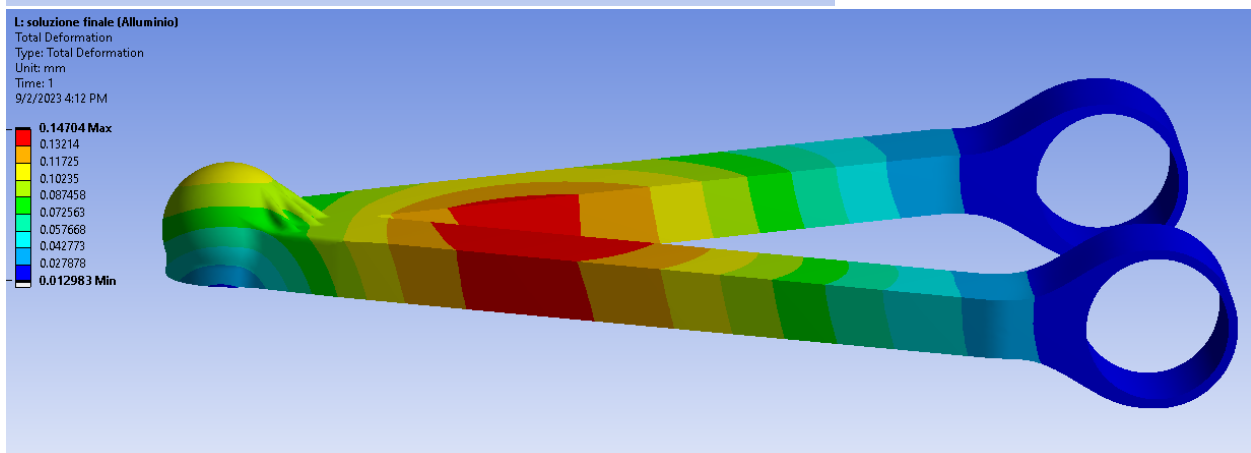
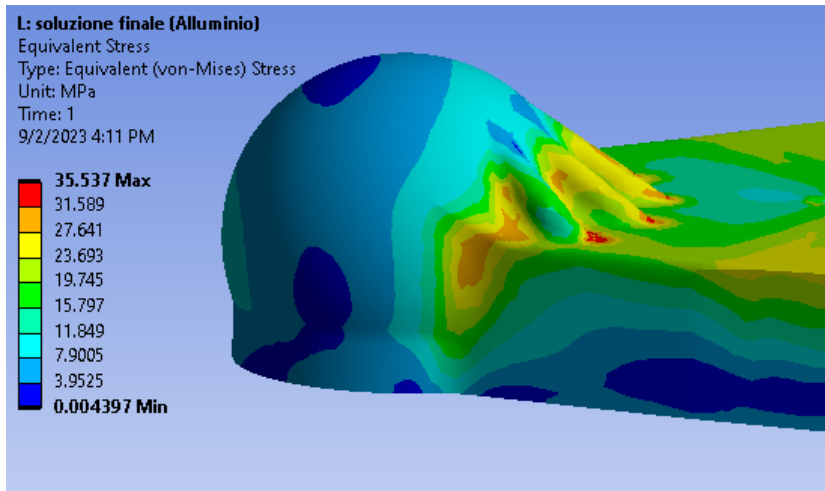


Figure 85. Final Iteration with lighter structure and Honeycomb TO and modified Ball Joint geometry;
 Max Stress=35.537 MPa; Def Max= 0.15mm

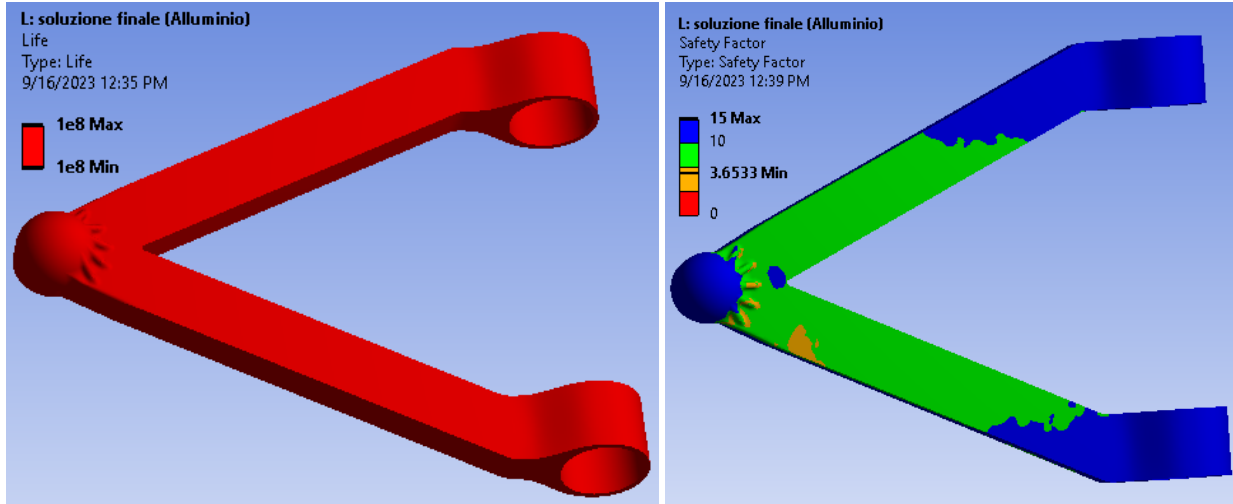


Figure 86. Life results for the optimized AL version, Life: 1e8 cycles min; SFc 3.65 min.

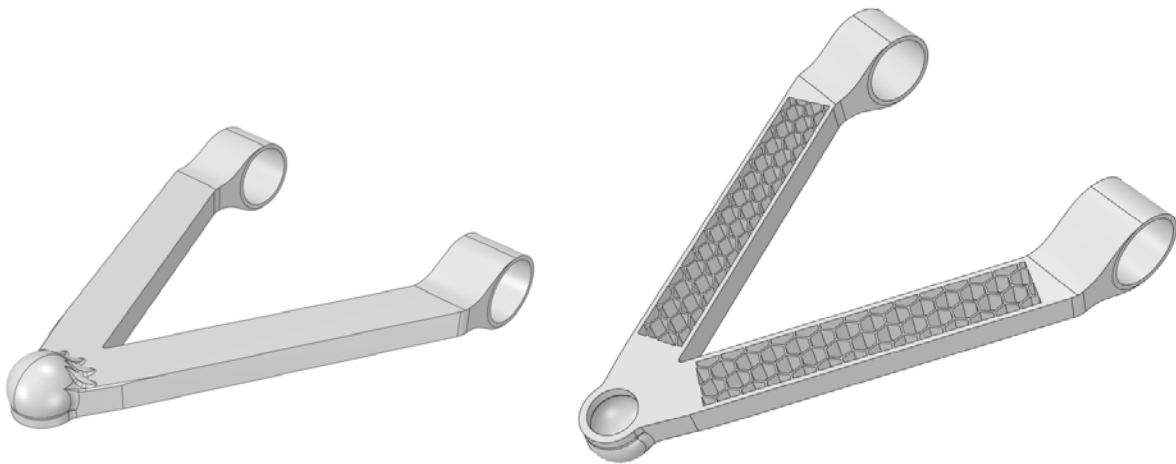


Figure 87. Optimized Upper Arm Solution - SLM.

11.2.2 PETG-CF Reinforced Core with Carbon Fiber laminate

This exercise was made in a similar method to the SLM Aluminum version, subsequent optimization iterations were performed on this part, described in Figure 88. This analysis was made by joining an internal core matrix made with CF reinforced PETG filament (Figure 90); adding 2 layers of woven carbon fiber twill with epoxy, as shown on Figure 96. Parameters of the design and part's geometry were optimized until reaching the lowest overall part Equivalent Stress, and Total Deformation, whilst delivering highest part life and safety factor Fatigue results. The Final iteration of this part is shown on Figures 91 – 92 and delivered a max Equivalent Stress of 18.562 MPa on the Polymeric reinforced matrix, whilst Figures 93 – 94 shown a Max Stress value of 102.05 MPa on the outer CF layers; a Total Deformation of Max Value = 0.36528 mm, and a Fatigue lower boundary life Cycle expectation of 9,6e4 cycles with a Safety Factor of 4.95 min. This final iteration obtained a reduced part weight of just 215 g, about 87% less than the

original part weight. The summary specifications of the final, optimized part (Figures 94, 95) are displayed in Table 27. The overall part fabrication cost was estimated in € 250 which is little less than 2 times the cost of fabrication of the stock part; but in the same manner as the lower arm stated before, the stock part cost does not include costs of tooling and subsequent costs for additional processing times that are 0 for the AM solution.

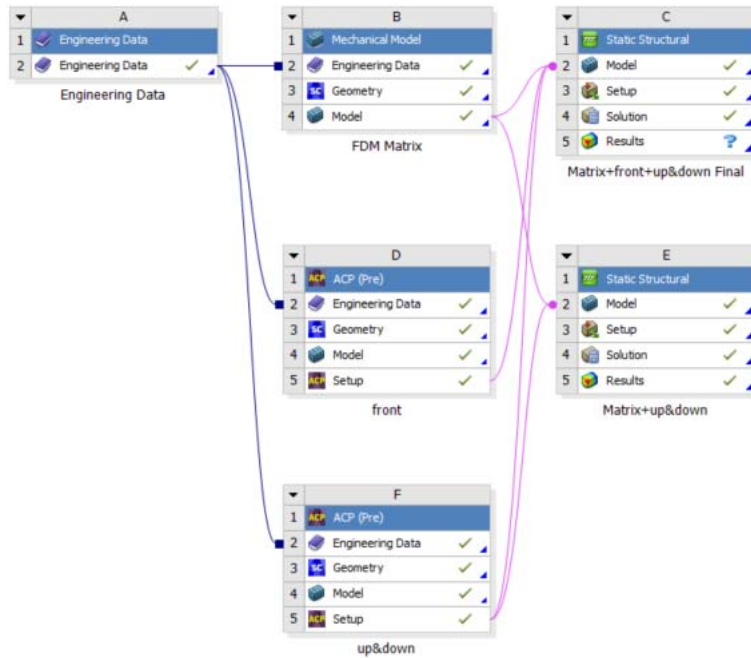


Figure 88. ANSYS Project Schematic layout of the Upper Arm focused on FDM matrix + Carbon Fiber Laminate



Figure 89. Materials used in the analysis.

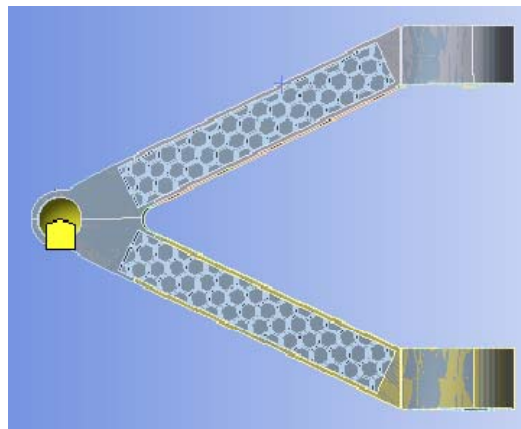


Figure 90. Matrix Geometry: Topologically Optimized Structure

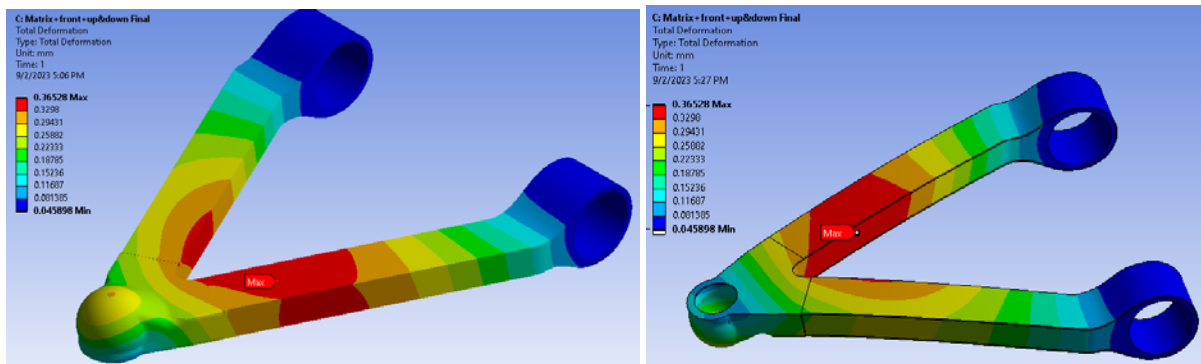


Figure 91. Total Deformation for total part; Max Value = 0.36528 mm

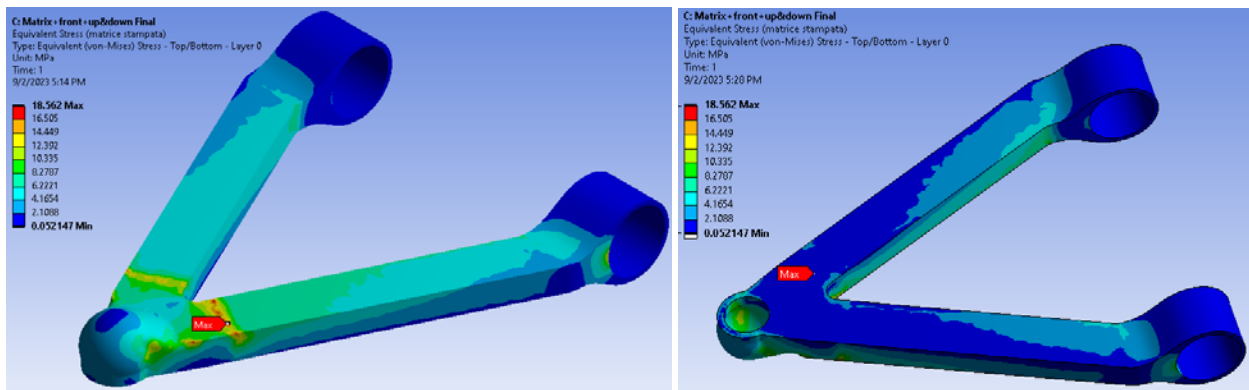


Figure 92. Equivalent Stress for PETG-CF AM Matrix; Max value of 18.562 MPa.

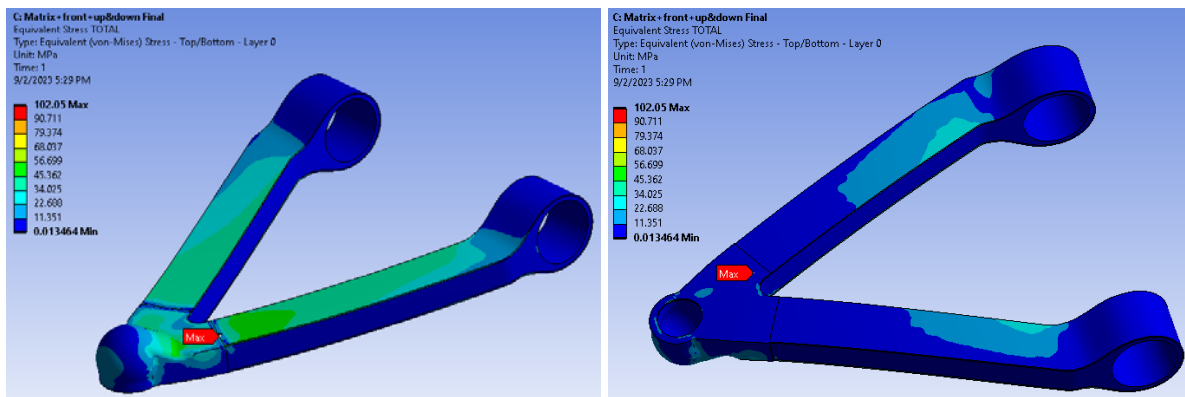


Figure 93. Equivalent Stress for Carbon Fiber layers; Max value of 102.05 MPa

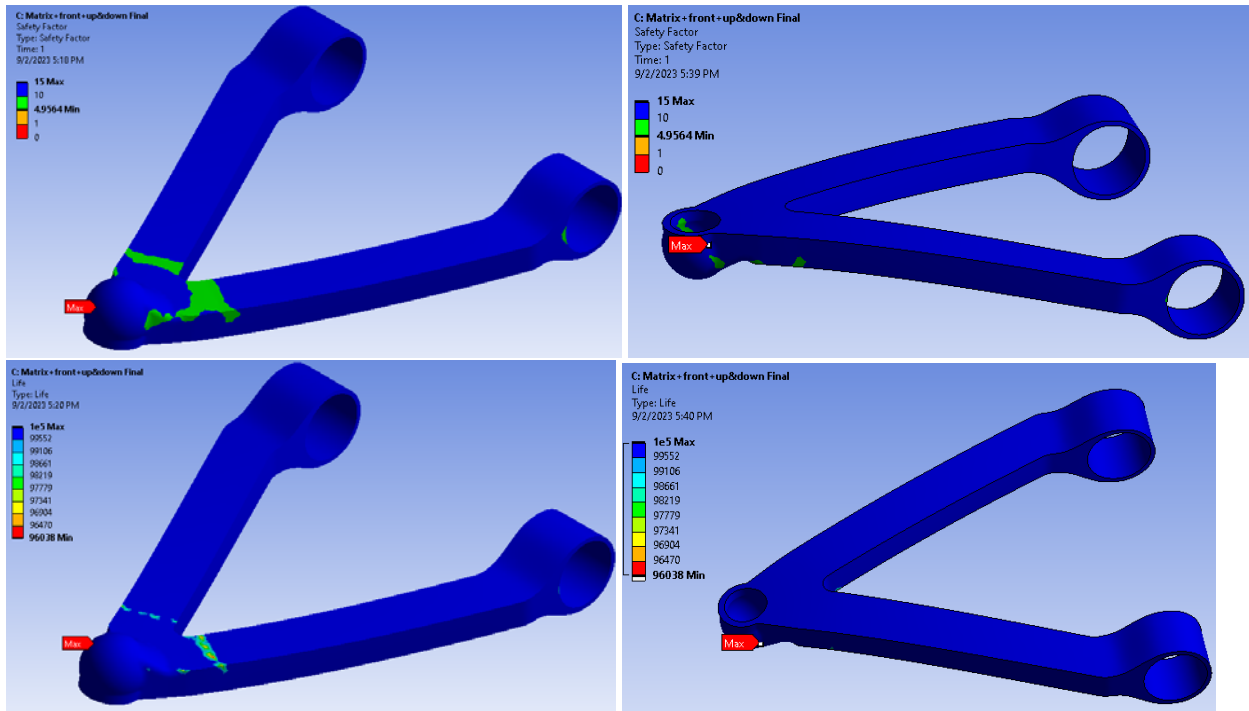


Figure 94. Safety Factor (Top) 4.95 min; and Fatigue Life Cycle (Down) 9,6e4 cycles for the Solution

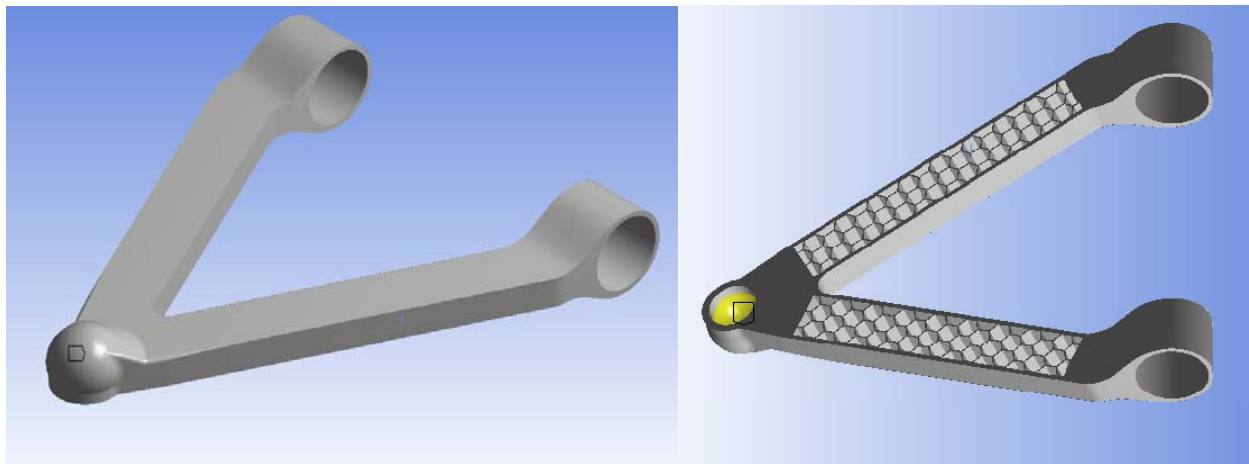


Figure 95. Optimized PETG Matrix



Figure 96. Carbon Fiber laminated Upper Arm Solution

Table 27. Optimized Lower Arm Summary; *: not considering tooling costs.

SUSPENSION UPPER ARM - OPTIMIZED			
Characteristic	Original - Stock	1) PETG + CF + Lamination	2)SLM AM (Lattice)
Overall Weight	1.95 Kg	214.1gr	1.25Kg
Material	Forged Steel	Core PETGCF + 2 x twill z=0.6 mm	AlSiMg10
Heat Treated	yes	No	yes
Total Part Cost (€) (est)	130*	250	680 (est)

12.Design Reengineering> methods for fast prototyping and optimal solution assessment

The parts optimized during this study were designed for Fast Prototyping. The selection of the type of process to create the prototype is based on the final requirements of the component to be produced. Different AM processes exist to create parts from the most economical, FDM-based filament printers, used

for polymeric filaments specially, towards the most sophisticated, yet expensive, metal powder printing (SLM) or Sintered Laser printing.

12.1 Upper Arm Prototyping

The upper arm prototype to be constructed was a 3D printed, scaled version of the analyzed design seen in Figure 94. This prototype was constructed following the optimized printing process and parameters obtained after following the optimization procedure stated on Figure 18, and nozzle orientation at 0 degrees for best mechanical characteristics (Kasmi et al., 2021); used printing parameters for this part are stated in Table 28.

The prototype was created using the equipment and materials available in the DIN laboratories, using the PETG-CF filament from Formfutura® (Table 16). The FDM equipment used was the Artillery Sidewinder X1® (Figure 51). The production of the 1:2 scaled part took 12.2 hours, for which a 1:1 scaled part with similar build parameters will take about 36 hours. The higher build time came after the optimization process, as a correct compromise must be given between part build time and overall material build quality; and the optimized Printing parameters are displayed in Table 28. This prototype did not include the metallic inserts on the bushing’s connectors, but it is recommended to include so to portray production-intent, prototype testing.

Table 28. Optimized Printing Parameters for PETG-CF Filament Material

Parameter	Value	Unit
QUALITY		
Layer Height	0.16	mm
Initial Layer Height	0.2	mm
Line Width	0.2	mm
Initial Layer Line Width	100	%
Printing nozzle orientation	0	deg
WALLS / LAYERS		
Wall lines	3	
Horizontal Expansion	0	mm
Top Layers	3	
Bottom Layers	3	
Infill Density	100	%
Infill Pattern	Lines	
Connect Infill Lines	Yes	
Infill Overlap Percentage	15	%
MATERIAL		
Printing Temperature	245	C
Printing Temperature Initial Layer	245	C
Build Plate Temperature	75	C
Build Plate Temp. Initial Layer	75	C
Flow	100	%
Initial Layer Flow	100	%
SPEED		

Print Speed	30	mm/s
Infill Speed	30	mm/s
Wall Speed	15	mm/s
Top/Bottom Speed	15	mm/s
Support Speed	30	mm/s
Travel Speed	100	mm/s
Initial Layer Print Speed	10	mm/s
Z Hop Speed	4	mm/s
TRAVEL		
Enable retraccion	Yes	
Retraccion Distance	2	mm
Retraccion Speed	25	mm/s
Z Hop when retracted	yes	
Z Hop Height	0.2	mm
Avoid Printed Parts When Travelling	yes	
COOLING		
Enable cooling	yes	
Fan Speed	100	%
Regular Fan Speed at Layer	4	
SUPPORT		
Generate Support	Yes	
Support Structure	Normal	
Support Placement	Touching Buildplate	
Support Overhang Angle	47	
Support Pattern	Zig Zag	
Support Wall Line Count	1	
Support Density	10	%
Support Horizontal Expansion	0	mm
OTHER PARAMETERS		
Print Sequence	All at Once	
Surface Mode	Surface	
Slicing Tolerance	Middle	
Minimum Polygon circumference	1	mm
Flow Rate Compensation factor	100	%
Small Feature Speed	50	%
Small Feature Initial Layer Speed	50	%

12.1.1 Part G-Coding for 3D printing: Slicing

The creation of the G-code to be loaded in the 3D printer machine was created by means of the Ultimaker® Cura V 5.1 Software (Figure 97); the version 5.1 allows the user to customize more than 90 different

parameters that are divided into part Quality, Infill characteristics, Top/Bottom layers as well as outer walls, Material-specific properties, Speed parameters, Cooling, and Support type, as well as a set of Experimental parameters aimed at obtaining a better surface quality. This software creates the G-code sequence aimed to build the part accurately according to the chosen parameters; it also gives an accurate part building time and estimates the material quantity to be used in the creation of the piece (Figure 98). The G-code created after slicing was then saved and transferred to the printer in which was run to create the part. This software also creates a line-by-line preview of the process so the operator can check the accuracy of the code and make the appropriate changes if needed.

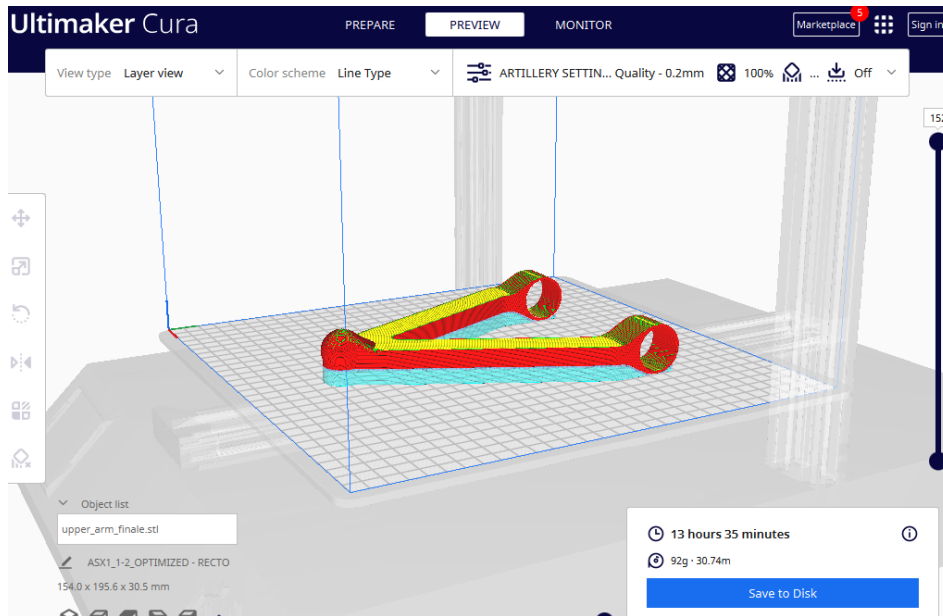


Figure 97. Ultimaker® Cura 5.1 Interface, shows 13h 35min building time with selected parameters

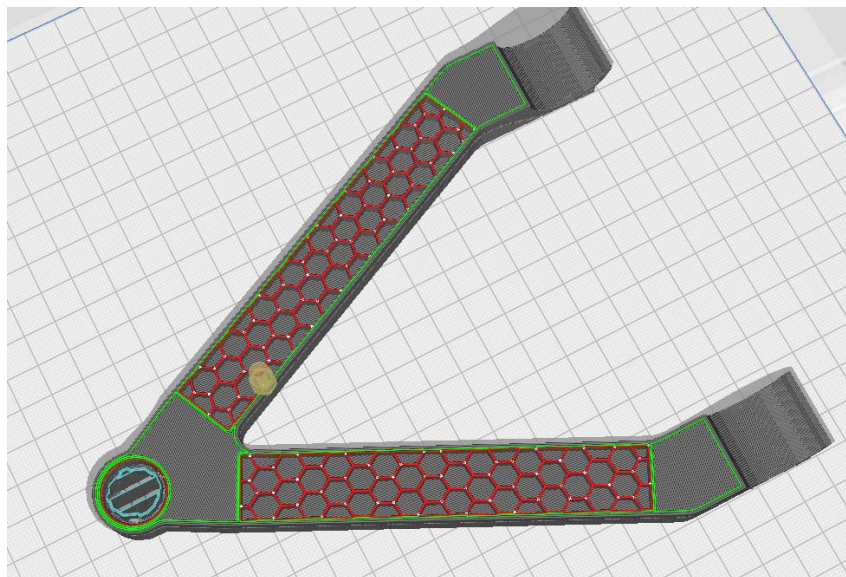


Figure 98. G-code preview line at 50% of the total printing time

12.1.2 FDM printing

FDM printing process was carried out in the Artillery Sidewinder X1 machine available at the DIN, the part was created and took the estimated time given in the slicing software; Images of the process can be seen in Figure 99 (at 50% of printing process), at layer 93, or the creation of the outer wall (Figure 100), until obtaining the completed print (with supports) (Figure 101), and the finished part (Figure 102, 103).

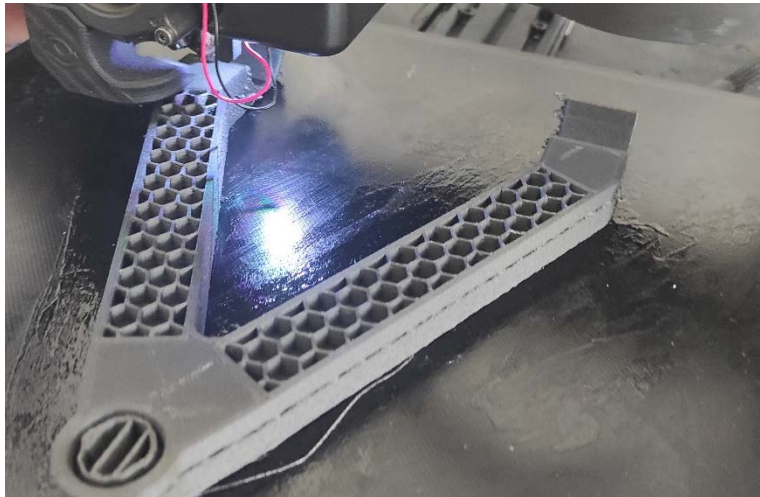


Figure 99. FDM printing of the Upper Arm at 50%

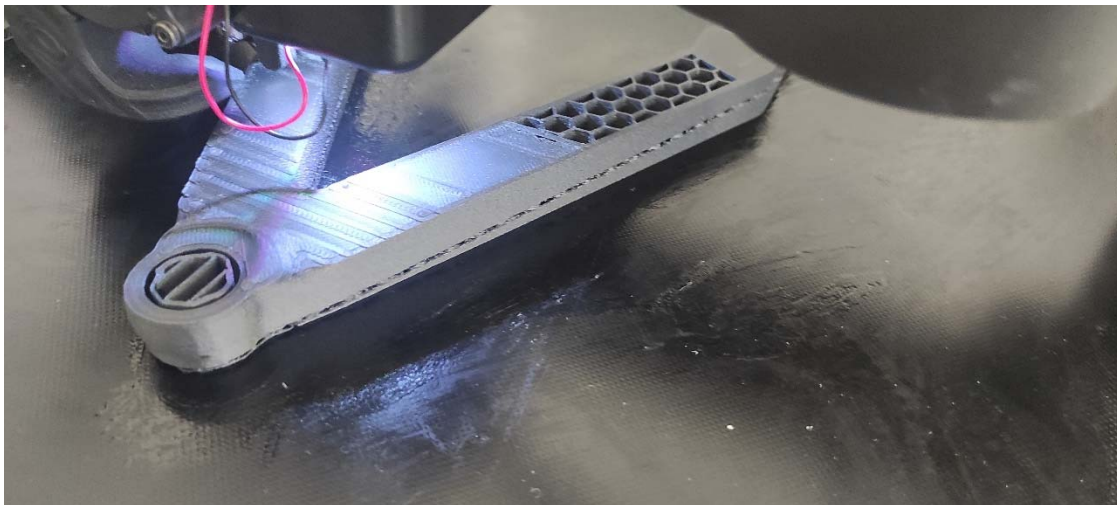


Figure 100. FDM printing of the Upper Arm at layer 93, the creation of the Top layer



Figure 101. Completed print (with supports)



Figure 102. Final printed part



Figure 103. Laminated version of the final printed element

12.1.3 3D scanning

The point cloud of the part was obtained after using the device with the aid of Geomagic® Control X software, which allowed to obtain a cloud point file (Figure 105b), and then process it in order to scale and fit both files overlapped, so a tolerance analysis can be performed. Control X software allows to portray 5 different types of analysis as seen in Figure 104. Comparison analysis was done, and results are shown in 2D, 3D mode (Figures 106-107) and the correlation Histogram on Figure 108 showed 94.064% of the scanned surface to be within the tolerance level of ± 0.25 mm.

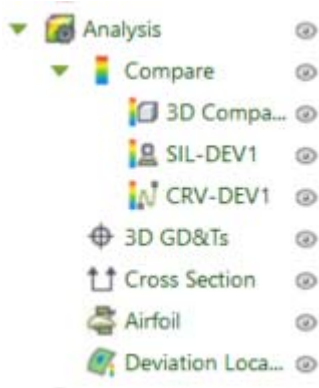


Figure 104. Analysis Tab from Geomagic control X 2020



Figure 105. a. Part positioning and Scan procedure with Faro® Quantum 3D Scanner.

b. Point cloud file obtained after scanning.

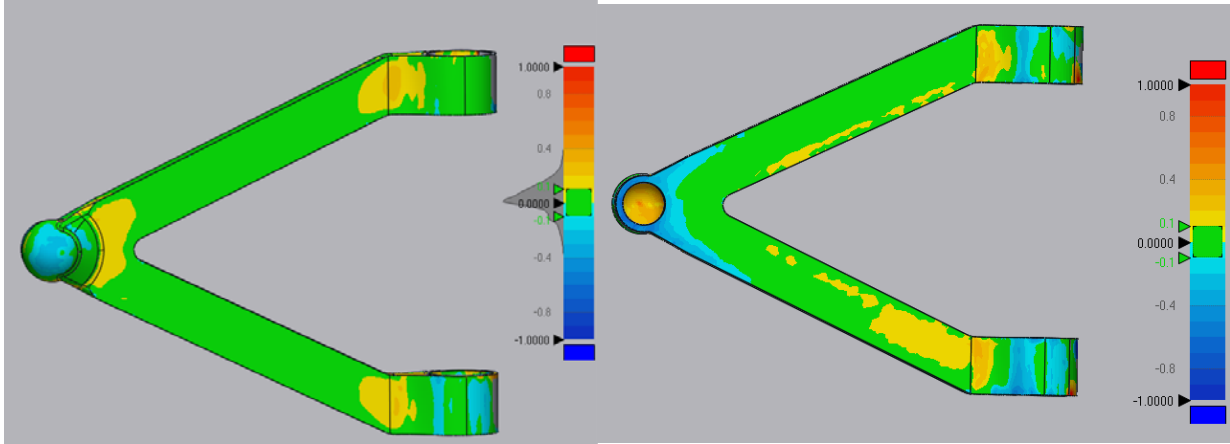


Figure 106. Comparison results of scanned part vs. CAD Values.

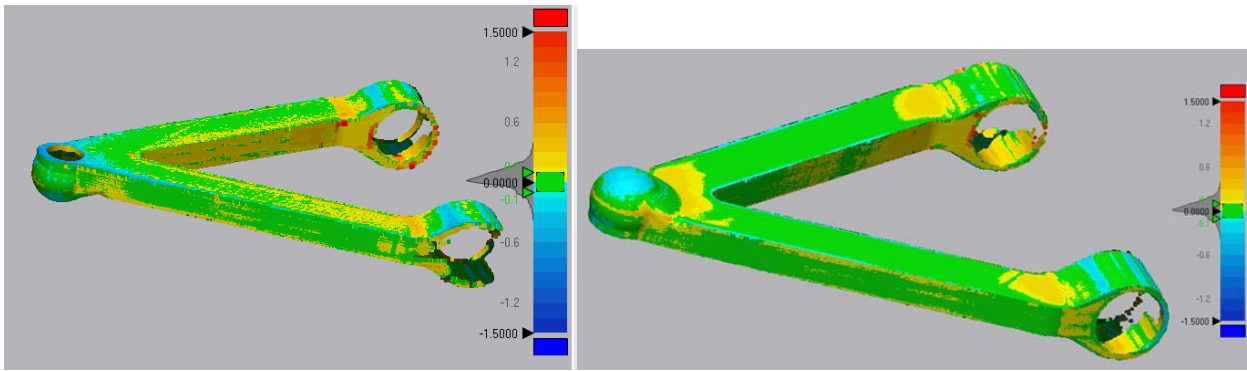


Figure 107. 3D Comparison results of scanned part vs. CAD Values.

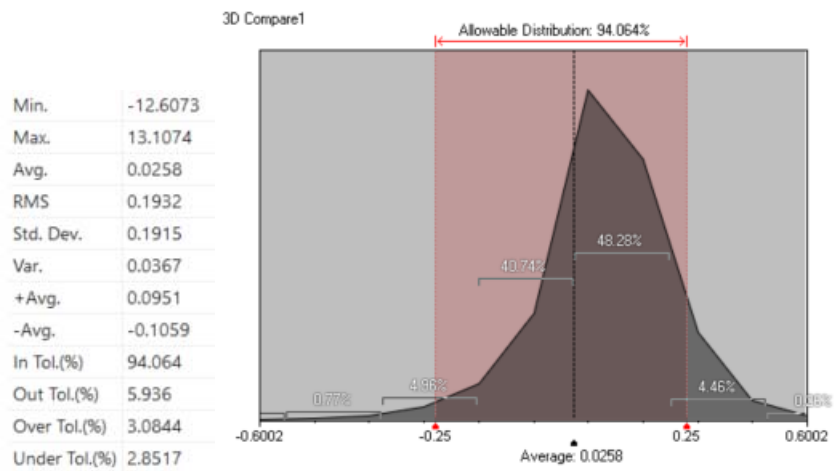


Figure 108. Tolerance variation results by 3D Scanning in Control X 2020.

12.1.3.1 Repeatability Assessment:

Second Printed part Scanning results:

The second Printed part was scanned following the same procedure as the first part in order to oversee the accuracy results of the entire manufacturing process (Figures 109, 110). The 93% of the entire surface showed measurements within tolerance range of ± 0.25 mm. These results are strictly dependent of the knowledge of the scanner operator and the accuracy of the creation of the point cloud. A better result can be obtained with proper scanning part positioning tooling and expertise of the tool operator.

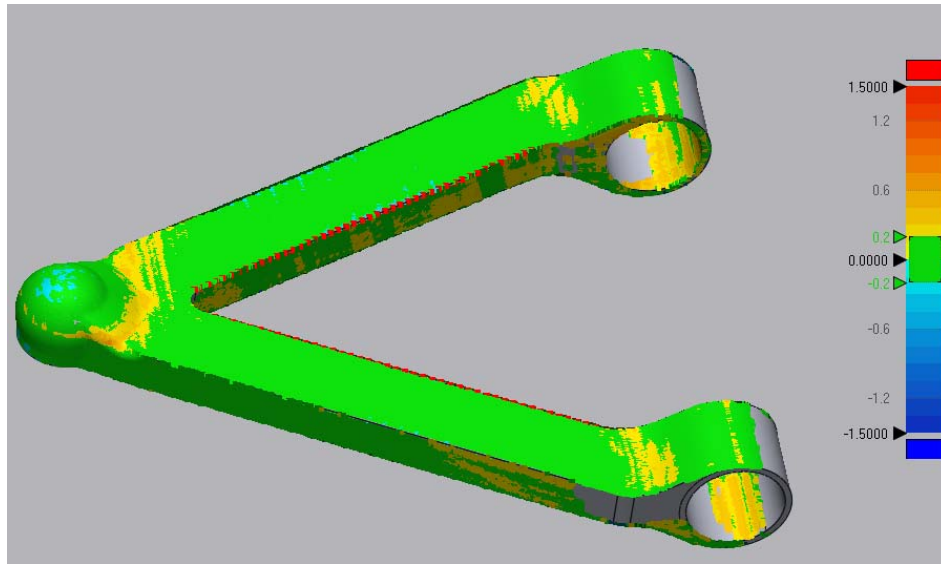


Figure 109. Tolerance variation results of second part

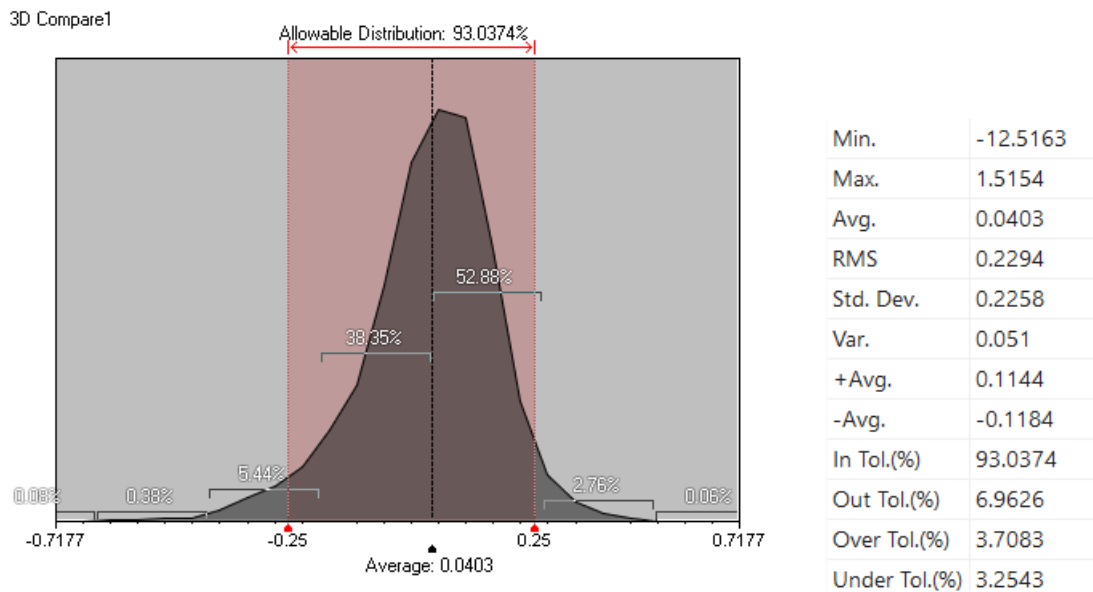


Figure 110. Tolerance variation results of the second part.

12.2 Lower Arm Prototyping

The lower arm prototyping was made using the existing equipment in the DIN laboratories, the printer chosen to print the obtained part was Sisma Mysint 100 (Figure 111), by which it was possible to create a part of scale 1:4. The total printing time was 11.4 hours with normal working printing conditions for the SLM printer given by the manufacturer, and following the parameters stated in Table 29. A support structure had to be included for this process in the same manner as the FDM printing, especially because of the geometry and positioning of the part in the printer.



Figure 111. Sisma® MySint 100 SLM Printer

Table 29. Main Printing Parameters for SLM

Main Printing Parameters used in SLM	
Layer width (μm)	30
Laser Spot Power (W)	150
Speed of laser beam (mm/s)	700
Wavelength (nm)	1070
Oxygen Concentration	0.30%
Inert Gas	Nitrogen, Argon



Figure 112. Part after SLM printing – First Iteration



Figure 113. Optimized Iteration of Lower Arm, with supports after SLM printing.



Figure 114. Optimized Lower Arm after heat treatment.

12.2.1 Lower Arm 3D Scanning

The first version of the printed arm gave a 90% of correlation of the printed surface within established tolerance (± 0.1 mm). This calculation does not include the bushings areas, as the printed part needs to be post-processed with a CNC machine in those areas to reach the decided tolerance.

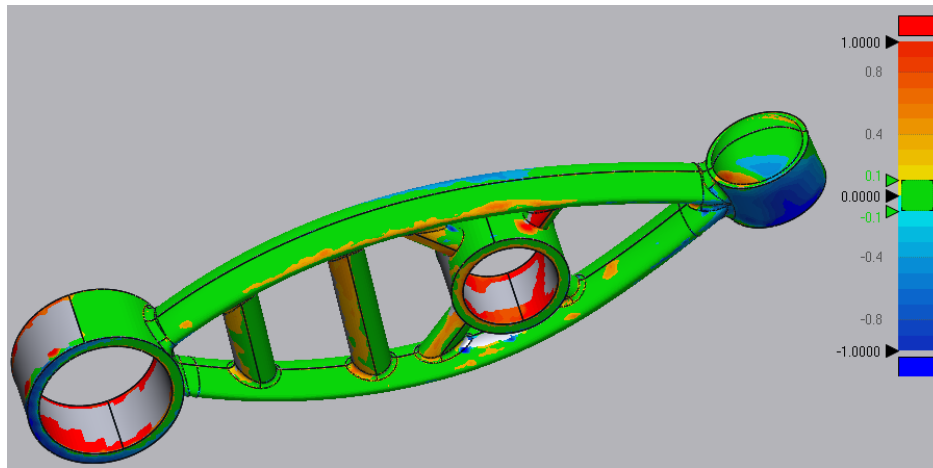


Figure 115. Lower Arm V1 tolerance correlation by means of 3D scanning

The SLM-printed optimized lower arm from Figure 114, printed at the highest tolerance-level capacity of the printer, showed a 83% of the entire surface within the tolerance of ± 0.1 mm; demonstrating that SLM AM process capability to create high accuracy parts within mechanic-level tolerances.

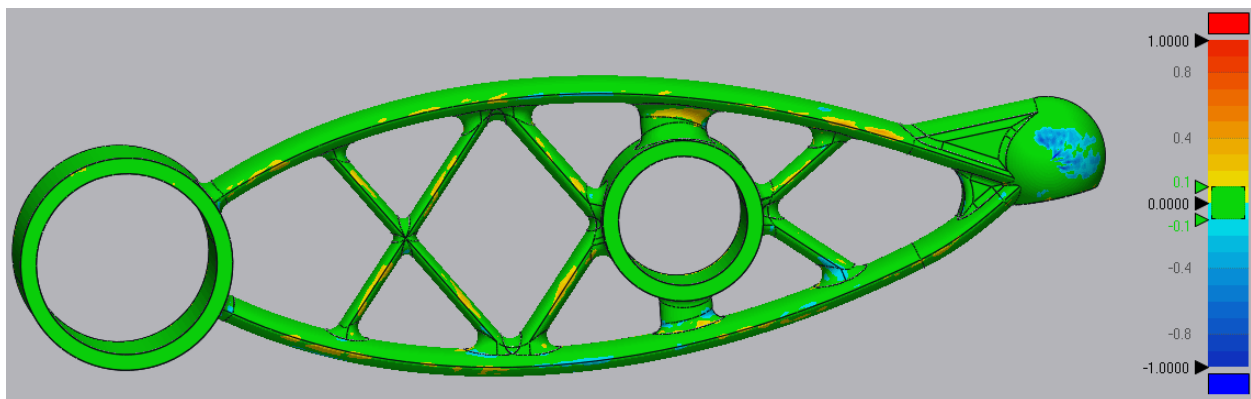


Figure 116. Optimized Lower Arm tolerance correlation by means of 3D scanning.

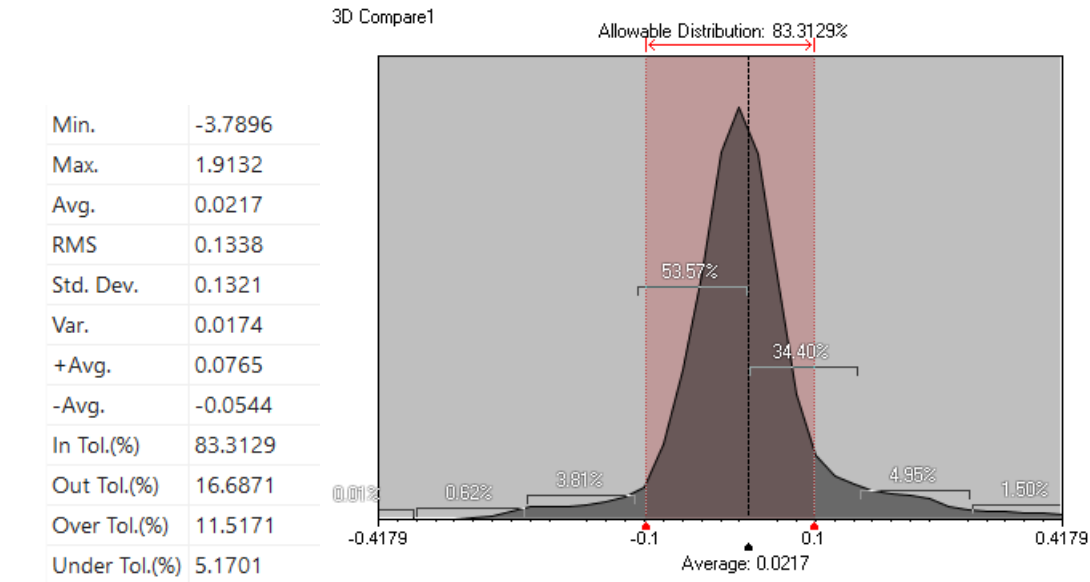


Figure 117. Tolerance variation results of the second part.

13.Achievements

First, a general, technical understanding about the behavior of AM processes was outlined; an optimization procedure was released in order to improve the internal material structural anisotropy; moreover, a mechanical characterization of PETG-CF FDM processed materials with CF twill laminate was performed to determine the mechanical resistance of a composite made from Twill woven Carbon fiber laminate with polymeric sourced, topologically optimized core structures.

Second, a deep understanding of the importance of following a methodology for product design was achieved; IDES method can combine diverse tools from the I4.0 era ought to be used for data and component analysis; the FEM analysis and other CAE tools can ease product reengineering in order to portray design for additive manufacturing efficiently. The use of these tools can drive line operators to accurately redesign, test, build and control the quality of produced parts.

Third, an exemplification of application of lightweighting of mechanical elements by means of the inclusion of the proposed composite structure with the IDES product design methodology has demonstrated the capability of the method to portray prototypes of products with an eyesight of industrialization by proposing a new product in the technical aspect and that at the same time is capable of meeting quality objectives established by the competition.

14. Conclusions

- AM technology has been under research and development for the past 40 years. This technology has demonstrated the capability for creating parts up to the highest quality standards.
- Nowadays, there is a wide range of AM equipment proposals that offer respectable levels of productivity and repeatability, but in any case, companies have to balance the overall initial machine and materials cost with the return of investment.
- Part quality and overall mechanical strength are strictly related to cost. This is why AM technology has become an interesting option for companies to portray its prototypes to test in a faster way. AM's higher initial costs are balanced with the 0 initial tooling cost.
- The use of additive manufacturing for final use parts and products is growing, but still faces challenges in quality, productivity, repeatability, and availability of materials. Industry leaders from both aerospace and energy will share some of ways they are addressing these challenges and opportunities to increase the use of additive manufacturing in the next years.
- The release of a valid method for AM part production that considers steps from parts reengineering and modelling, material and equipment set-up, execution and final quality control is ultimately needed by companies.
- The release of a valid path to exploit the possibilities of 4.0 technologies to apply in the industry is needed, facing the challenges of its limitations by acting on every step in this process.
- Companies require that new operators learn the proper skills needed to operate equipment related to Digital Engineering, part manufacturing with AM, and quality control via laser scanner in order to consider a switch to these methods.
- The use of IDES method exploits the design structure complexity to enable product-driven efficiency and accuracy culture across the company organization. This engagement must be exploited to guarantee a product that answers immediately to the customer and the industry; and a quick reaction to market demand fluctuation and would be a key guideline for companies ought to succeed.

15. Future works

- To develop subsequent technical exercises by applying the methods, tools, and processes englobed within IDES to satisfy modern era product development requirements.
- Continue to develop product engineering processes by exploiting the possibilities of developing an integral product management level of information that, can give push businesses into adopting a more centered source of information to drive management solutions for OEMs.
- The use of additive manufacturing for final use parts and products is growing, but still faces challenges in quality, productivity, repeatability, and availability of materials. Industry leaders from both aerospace and energy will share some of ways they are addressing these challenges and opportunities to increase the use of additive manufacturing in the next years.

16. Bibliography

- 3D Molier. (2021). *Tesla Model S Front Suspension*. <http://3dsmolier.com/3d-model-tesla-model-s-front-suspension-3>
- Ahmed, S., Irshad, L., & Demirel, H. O. (2021). Prototyping human-centered products in the age of industry 4.0. *Journal of Mechanical Design*, 143(7).
- Ali, H. Y., Danish, R. Q., & Asrar-ul-Haq, M. (2020). How corporate social responsibility boosts firm financial performance: The mediating role of corporate image and customer satisfaction. *Corporate Social Responsibility and Environmental Management*, 27(1), 166–177.
- Alt, R., Ehmke, J. F., Haux, R., Henke, T., Mattfeld, D. C., Oberweis, A., Paech, B., & Winter, A. (2019). Towards customer-induced service orchestration-requirements for the next step of customer orientation. *Electronic Markets*, 29(1), 79–91.
- Ashima, R., Haleem, A., Bahl, S., Javaid, M., Mahla, S. K., & Singh, S. (2021). Automation and manufacturing of smart materials in Additive Manufacturing technologies using Internet of Things towards the adoption of Industry 4.0. *Materials Today: Proceedings*, 45, 5081–5088.
- Assur, N., & Rowshankish, K. (2022). The data-driven enterprise of 2025. *McKinsey, USA*.
- Balamurugan, E., Flaih, L. R., Yuvaraj, D., Sangeetha, K., Jayanthiladevi, A., & Kumar, T. S. (2019). Use case of artificial intelligence in machine learning manufacturing 4.0. *2019 International Conference on Computational Intelligence and Knowledge Economy (ICCIKE)*, 656–659.
- Berryman, M. L. (2002). DFSS and big payoffs. *Lean & Six Sigma Review*, 2(1), 23.
- Bolaños-Ruiz, E. A. (2023). Technology Roadmapping and TRIZ: A Practical Approach for Inventive Problem-Solving and Product Innovation. In *TRIZ in Latin America: Case Studies* (pp. 155–173). Springer.
- Burton, R. M., & Obel, B. (2018). The science of organizational design: fit between structure and coordination. *Journal of Organization Design*, 7(1), 1–13.
- Chen, P.-C., Chou, C. C., & Chiang, C. H. (2021). Systematically Studying Dissolution Process of 3D Printed Acrylonitrile Butadiene Styrene (ABS) Mold for Creation of Complex and Fully Transparent Polydimethylsiloxane (PDMS) Fluidic Devices. *BioChip Journal*, 1–8.
- Cucinotta, F., Raffaele, M., & Salmeri, F. (2021). A Topology Optimization Method for Stochastic Lattice Structures. *Advances on Mechanics, Design Engineering and Manufacturing III: Proceedings of the International Joint Conference on Mechanics, Design Engineering & Advanced Manufacturing, JCM 2020, June 2-4, 2020*, 235–240.
- Daft, R. L., Murphy, J., & Willmott, H. (2010). *Organization theory and design: Cengage learning EMEA. Hampshire*.
- Dalpadulo, E., Gherardini, F., Pini, F., & Leali, F. (2020). Integration of topology optimisation and design variants selection for additive manufacturing-based systematic product redesign. *Applied Sciences*, 10(21), 7841.
- Delpa, V., Kenné, J.-P., & Hof, L. A. (2022). Circular manufacturing 4.0: towards internet of things embedded closed-loop supply chains. *The International Journal of Advanced Manufacturing*

Technology, 118(9), 3241–3264.

- Dilberoglu, U. M., Gharehpapagh, B., Yaman, U., & Dolen, M. (2021). Current trends and research opportunities in hybrid additive manufacturing. *The International Journal of Advanced Manufacturing Technology*, 113(3), 623–648.
- Dutta, G., Kumar, R., Sindhvani, R., & Singh, R. K. (2021). Digitalization priorities of quality control processes for SMEs: A conceptual study in perspective of Industry 4.0 adoption. *Journal of Intelligent Manufacturing*, 32(6), 1679–1698.
- EOS Metal Solutions. (2022a). *Aluminium AlSi10Mg Material Data Sheet*. https://www.eos.info/03_system-related-assets/material-related-contents/metal-materials-and-examples/metal-material-datasheet/aluminium/material_datasheet_eos_aluminium-alsi10mg_en_web.pdf
- EOS Metal Solutions. (2022b). *Aluminium AlSi10Mg Material Data Sheet*.
- Ericsson, E., Gingnell, L., & Lilliesköld, J. (2015). Implementing Design for Six Sigma in large Swedish product developing organisations—an interview study. *Total Quality Management & Business Excellence*, 26(5–6), 648–660.
- Ferretti, P., Leon, C., Sali, M., Frizziero, L., Donnici, G., Liverani, A. (2021). *Application of TPU – Sourced 3D Printed FDM Organs for Improving the Realism in Surgical Planning and Training* (International Conference on Industrial Engineering and Operations Management Singapore (ed.)). International Conference on Industrial Engineering and Operations Management Singapore.
- Ferretti, P., Leon-Cardenas, C., Santi, G. M., Sali, M., Ciotti, E., Frizziero, L., Donnici, G., & Liverani, A. (2021). Relationship between FDM 3D Printing Parameters Study: Parameter Optimization for Lower Defects. *Polymers*, 13(13), 2190. <https://doi.org/10.3390/polym13132190>
- Fiebig, S., Sellschopp, J., Manz, H., Vietor, T., Axmann, K., & Schumacher, A. (2015). Future challenges for topology optimization for the usage in automotive lightweight design technologies. *Proc. of 11th World Congress on Structural and Multidisciplinary Optimization, Sydney, Australia*, 142.
- Francia, D., Caligiana, G., Liverani, A., Frizziero, L., & Donnici, G. (2018). PrinterCAD: a QFD and TRIZ integrated design solution for large size open moulding manufacturing. *International Journal on Interactive Design and Manufacturing*, 12(1), 81–94. <https://doi.org/10.1007/s12008-017-0375-2>
- Frizziero, L., Donnici, G., Liverani, A., Alessandri, G., Menozzi, G. C., & Varotti, E. (2019). Developing innovative crutch using IDeS (industrial design structure) methodology. *Applied Sciences (Switzerland)*, 9(23). <https://doi.org/10.3390/app9235032>
- Frizziero, L., Leon-Cardenas, C., Colasurdo, G., Vicaretti, A., & Liverani, A. (2022). IDeS (Industrial Design Structure) Method Applied to the Automotive Design Framework: Two Sports Cars with Shared Platform. In *Inventions* (Vol. 7, Issue 2). <https://doi.org/10.3390/inventions7020036>
- Frizziero, L., Liverani, A., Donnici, G., Conti, E., Dello Preite, B., Lamanna, U., Leon-Cardenas, C., & Garulli, M. (2021). GD (Generative Design) Applied to a Plastics Recovery Drone (PRD) Using IDeS (Industrial Design Structure). *Inventions*, 6(4), 82.
- Frizziero, L., Pagliari, C., Donnici, G., Liverani, A., Santi, G. M., Papaleo, P., Napolitano, F., Leon-Cardenas, C., Trisolino, G., & Zarantonello, P. (2021). Effectiveness assessment of CAD simulation in complex orthopedic surgery practices. *Symmetry*, 13(5), 850.

- Frizziero, L., Santi, G. M., Leon-Cardenas, C., Donnici, G., Liverani, A., Napolitano, F., Papaleo, P., Pagliari, C., Antonioli, D., & Stallone, S. (2021). An innovative and cost-advantage cad solution for cubitus varus surgical planning in children. *Applied Sciences*, *11*(9), 4057.
- Frizziero, L., Santi, G. M., Leon-Cardenas, C., Donnici, G., Liverani, A., Papaleo, P., Napolitano, F., Pagliari, C., Di Gennaro, G. L., & Stallone, S. (2021). In-House, Fast FDM Prototyping of a Custom Cutting Guide for a Lower-Risk Pediatric Femoral Osteotomy. *Bioengineering*, *8*(6), 71.
- Futura B.V., F. (2022). *CarbonFil® Technical Data Sheet*. <https://formfutura.com/product/carbonfil/>
- Gonçalves, J. F., Moreira, J. B. D., Salas, R. A., Ghorbani, M. M., Rubio, W. M., & Silva, E. C. N. (2020). Identification problem of acoustic media in the frequency domain based on the topology optimization method. *Structural and Multidisciplinary Optimization*, *62*, 1041–1059.
- Gordeev, E. G., Galushko, A. S., & Ananikov, V. P. (2018). Improvement of quality of 3D printed objects by elimination of microscopic structural defects in fused deposition modeling. *PLoS One*, *13*(6), e0198370. <https://doi.org/10.1371/journal.pone.0198370>
- Gupta, B. B., & Quamara, M. (2020). An overview of Internet of Things (IoT): Architectural aspects, challenges, and protocols. *Concurrency and Computation: Practice and Experience*, *32*(21), e4946.
- Han, J. H., & Lee, J. Y. (2021). Digital healthcare industry and technology trends. *2021 IEEE International Conference on Big Data and Smart Computing (BigComp)*, 375–377.
- IBISWorld. (2023). *Global Car & Automobile Manufacturing - Market Size 2005–2029*. <https://www.ibisworld.com/global/market-size/global-car-automobile-manufacturing/>
- Ikumapayi, O. M., Akinlabi, E. T., Mwema, F. M., & Ogbonna, O. S. (2020). Six sigma versus lean manufacturing—An overview. *Materials Today: Proceedings*, *26*, 3275–3281.
- ISO 17296-2:2015 Additive manufacturing — General principles — Part 2: Overview of process categories and feedstock, (2020).
- Jørgensen, K. A. (2009). Product configuration and product family modelling. *Department of Production, Aalborg University*.
- Kasmi, S., Ginoux, G., Allaoui, S., & Alix, S. (2021). Investigation of 3D printing strategy on the mechanical performance of coextruded continuous carbon fiber reinforced PETG. *Journal of Applied Polymer Science*, *138*(37), 50955.
- Kjaer, L. L., Pigosso, D. C. A., Niero, M., Bech, N. M., & McAlloone, T. C. (2019). Product/service-systems for a circular economy: The route to decoupling economic growth from resource consumption? *Journal of Industrial Ecology*, *23*(1), 22–35.
- Krupennikov, O., Nazarov, M., & Kiselev, E. (2022). Investigation of the Efficiency of Manufacturing Polymer Molds by FDM-Printing. *Materials Research Proceedings*, *21*, 117–121. <https://doi.org/https://doi.org/10.21741/9781644901755-21>
- Kwon, H.-J., Sunthornvarabhas, J., Park, J.-W., Lee, J.-H., Kim, H.-J., Piyachomkwan, K., Sriroth, K., & Cho, D. (2014). Tensile properties of kenaf fiber and corn husk flour reinforced poly (lactic acid) hybrid bio-composites: Role of aspect ratio of natural fibers. *Composites Part B: Engineering*, *56*, 232–237.
- Lazorík, P. (2021). SMART Production System with Full Digitalization for Assembly and Inspection in Concept of Industry 4.0. *Future Access Enablers for Ubiquitous and Intelligent Infrastructures: 5th*

- EAI International Conference, FABULOUS 2021, Virtual Event, May 6–7, 2021, Proceedings*, 382, 181.
- Lenort, R., Wicher, P., & Zapletal, F. (2023). On influencing factors for Sustainable Development goal prioritisation in the automotive industry. *Journal of Cleaner Production*, 387, 135718.
- Leon-Cardenas, C., Ferretti, P., Sali, M., Santi, G. M., Gianese, F., Crescentini, N., Frizziero, L., Donnici, G., & Liverani, A. (n.d.). *FDM-sourced Shinbone Cutting Guide in Polylactic acid-based Polymers: Heat Sterilization Effects on Part Quality*.
- Li, S., Yuan, S., Zhu, J., Wang, C., Li, J., & Zhang, W. (2020). Additive manufacturing-driven design optimization: Building direction and structural topology. *Additive Manufacturing*, 36, 101406.
- Li, Y., Feng, Z., Hao, L., Huang, L., Xin, C., Wang, Y., Bilotti, E., Essa, K., Zhang, H., & Li, Z. (2020). A review on functionally graded materials and structures via additive manufacturing: from multi-scale design to versatile functional properties. *Advanced Materials Technologies*, 5(6), 1900981.
- Lin, W. D., Low, Y. H., Chong, Y. T., & Teo, C. L. (2018). Integrated cyber physical simulation modelling environment for manufacturing 4.0. *2018 IEEE International Conference on Industrial Engineering and Engineering Management (IEEM)*, 1861–1865.
- Lipu, M. S. H., Hannan, M. A., Karim, T. F., Hussain, A., Saad, M. H. M., Ayob, A., Miah, M. S., & Mahlia, T. M. I. (2021). Intelligent algorithms and control strategies for battery management system in electric vehicles: Progress, challenges and future outlook. *Journal of Cleaner Production*, 292, 126044.
- Maas, J. (2000). Driving customer equity: How lifetime customer value is reshaping corporate strategy. *MIT Sloan Management Review*, 41(4), 106.
- Maute, K., & Ramm, E. (1995). Adaptive topology optimization. *Structural Optimization*, 10, 100–112.
- Medini, K., Andersen, A.-L., Wuest, T., Christensen, B., Wiesner, S., Romero, D., Liu, A., & Tao, F. (2019). Highlights in customer-driven operations management research. *Procedia Cirp*, 86, 12–19.
- Miles, M., & Roberts, D. (2019). *Overcoming Barriers to Implementing and Sustaining Product Development Tools*. <https://doi.org/10.13140/RG.2.2.34038.45126>
- Minnoye, A. L. M., Tajdari, F., Doubrovski, E. L., Wu, J., Kwa, F., Elkhuizen, W. S., Huysmans, T., & Song, Y. (2022). Personalized product design through digital fabrication. *International Design Engineering Technical Conferences and Computers and Information in Engineering Conference*, 86212, V002T02A054.
- MInus, M., & Kumar, S. (2005). The processing, properties, and structure of carbon fibers. *Jom*, 57, 52–58.
- Mouaky, M., Benabbou, L., & Berrado, A. (2018). DMADV approach to evaluate the Adaptive Kanban performance for inventory management process: the case of Moroccan public pharmaceutical supply chain. *Supply Chain Forum: An International Journal*, 19(3), 178–190.
- Mukherjee, S., Lu, D., Raghavan, B., Breikopf, P., Dutta, S., Xiao, M., & Zhang, W. (2021). Accelerating large-scale topology optimization: State-of-the-art and challenges. *Archives of Computational Methods in Engineering*, 1–23.
- Munk, D. J., Vio, G. A., & Steven, G. P. (2015). Topology and shape optimization methods using evolutionary algorithms: a review. *Structural and Multidisciplinary Optimization*, 52, 613–631.
- Narver, J. C., & Slater, S. F. (1990). The effect of a market orientation on business profitability. *Journal of*

Marketing, 54(4), 20–35.

- Nazarova, H., Kashchena, N., Nesterenko, I., Kovalevska, N., & Kashperska, A. (2022). Theoretical and methodological aspects of improving the functioning of the accounting system. *Amazonia Investiga*, 11(54), 243–255.
- Neneh, B. N. (2018). Customer orientation and SME performance: the role of networking ties. *African Journal of Economic and Management Studies*.
- Oyner, O. K., & Latyshova, L. S. (2009). An impact of companies market oriented behaviour upon business efficiency. *Proceedings of the Xth International Scientific Conference for Economic and Society Development. Moscow: GU-HSE*, 287–296.
- Pan, C., Han, Y., & Lu, J. (2020). Design and optimization of lattice structures: A review. *Applied Sciences*, 10(18), 6374.
- Paprocki, M. (2019). Contemporary trends in the design and management of product development. *Mechanik*, 92(1 SE-Articles), 64–66. <https://doi.org/10.17814/mechanik.2019.1.14>
- Parmar, H., Khan, T., Tucci, F., Umer, R., & Carlone, P. (2022). Advanced robotics and additive manufacturing of composites: towards a new era in Industry 4.0. *Materials and Manufacturing Processes*, 37(5), 483–517.
- Patel, M., & Desai, D. A. (2018). Critical review and analysis of measuring the success of Six Sigma implementation in manufacturing sector. *International Journal of Quality & Reliability Management*.
- Patel, S. (2017). *The Tactical Guide to Six Sigma Implementation*. Productivity Press.
- Perez, O., Saucedo, S., & Cruz, J. (2018). *Manufacturing 4.0: The Use of Emergent Technologies in Manufacturing*. Palibrio.
- Peterson, M., & Summers, J. D. (2021). Recommended methods supporting adoption of the agile philosophy for hardware development. *International Design Engineering Technical Conferences and Computers and Information in Engineering Conference*, 85420, V006T06A013.
- Piancastelli, L., Frizziero, L., & Donnici, G. (2014). Learning by failures: The “Astura II” concept car design process. *ARPN Journal of Engineering and Applied Sciences*, 9(10), 2009–2015. <https://www.scopus.com/inward/record.uri?eid=2-s2.0-84908459202&partnerID=40&md5=03162e4fb50b3bd7025fc55c15bd679a>
- Plocher, J., & Panesar, A. (2019). Review on design and structural optimisation in additive manufacturing: Towards next-generation lightweight structures. *Materials & Design*, 183, 108164.
- Polymaker. (2022). *PolyLite PLA-CF*. V5.1. <https://us.polymaker.com/products/polylite-pla-cf>
- Powell, D. J., & Bartolome, C. P. F. (2020). Enterprise-wide value stream mapping: from dysfunctional organization to cross-functional, collaborative learning and improvement. *2020 IEEE International Conference on Industrial Engineering and Engineering Management (IEEM)*, 551–555.
- Raj, A., Dwivedi, G., Sharma, A., de Sousa Jabbour, A. B. L., & Rajak, S. (2020). Barriers to the adoption of industry 4.0 technologies in the manufacturing sector: An inter-country comparative perspective. *International Journal of Production Economics*, 224, 107546.
- Rajeshirke, M., Alkunte, S., Huseynov, O., & Fidan, I. (2023). Fatigue analysis of additively manufactured

- short carbon fiber-reinforced PETG Components. *The International Journal of Advanced Manufacturing Technology*, 1–18.
- Romero, P. E., Arribas-Barrios, J., Rodriguez-Alabanda, O., González-Merino, R., & Guerrero-Vaca, G. (2021). Manufacture of polyurethane foam parts for automotive industry using FDM 3D printed molds. *CIRP Journal of Manufacturing Science and Technology*, 32, 396–404.
- Salifu, S., Desai, D., Ogunbiyi, O., & Mwale, K. (2022). Recent development in the additive manufacturing of polymer-based composites for automotive structures—A review. *The International Journal of Advanced Manufacturing Technology*, 119(11–12), 6877–6891.
- Sarvankar, S. G., & Yewale, S. N. (2019). Additive manufacturing in automobile industry. *Int. J. Res. Aeronaut. Mech. Eng*, 7(4), 1–10.
- Seno, J. P., Pimenta, M. L., Hilletoft, P., & Eriksson, D. (2019). Cross-functional interconnectedness as an enabler of customer value. *Journal of Business & Industrial Marketing*.
- Shivajee, V., Singh, R. K., & Rastogi, S. (2019). Manufacturing conversion cost reduction using quality control tools and digitization of real-time data. *Journal of Cleaner Production*, 237, 117678.
- Shokri, A., & Li, G. (2020). Green implementation of Lean Six Sigma projects in the manufacturing sector. *International Journal of Lean Six Sigma*.
- Silva, C. S., Borges, A. F., & Magano, J. (2021). Quality Control 4.0: a way to improve the quality performance and engage shop floor operators. *International Journal of Quality & Reliability Management*.
- Soderborg, N. R. (2004). Design for six sigma at Ford. *Six Sigma Forum Magazine*, 4(1).
- Specs, U. (2020). *Tesla Model S Specifications*. <https://www.ultimatespecs.com/car-specs/Tesla/116348/Tesla-Model-S-Performance.html>
- Sudbury, T. Z., Springfield, R., Kunc, V., & Duty, C. (2017). An assessment of additive manufactured molds for hand-laid fiber reinforced composites. *The International Journal of Advanced Manufacturing Technology*, 90(5), 1659–1664.
- Tambare, P., Meshram, C., Lee, C.-C., Ramteke, R. J., & Imoize, A. L. (2021). Performance measurement system and quality management in data-driven Industry 4.0: A review. *Sensors*, 22(1), 224.
- Thaichon, P., Surachartkumtonkun, J., Quach, S., Weaven, S., & Palmatier, R. W. (2018). Hybrid sales structures in the age of e-commerce. *Journal of Personal Selling & Sales Management*, 38(3), 277–302. <https://doi.org/10.1080/08853134.2018.1441718>
- Varotsis, A. B. (2022). *What are lattice structures?* <https://www.ntop.com/resources/blog/guide-to-lattice-structures-in-additive-manufacturing/>
- Volkov, D. V., Vinogradova, M. V., & Kulyamina, O. S. (2018). The synthesis of modern consumer preferences with the use of social networks in supply chain. *International Journal of Supply Chain Management*, 7(5), 851–857.
- Wang, F.-K., Yeh, C.-T., & Chu, T.-P. (2016). Using the design for Six Sigma approach with TRIZ for new product development. *Computers & Industrial Engineering*, 98, 522–530.
- Wang, P. H., Kim, G., & Sterkenburg, R. (2019). Investigating the Effectiveness of a 3D Printed Composite

Mold. *Int J of Aerospace and Mechanical Engineering*, 13(11).

Xiong, J., Hsiang, E.-L., He, Z., Zhan, T., & Wu, S.-T. (2021). Augmented reality and virtual reality displays: emerging technologies and future perspectives. *Light: Science & Applications*, 10(1), 1–30.

Yap, C. Y., Chua, C. K., Dong, Z. L., Liu, Z. H., Zhang, D. Q., Loh, L. E., & Sing, S. L. (2015). Review of selective laser melting: Materials and applications. *Applied Physics Reviews*, 2(4).

Yousaf, M. S., Detwiler, D., Duddeck, F., Menzel, S., Ramnath, S., Zurbrugg, N., & Bujny, M. (2023). Similarity-driven topology optimization for statics and crash via energy scaling method. *Journal of Mechanical Design*, 145(10).

EL PLAN ES HACER LA METODOLOGIA COMPLETA PARA PODER PRODUCIR ELEMENTOS INDUSTRIALMENTE ACEPTABLES

- 1) DEFINICION DE INSUMOS
 - a. PARTE OPTIMIZADA PARA LA AM
 - b. MATERIALES> CON HOJAS TECNICAS Y PRUEBAS DE DESEMPEÑO
 - c. EQUIPO DE IMPRESION
- 2) OPTIMIZACION PARAMETROS DE TRABAJO PARA EL SET DE INSUMOS VISTOS EN PASO 1, SIMULACIONES DE LA PARTE OPTIMIZADA PARA CONGELAR EL MODELO
- 3) ELABORACION DE LA PARTE FISICA
- 4) PROCEDIMIENTOS DE CONTROL DE CALIDAD DE LA PARTE